

Manuscript Number: ECM-D-16-00352R1

Title: Photocatalytic reduction of CO<sub>2</sub> by CO co-feed combined with photocatalytic water splitting in a novel twin reactor

Article Type: Original research paper

Section/Category: 3. Clean Energy and Sustainability

Keywords: twin reactor; CO<sub>2</sub> reduction; water splitting; photocatalysis; methanol; sun light intensity

Corresponding Author: Prof. Lijun Yang, Ph. D.

Corresponding Author's Institution: North China Electric Power University

First Author: Shang Li

Order of Authors: Shang Li; Lijun Yang, Ph. D.; Oluwafunmilola Ola; Mercedes Maroto-Valer; Xiaoze Du; Yongping Yang

Abstract: As a promising way to control greenhouse gas emission and alleviate global energy shortage, photocatalytic reduction of carbon dioxide attracts more attentions in recent years since it can produce fuels efficiently with the combination of H<sub>2</sub> through water splitting. In this work, a computational model which characterizes the photocatalytic reduction of carbon dioxide by CO co-feed in a novel twin reactor is developed with three subsidiaries of chemical reaction kinetics, gas-liquid mass transfer, and transient sun light intensity distribution. Thanks to previous experimental work as the reliable verification for the numerical simulation, the variations of the CH<sub>3</sub>OH concentration with the CO/CO<sub>2</sub> ratio of gas mixture, pressure and temperature are obtained and analyzed. The results show that the carbon in CO can form CH<sub>3</sub>OH directly, however the excessive CO will react with HCOOCH<sub>3</sub> to form CH<sub>3</sub>CHO, which results in a reduced CH<sub>3</sub>OH concentration. Besides, the CH<sub>3</sub>OH concentration subsequently increases as the temperature and pressure increase, and the CH<sub>3</sub>OH product and reaction rate vary widely with time due to the changing sun light intensity during the day.

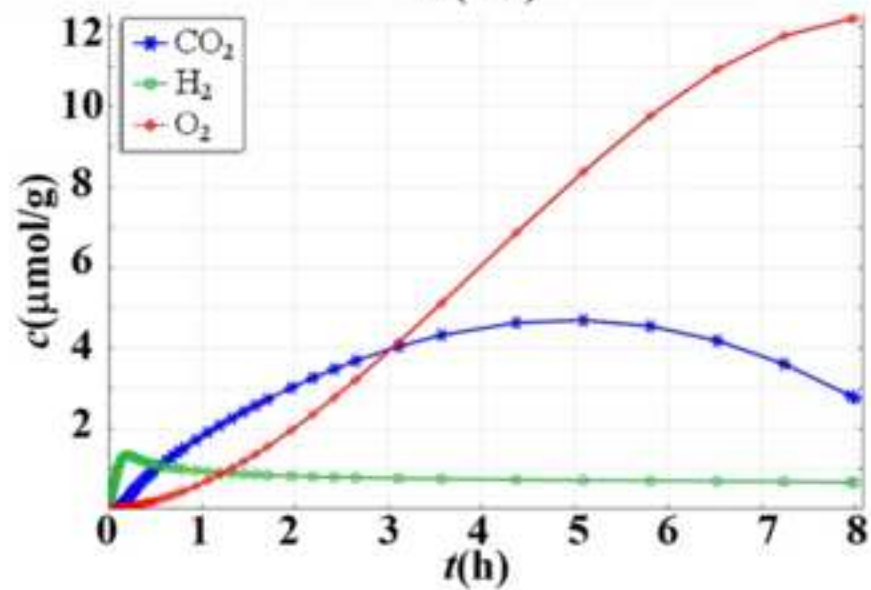
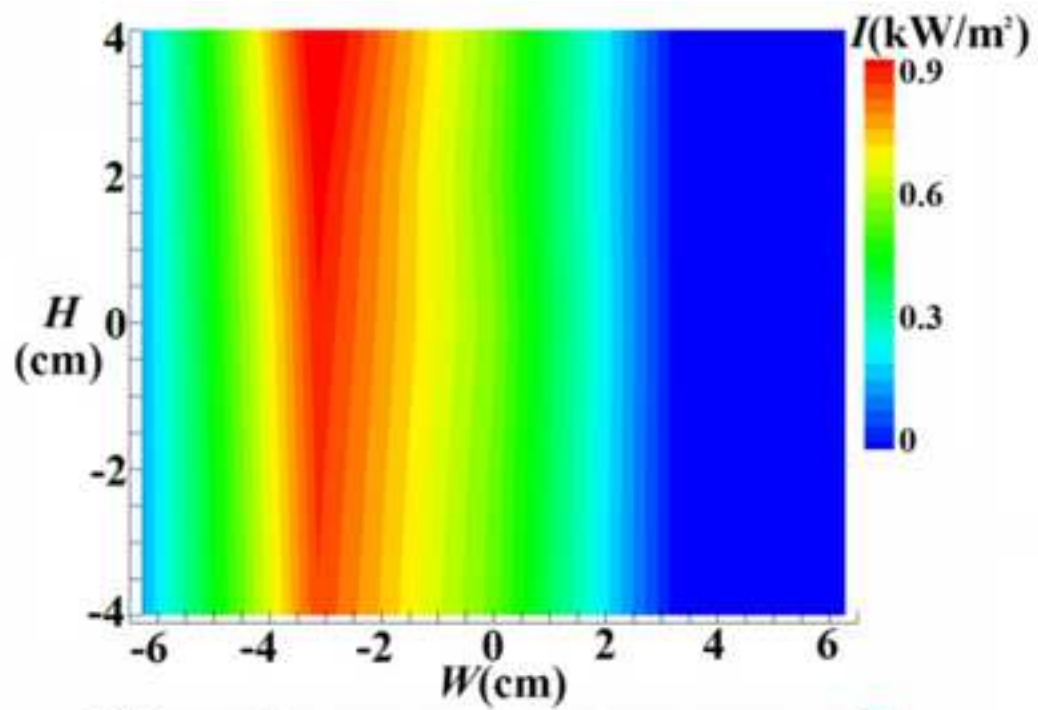
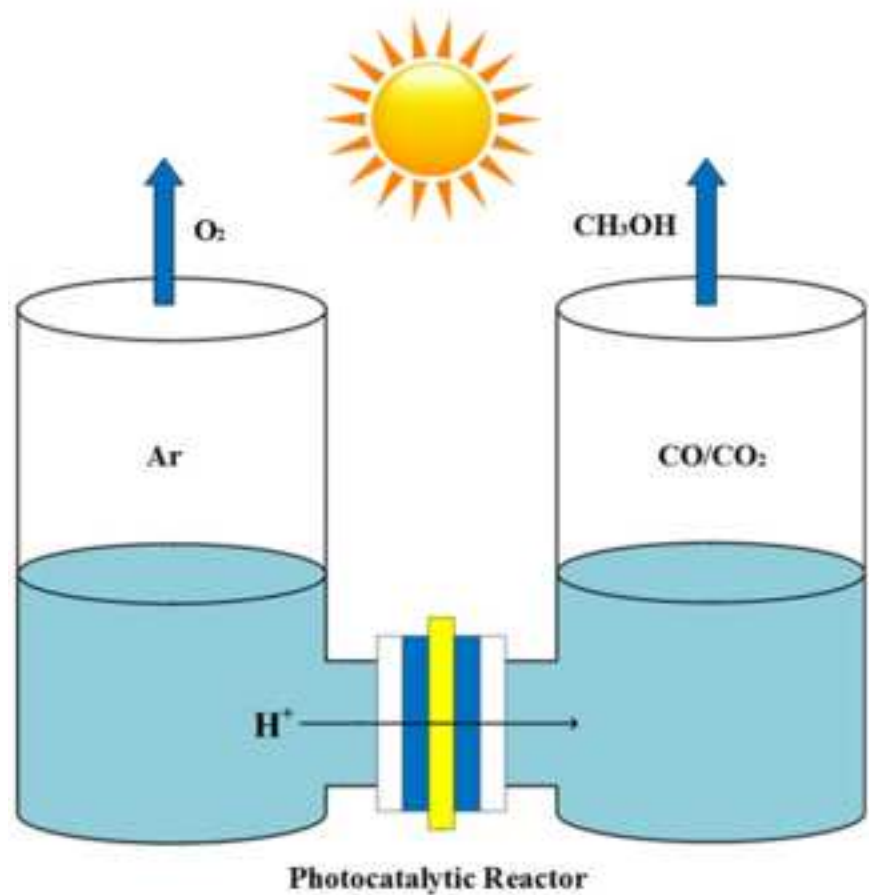
Dear Editor

Thanks for your comments and suggestions on our manuscript. Those comments are all valuable and very helpful for revising and improving our paper, as well as important for guiding our researches. We have modified the manuscript accordingly and seriously. Detailed corrections are listed in the response file and the revised manuscript.

Sincerely yours  
Corresponding author: Lijun Yang

Email: yanglj@ncepu.edu.cn

School of Energy Power and Mechanical Engineering,  
North China Electric Power University,  
Beijing 102206, China



## Research Highlights

Photocatalytic CO<sub>2</sub> reduction combined with H<sub>2</sub> through water splitting is studied.

The carbon in CO can form CH<sub>3</sub>OH directly, so can increase CH<sub>3</sub>OH concentration.

Excessive CO will react with HCOOCH<sub>3</sub>, resulting in a reduced CH<sub>3</sub>OH concentration.

CH<sub>3</sub>OH concentration increases with increasing the reactor temperature and pressure.

CH<sub>3</sub>OH product and reaction rate vary widely with time due to changing sun light.

1                    Photocatalytic reduction of CO<sub>2</sub> by CO co-feed  
2                    combined with photocatalytic water splitting in a novel  
3                    twin reactor

4                    Shang Li<sup>1</sup>, Lijun Yang\*<sup>1</sup>, Oluwafunmilola Ola\*<sup>2</sup>, Mercedes Maroto-Valer<sup>2</sup>, Xiaoze  
5                    Du<sup>1</sup>, Yongping Yang<sup>1</sup>

6                    1. Key Laboratory of Condition Monitoring and Control for Power Plant Equipments of  
7                    Ministry of Education,  
8                    School of Energy Power and Mechanical Engineering, North China Electric Power  
9                    University, Beijing 102206, China

10                    2. Centre for Innovation in Carbon Capture and Storage (CICCS),  
11                    School of Engineering and Physical Sciences, Heriot-Watt University, Edinburgh, EH14 4AS,  
12                    UK

13  
14                    **ABSTRACT**

15                    As a promising way to control greenhouse gas emission and alleviate global energy  
16                    shortage, photocatalytic reduction of carbon dioxide attracts more attentions in recent  
17                    years since it can produce fuels efficiently with the combination of H<sub>2</sub> through water  
18                    splitting. In this work, a computational model which characterizes the photocatalytic

---

\* Corresponding author: Lijun Yang. Tel: +86 10 61773373; Fax: +86 10 61773877. E-mail address:

[yanglj@ncepu.edu.cn](mailto:yanglj@ncepu.edu.cn)

Oluwafunmilola Ola. Tel: +44 (0) 131 451 4737. E-mail address: [O.O.Ola@hw.ac.uk](mailto:O.O.Ola@hw.ac.uk)

19 reduction of carbon dioxide by CO co-feed in a novel twin reactor is developed with  
20 three subsidiaries of chemical reaction kinetics, gas-liquid mass transfer, and transient  
21 sun light intensity distribution. Thanks to previous experimental work as the reliable  
22 verification for the numerical simulation, the variations of the CH<sub>3</sub>OH concentration  
23 with the CO/CO<sub>2</sub> ratio of gas mixture, pressure and temperature are obtained and  
24 analyzed. The results show that the carbon in CO can form CH<sub>3</sub>OH directly, however  
25 the excessive CO will react with HCOOCH<sub>3</sub> to form CH<sub>3</sub>CHO, which results in a  
26 reduced CH<sub>3</sub>OH concentration. Besides, the CH<sub>3</sub>OH concentration subsequently  
27 increases as the temperature and pressure increase, and the CH<sub>3</sub>OH product and  
28 reaction rate vary widely with time due to the changing sun light intensity during the  
29 day.

30 **Key words:** twin reactor, CO<sub>2</sub> reduction, water splitting, photocatalysis, methanol, sun  
31 light intensity

32

33 **Nomenclature**

<i>c</i>	concentration	$\text{mol}\cdot\text{m}^{-3}$
<i>D</i>	diffusion coefficient	$\text{m}^2\cdot\text{s}^{-1}$
<i>I</i>	light intensity	$\text{W}\cdot\text{m}^{-2}$
<i>k</i>	kinetic rate constant	$\text{m}^4\cdot\text{s}^{-1}\cdot\text{mol}^{-2}$
<i>L</i>	reactor height	mm
<i>M</i>	molecular weight	$\text{g}\cdot\text{mol}^{-1}$
<i>p</i>	pressure	Pa
<i>r</i>	reaction rate	$\text{mol}\cdot\text{m}^{-3}\cdot\text{s}^{-1}$
<i>R</i>	radius	mm
<i>t</i>	time	s
<i>T</i>	temperature	K
<i>V</i>	molar volume	$\text{cm}^3\cdot\text{mol}^{-1}$
<i>N</i>	mass transfer rate	$\text{mol}\cdot\text{m}^{-2}\cdot\text{s}^{-1}$
<i>K</i>	mass transfer coefficient	$\text{s}\cdot\text{mol}\cdot\text{kg}^{-1}\cdot\text{m}^{-1}$
<i>H</i>	Henry constant	$\text{Pa}\cdot\text{m}^3\cdot\text{mol}^{-1}$
<i>V</i>	ionic strength	$\text{mol}\cdot\text{m}^{-3}$
<i>E</i>	electric field intensity	$\text{V}\cdot\text{m}^{-1}$
<i>z</i>	ionic valence	
<i>h</i>	solubility coefficient	

$X$	sun unit vector
$Y$	sun unit vector
$Z$	sun unit vector
$m$	energy coefficient
$Rf$	reflectivity
$Tr$	transmissivity
$Ab$	absorptivity
$n$	refractivity
$L$	latitude
$Day$	day of year
$Hr$	local solar time

34 Greek letters

$\delta$	film thickness	mm
$\nu$	chemical calculated number	
$\rho$	density	$\text{kg}\cdot\text{m}^{-3}$
$\varphi$	correction coefficient of Henry constant	
$\psi$	proportional coefficient	S
$\omega$	hour angle	
$\delta$	declination	
$\alpha$	solar altitude	



$\gamma$  solar azimuth

Subscript and superscript

$A$  material

$B$  material

$F$  material

$O$  material

$a$  chemical calculated number

$b$  chemical calculated number

$f$  chemical calculated number

$o$  chemical calculated number

$L$  liquid phase

$G$  gas phase

$j$  number of reaction

$i$  number of reactant or ion

$m$  interface

$s$  sun

$x$  carbon source from carbon dioxide

$y$  carbon source from carbon monoxide

## 36 **1. Introduction**

37 Since fossil fuels dominate more than 85% of energy consumption all over the  
38 world at the status quo, the rapid depletion has concentrated the growing concerns on  
39 the global energy crisis and an increasing carbon dioxide (CO<sub>2</sub>) emission, which  
40 motivates researchers exploring the CO<sub>2</sub> reduction and utilization[1-5]. In the past  
41 decades, the conversion of CO<sub>2</sub> to value-added chemicals and renewable fuels has  
42 been investigated by various methods such as thermal conversion, plasma conversion  
43 and photoreduction[6]. Among various technologies of energy conservation and  
44 emission reduction[7-9], the photocatalytic CO<sub>2</sub> reduction into hydrocarbon fuels is a  
45 promising and eco-friendly method to prevent the increasing of greenhouse gases and  
46 depletion of fossil resources[5, 10, 11]. Since the first demonstration in 1979 by Inoue  
47 et al.[12], the approach of photocatalytic CO<sub>2</sub> reduction has received increasing  
48 attentions [13-15].

49 For the traditional photo-technology, CO<sub>2</sub> can be reduced by water (H<sub>2</sub>O) to CO,  
50 CH<sub>4</sub>, HCOOH, HCHO and CH<sub>3</sub>OH over semiconductor materials such as TiO<sub>2</sub>, ZnO,  
51 WO<sub>3</sub>, SiC, CdS, and GaP[16-19]. However, CO<sub>2</sub> is hardly reducible since H<sub>2</sub>O is a  
52 weak reductant. What's worse, the hydrocarbon products can be easily oxidized,  
53 which results in a low output ratio of hydrocarbons unexpectedly. In recent years, the  
54 technology of hydrogen production from photocatalytic water splitting has achieved a  
55 rapid progress [20, 21]. In 1987, Thampi et al.[22] reported that under the action of

56 TiO<sub>2</sub> nanoparticles catalyst, CH<sub>4</sub> was produced from the gas mixture of H<sub>2</sub> and CO<sub>2</sub>  
57 with the production rate of about 116μL/h. And in 2007, Lo et al.[23] confirmed that  
58 the CO<sub>2</sub> photoreduction was improved by a mixture of H<sub>2</sub> and H<sub>2</sub>O compared with  
59 that using solely H<sub>2</sub> or H<sub>2</sub>O. Many studies on CO<sub>2</sub> hydrogenation to yield organics  
60 have been reported, which provide a theoretical basis for the chemical reactions of  
61 photocatalytic reduction of carbon dioxide with the combination of H<sub>2</sub> through water  
62 splitting. Twin reactor system can combine the water splitting with CO<sub>2</sub> reduction  
63 because the reducibility of H<sub>2</sub> is better than H<sub>2</sub>O, so the CO<sub>2</sub> photo-reduction with H<sub>2</sub>  
64 through water splitting is more viable to produce fuels at a higher yield rate [11], as it  
65 has also been experimentally investigated in previous studies [24-26].

66 Twin reactor usually consists of two components for photocatalytic water splitting  
67 and photocatalytic CO<sub>2</sub> reduction, which are divided by an ion exchange unit. H<sup>+</sup> from  
68 water splitting is directly used to perform the CO<sub>2</sub> photo-hydrogenation with the  
69 participation of the light at the room temperature. The conversion of CO<sub>2</sub> into  
70 hydrocarbons is feasible from the thermodynamic viewpoint. For instance, the  
71 photoreduction of CO<sub>2</sub> to produce CH<sub>3</sub>OH can be represented by five possible  
72 reactions as listed in Table 1. The enthalpies ( $\Delta H^0$ ) of all the five reactions are  
73 negative at room temperature, which proves that the reactions are exothermic. The  
74 Gibbs free energies ( $\Delta G^0$ ) of the reactions (1), (4) and (5) are negative, meaning that  
75 the reactions are spontaneous, equilibrium favorable. Moreover, although the  $\Delta G^0$  of

76 the reactions (2) and (3) are positive, meaning that they are thermodynamically not  
77 spontaneous, those values are still much lower than that of water splitting ( $\Delta H^0 =$   
78  $285.8 \text{ kJ/mol}$ ;  $\Delta G^0 = 237.1 \text{ kJ/mol}$ ). Hence, the photocatalysts can convert photon  
79 energy into chemical energy accompanied by this slightly positive change in the  
80 Gibbs free energy[25]. The combination of photocatalytic  $\text{CO}_2$  reduction with water  
81 splitting in the twin reactor presents a better performance than the  $\text{CO}_2$  reduction by  
82  $\text{H}_2\text{O}$ , and prevents the oxygenation of hydrocarbon products.

83 CO was considered as a co-feed to enhance the production efficiency of  $\text{CH}_3\text{OH}$ ,  
84 and a certain amount of CO mixed with the reaction gases can promote  $\text{CH}_3\text{OH}$   
85 production under the same conditions because CO is thermodynamically more  
86 favorable as compared to the  $\text{CO}_2$ . However, due to the limitation of experimental  
87 conditions, it did not address how the CO affects the methanol production. When the  
88 reaction gas is pure CO,  $\text{CH}_3\text{OH}$  cannot be produced, which was not clarified in detail  
89 by previous studies. Other operating conditions such as the pressure and temperature  
90 in the twin reactor, which are crucial to the photocatalytic reduction of  $\text{CO}_2$ , were also  
91 not deeply investigated. What's more, there are few related studies about the sun light  
92 effect on the photocatalytic  $\text{CO}_2$  reduction in twin reactors, since most of the  
93 experiments were carried out in an indoor environment with the artificial light instead  
94 of natural sources. Adopting the software SOLTRACE in this work, the principle of  
95 CO effect on the  $\text{CH}_3\text{OH}$  production and the impacts of operation conditions on the

96 conversion efficiency from CO<sub>2</sub> to CH<sub>3</sub>OH in the twin reactor are deeply investigated  
97 by unveiling the sun light distribution as well as the photocatalytic CO<sub>2</sub> reduction  
98 mechanism. It can be of benefit to the optimal design and operation of twin reactors  
99 by investigating the photocatalytic reduction of CO<sub>2</sub> by CO co-feed combined with  
100 photocatalytic water splitting.

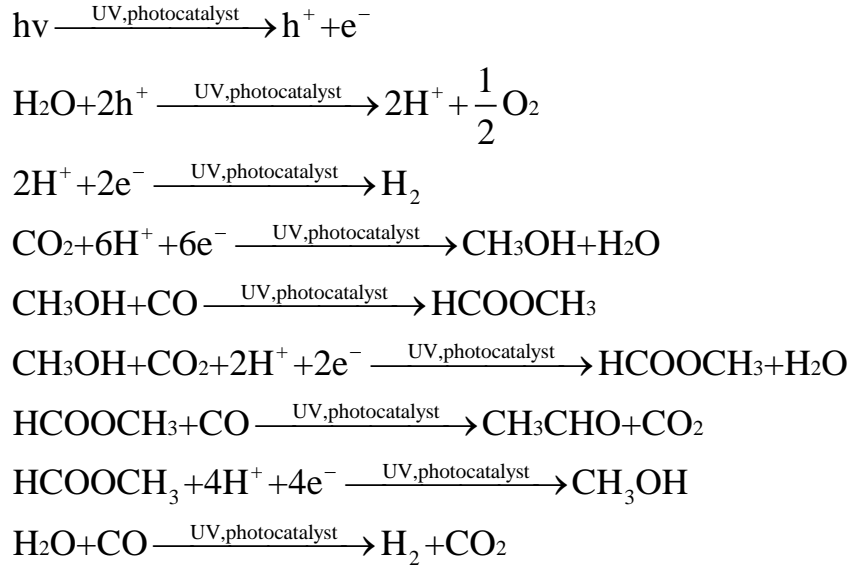
## 101 **2. Model development**

### 102 *2.1 Physical model*

103 The physical model of the twin reactor can be simplified as Fig.1, which has been  
104 described in detail and experimentally investigated in some of the photocatalytic  
105 characteristics [24-26]. With a Nafion membrane for segregation, 0.15 g of  
106 Pt/CuAlGaO<sub>4</sub> and 0.15 g of Pt/SrTiO<sub>3</sub>:Rh in 2mM FeCl<sub>2</sub> were placed in the CO<sub>2</sub>  
107 reduction reactor solution, while 0.30 g of commercial WO<sub>3</sub> in 2mM FeCl<sub>3</sub> solution  
108 were put in the water splitting reactor. In the novel twin reactor, one of the key  
109 components is the modified Nafion membrane that allows not only the transport of  
110 hydrogen ions, but also the exchange of the electron mediators (Fe<sup>2+</sup>/Fe<sup>3+</sup>). The  
111 electron is shuffled via the electron mediator (Fe<sup>2+</sup>/Fe<sup>3+</sup>) through membrane. The mass  
112 and charge balances are kept concurrently by the diffusion of H<sup>+</sup> through the  
113 membrane[27]. The pH of the solution is 2.6 (adjusted by adding sulfuric acid) and  
114 the volume of each compartment of the twin reactor is 225 mL. The H<sup>+</sup> generated by  
115 H<sub>2</sub>O splitting goes through the Nafion membrane and forms H<sub>2</sub>, which reacts with

116 CO<sub>2</sub> to produce organic compounds. In this work, the multi-physics coupling software  
117 is used to simulate the above process with the following necessary assumptions, based  
118 on which the model can be well simplified without introducing unexpected errors.

- 119 1) Since the driving force of the photoreaction originates from the light energy  
120 but not the thermal energy (i.e. molecular kinetics at high temperatures) in  
121 the traditional catalytic reaction, most photoreactions work at about the room  
122 temperature. As a result, the thermodynamic effects of the reactions at  
123 various temperatures can be ignored because of the extremely weak  
124 provoking energy in the photocatalysis.
- 125 2) Thanks to the magnetic stirrer in the experiment for the uniform catalyst  
126 distribution in the solution, the reaction rate is assumed to be a function of  
127 the time rather than the location.
- 128 3) Since CO and CO<sub>2</sub> are free from liquidation at the room temperature and  
129 atmospheric pressure, the mixture can be seen as an ideal gas so as to easily  
130 calculate the partial pressure based on the ideal gas equation. Besides, the  
131 chemical process at the interface of the gas and liquid is not taken into  
132 account.
- 133 4) The effects of the catalyst surface topography, concentration, band gap, and  
134 absorption or desorption existing on the surface of catalyst particles are  
135 ignored.
- 136 5) The chemical reactions in the twin reactor take the following forms, which  
137 are regarded as single step reactions [25].



138

139 With the aforementioned equations, the inferior middle processes are reasonably  
140 ignored for clearly uncovering the chemical mechanism from the reactants to  
141 products.

## 142 2.2 Chemical reaction kinetics model

143 For the chemical reaction  $aA + bB = fF + oO$  under constant volume conditions, the  
144 reaction rate can be expressed as follows:

$$r = -\frac{1}{a} \frac{dc_A}{dt} = -\frac{1}{b} \frac{dc_B}{dt} = \frac{1}{f} \frac{dc_F}{dt} = \frac{1}{o} \frac{dc_O}{dt} \quad (1)$$

145

146 When the reaction is an elementary reaction, the above formula can be written as:

$$r = kc_A^a c_B^b \quad (2)$$

147

148 Where  $k$  is the reaction rate constant.

149 In previous studies, it has been noticed that the photocatalytic reaction rate follows  
150 a power law expression of the light intensity[28]. By experimental studies, Herrmann  
151 suggested that the reaction rate is proportional to the light intensity at low light

152 intensities, and when the light intensity is high, the reaction rate is proportional to the  
 153 square root of the light intensity [29]. According to the work of Wang et al., the  
 154 photocatalytic reaction rate was considered proportional to the n-th power of the light  
 155 intensity[17], where n is a factor to describe the reaction rate dependency on light  
 156 irradiance. The higher n value of the reactor represents that the incident photons can  
 157 be more effectively utilized for photocatalytic reactions[30]. Therefore, the reversible  
 158 catalytic reaction rate equation can be written with the following form:

$$159 \quad r_j = I^m \left( k_j \prod_{i=1}^{\nu_i} c_i^{\nu_i} \right) \quad (3)$$

160 Where  $r_j$  is the reaction rate,  $k_j$  is the kinetic rate constant,  $c_i$  is the concentration,  $\nu_i$  is  
 161 the chemical calculated number,  $I$  is the light intensity,  $m$  is the energy coefficient.

### 162 2.3 Mass transfer model

163 Many physical models, such as two-film, Higbie penetration, Danckwerts surface  
 164 renewal and turbulent mass transfer theories, all formerly clarified the process of  
 165 gas-liquid mass transfer. With two-film theory adopted in this work, a static film on  
 166 each side of the gas-liquid interface is assumed as the gas membrane and liquid  
 167 membrane. Moreover, the mass transfer rate of gas-liquid interphase depends on the  
 168 diffusion rate of gas and liquid membranes.

$$169 \quad N = \frac{D_G}{RT\delta_G}(p_G - p_m) = \frac{D_L}{\delta_L}(c_m - c_L) \quad (4)$$

170 Where  $N$  is the mass transfer rate,  $D_G$  and  $D_L$  are the diffusion coefficients of  
 171 components in gases and liquids respectively.  $\delta_G$  and  $\delta_L$  are the gas and liquid film  
 172 thicknesses, which are about 0.1mm according to the experiment.  $c_m$  and  $p_m$  represent



173 the concentration and partial pressure at the interface of the membranes.  $p_G$  is the  
 174 partial pressure of components in gas phase while  $c_L$  is the concentration of  
 175 components in liquid phase.  $R$  is the perfect gas constant and  $T$  is temperature.

176 By eliminating the interface concentration  $c_m$  and the interface pressure  $p_m$  in the  
 177 above formula, the mass transfer rate is expressed as:

$$178 \quad N = K_G(p_G - p^*) = K_L(c^* - c_L) \quad (5)$$

$$p^* = Hc_L; c^* = \frac{p_G}{H}$$

179 Where  $p^*$  is the partial pressure in equilibrium with  $c_L$ ,  $c^*$  is the concentration in  
 180 equilibrium with  $p_G$ ,  $H$  is the Henry constant,  $K_G$  and  $K_L$  represent gas phase total  
 181 mass transfer coefficient and liquid phase total mass transfer coefficient:

$$182 \quad K_G = \frac{1}{\frac{RT\delta_G}{D_G} + \frac{H\delta_L}{D_L}} \quad (6)$$

$$K_L = \frac{1}{\frac{RT\delta_G}{HD_G} + \frac{\delta_L}{D_L}}$$

183 When the solution contains electrolytes, electrolyte ions will reduce the solubility  
 184 of gases[31]. The Henry constant of gas in pure H<sub>2</sub>O is different from that in the  
 185 electrolyte solution, hence the correction coefficient of Henry constant  $\varphi$  has been  
 186 introduced in the research of Ueyama and Hatanaka [31]:

$$187 \quad H = \varphi H^0$$

$$\lg \varphi = \sum h_i V_i \quad (7)$$

188  $H^0$  and  $H$  are Henry constants for the gas in the water and electrolyte, respectively.  $V_i$   
 189 is the electrolyte ionic strength calculated by Eq.(8) as followed, and  $h_i$  is the reduced  
 190 coefficient of solubility caused by electrolyte, which is calculated by  $h = h^+ + h^- + h^*$ .  $h^+$ ,

191  $h^-$ ,  $h^*$  are influenced by the positive and negative ions, and the dissolved gases.

192 
$$V_i = \frac{1}{2} \sum c_j z_j^2 \quad (8)$$

193 Where,  $c_j$  is the ion concentration,  $z_j$  is the ion valence.

194 The electrolytes in the system are  $H^+$ ,  $Fe^{2+}$ ,  $Fe^{3+}$ ,  $Cl^-$  and  $SO_4^{2-}$  according to the  
195 related experiments.

196 As the physical model introduced above, the pH which has an impact on gas  
197 dissolution process, is set as 2.6 (adjusted by adding sulfuric acid) of the solution. In  
198 this work,  $H^+$  is considered with the same electrolyte as  $Fe^{2+}$ ,  $Fe^{3+}$  and  $Cl^-$ , so the pH  
199 effects on the solubility of  $CO_2$  are illustrated by the correction coefficient  $\varphi$ .

200 Diffusion coefficients of  $CO_2$  in the mixed gas and the solution can be calculated  
201 according to the following formula [32, 33]:

202 
$$\log D_L = -8.1764 + \frac{712.5}{T} - \frac{2.591 \times 10^5}{T^2}$$
$$D_G = \frac{435.7T^{3/2}}{P(V_A^{1/3} + V_B^{1/3})^2} \sqrt{\frac{1}{M_A} + \frac{1}{M_B}} \quad (9)$$

203 Where  $A$ ,  $B$  are two kinds of gas in the reactor,  $p$  is the total pressure,  $T$  is the  
204 temperature in the reactor and equals to 293K and  $M$  is the molar mass of the gas.  $V$  is  
205 the molar volume with the constant of 22.4 L/mol, due to the fact that the  $CO_2$  and  
206  $CO$  are ideal gases in the reactor.

#### 207 2.4 Sun light model

208 Since the photocatalytic  $CO_2$  reduction cannot work without sun light input in the  
209 twin reactor, most of the experiments were carried out in an indoor environment with

210 the artificial light for substitute. Unfortunately, few related studies emphasized on the  
 211 sun light distribution. While in this work, with the software SOLTRACE based on the  
 212 theory from Spencer and Murty[34], the sun light distribution is obtained and  
 213 analyzed for its optical performance, which is highly affected by the light diffusion as  
 214 a key factor that can be predicted by setting up accurate parameters in SOLTRACE.

215 The angular intensity distribution and position of the light together define the  
 216 natural energy source, and in Beijing (northern latitude  $40^{\circ}5'$ , east longitude  $116^{\circ}16'$ ),  
 217 the 200nd day during the year with the maximum sun declination is usually selected  
 218 for sunlight acquisition. Although the Gaussian and Pillbox apparatus can together  
 219 determine the sun shape, it cannot represent the real sunlight condition due to the  
 220 complex atmospheric factors as well as inevitable errors from the optical equipment.  
 221 Since the Gaussian leads to an obviously higher error than pillbox, it is dismissed in  
 222 this paper. The sunlight position ( $X_s, Y_s, Z_s$ ) can be calculated by latitude ( $L$ : +N, -S),  
 223 day of year ( $Day$ ) and local solar time ( $Hr$ ) as follows.

$$\begin{aligned}
 X_s &= \sin\gamma_s \cos\alpha_s \\
 Y_s &= \sin\alpha_s \\
 Z_s &= \cos\gamma_s \cos\alpha_s
 \end{aligned}
 \tag{10}$$

225 Where  $\alpha_s$  is the solar altitude and  $\gamma_s$  is the solar azimuth, which can be obtained by  
 226 the following form.

$$\begin{aligned}
 \alpha_s &= \sin^{-1}(\cos L \cos \delta \cos \omega + \sin L \sin \delta) \\
 \gamma_s &= \cos^{-1}\left[\frac{\sin \alpha_s \sin L - \sin \delta}{\cos \alpha_s \cos L}\right]
 \end{aligned}
 \tag{11}$$

228 Where  $\omega$  is the hour angle,  $\omega=15(Hr-12)$ .  $Hr$  is the local solar time, which is set  
 229 from 8:00 to 16:00.  $\delta$  is the declination,  $\delta= 23.45\sin (360(284+Day)/365)$ .  $Day$  is set  
 230 as 200, implying the maximum sun declination, and  $L$  as  $40^{\circ}5'$ , representing the  
 231 latitude of Beijing.

232 Optical properties can be obtained from the movement of rays when they hit the  
 233 surfaces. According to the experiment of Chen et al.[25], the body of the reactor is  
 234 made of glass which can be treated as fully transparent, so the absorptivity is set to 0.  
 235 The reflectivity and the transmissivity of the twin reactor can be obtained by the  
 236 following forms.

$$237 \quad Rf = \frac{(n_1 - n_2)}{(n_1 + n_2)} \quad (12)$$

$$Rf + Tr = 1$$

238 Where  $Rf$  is reflectivity,  $Tr$  is transmissivity,  $n$  is refractivity that can be obtained  
 239 from the relevant literature. In addition, due to the effect of the element surface shape  
 240 on ray direction, surface slope error and surface specularity can be included, which  
 241 together affect ray interaction at the surface in a combined form as follows

$$242 \quad \sigma_{\text{optical}} = (4\sigma_{\text{slope}}^2 + \sigma_{\text{specularity}}^2)^{1/2} \quad (13)$$

243 Where  $\sigma_{\text{optical}}$  is the comprehensive factor,  $\sigma_{\text{slope}}$  means the surface slope error, and  
 244  $\sigma_{\text{specularity}}$  represents the surface specularity error.

## 245 2.5 Evaluation of model parameters

246 The variables and constants used in this model are listed in Table 2 with specific

247 meanings. The geometric parameters were obtained based on the real dimensions of  
248 the reactor and the kinetics parameters by fitting the experimental data. Since the  
249 reaction rate constant is not known in advance, should it be assumed at first. The  
250 CH<sub>3</sub>OH production can be numerically calculated and then compared with the  
251 experimental data. If the error is not within the allowed value, should the reaction rate  
252 constant as aforementioned above be reassumed for expecting results. The mass  
253 transfer parameters were estimated by Eqs.(7-9) with the initials referring to the  
254 experiment, and the sun position parameters by Eqs.(10) and (11) with the optical  
255 variables determined by Eqs.(12) and (13).

## 256 *2.6 Validation of numerical results*

257 Adopting the reaction engineering and diluted species transport modules, Eqs.(2-3)  
258 and (4-9) can be solved respectively by the commercial software COMSOL. Besides,  
259 the reaction rate can be iterated as the light intensity was taken into account by  
260 setting global variables.

261 The initial conditions with pure CO<sub>2</sub> are simulated as shown in Figs. 2 and 3. As  
262 observed, the H<sub>2</sub> concentration increases sharply at the beginning since the H<sup>+</sup>  
263 generated by water decomposition penetrates directly through the ion exchange  
264 membrane to form H<sub>2</sub>. Meanwhile, the O<sub>2</sub> concentration in the water splitting reactor  
265 also rises with a half production of H<sub>2</sub>. However as the O<sub>2</sub> increases stably, the H<sub>2</sub> in  
266 the CO<sub>2</sub> reduction reactor no longer increases and keeps at the rate of nearly

267 0.85 $\mu\text{mol/g}$ , showing that  $\text{H}_2$  already reaches a balance since it generated by water  
268 splitting transforms directly into the  $\text{CH}_3\text{OH}$  and other organic compounds. So at the  
269 beginning five hours, even the increasing rate declines gradually, the  $\text{CH}_3\text{OH}$  rises  
270 conspicuously with an average speed of 0.8  $\mu\text{mol/g/h}$ , while it then keeps almost no  
271 change with the ultimate concentration of 4 $\mu\text{mol/g}$  as shown in Fig. 3. Besides, Fig. 3  
272 shows that the average error between the simulation and experimental results is about  
273 13.12%, which is quite small. Moreover, Fig. 4 shows the concentration of methyl  
274 formate ( $\text{HCOOCH}_3$ ) and acetaldehyde ( $\text{CH}_3\text{CHO}$ ) as the two by-products during the  
275 reaction process, which reaches 1.5 $\mu\text{mol/g}$  and 0.4  $\mu\text{mol/g}$  with the average rate of  
276 0.1875  $\mu\text{mol/g/h}$  and 0.05  $\mu\text{mol/g/h}$  respectively within the 8 hours. The  $\text{CO}_2$  and  $\text{CO}$   
277 composite process is also numerically calculated with the initial partial pressure of  
278  $\text{CO}$  set in accordance with the mixing ratio of 1:10 and 1:5 respectively as shown in  
279 Figs. 5 and 6, which clearly present that the final  $\text{CH}_3\text{OH}$  concentrations are  
280 7.8  $\mu\text{mol/g}$  and 7.4 $\mu\text{mol/g}$  after 8 hours with the relative errors between the  
281 simulating and experimental results of 4.41% and 2.92% respectively.

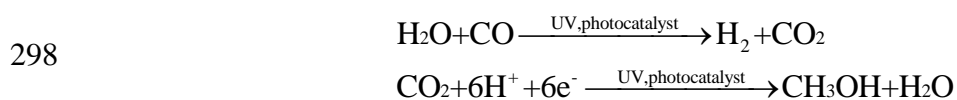
282 The comparisons show that the numerical and experimental results agree well with  
283 each other, so the modelling approach is reliable and accurate enough to predict the  
284 photocatalytic  $\text{CO}_2$  reduction performances in the twin reactor system. Since the  
285 photocatalytic  $\text{CO}_2$  reduction gradually recedes with an ultimately constant  $\text{CH}_3\text{OH}$   
286 concentration, the working conditions of the twin reactor system can be optimized by

287 means of numerical simulations.

### 288 **3. Results and discussion**

#### 289 *3.1 Effects of gas mixture ratio*

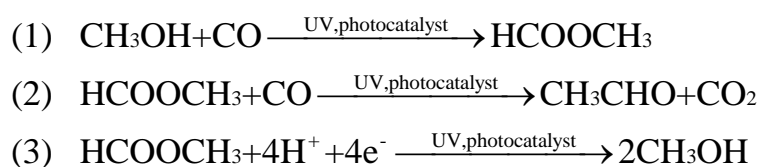
290 Pure CO as the reactant gas is specifically simulated so as to unveil its  
291 characteristics during the overall process at the ambient pressure and temperature of  
292 1atm and 293K respectively. Fig. 7 shows that the H<sub>2</sub> presents almost twice the  
293 concentration of O<sub>2</sub>, while the CH<sub>3</sub>OH concentration displays nearly zero due to the  
294 non-conversion from hydrogen, which clearly shows the unavailable direct chemical  
295 reaction between the pure CO and hydrogen or hydrogen ions. However, very small  
296 amount of CH<sub>3</sub>OH (less than 0.1μmol/g) exists inevitably due to the following  
297 reaction in the reduction reactor:



299 The overall process at various gas mixture ratios of CO to CO<sub>2</sub> was numerically  
300 simulated during the whole 20 hours with the carbon elements symbolized as C<sub>x</sub> from  
301 CO<sub>2</sub> and C<sub>y</sub> from CO for easy analysis of the carbon trails existing in methanol. Fig.8  
302 displays the processing amount of C<sub>x</sub>H<sub>3</sub>OH as well as C<sub>y</sub>H<sub>3</sub>OH at the CO to CO<sub>2</sub> ratio  
303 of 1:10. During the first 8 hours, it can be observed that the C<sub>x</sub>H<sub>3</sub>OH has a higher  
304 production rate of 0.53 μmol/g/h, while only 0.45 μmol/g/h for the C<sub>y</sub>H<sub>3</sub>OH. After  
305 then, it changes little for the concentration of C<sub>x</sub>H<sub>3</sub>OH with a stable amount of  
306 4.2μmol/g at the 20th hour. But for C<sub>y</sub>H<sub>3</sub>OH, the concentration always increases and

307 eventually reaches about 4.6  $\mu\text{mol/g}$  after 20 hours. It shows that the CO can easily  
 308 transform into the methanol and other organic compounds through the chemical  
 309 chains as aforementioned above compared with  $\text{CO}_2$ . As shown in Fig. 9, the  
 310 production of  $\text{C}_x\text{H}_3\text{OH}$  declines with the CO to  $\text{CO}_2$  ratio of 1:5 compared with the  
 311 case of 1:10, and only arrives at 3.6 $\mu\text{mol/g}$  for the maximum concentration. As for  
 312  $\text{C}_y\text{H}_3\text{OH}$ , the concentration reaches the peak of nearly 3.75  $\mu\text{mol/g}$  at the time of 7.5h,  
 313 then it decreases to 2.1  $\mu\text{mol/g}$  after 20 hours and finally presents a declining  
 314 tendency. Since CO plays a double role during the  $\text{CH}_3\text{OH}$  production, may the  
 315  $\text{CH}_3\text{OH}$  increase due to its positive effect with a small amount, while should other  
 316 organic compounds unexpectedly emerge with an excessive CO ratio. Fig. 10 shows  
 317 the  $\text{CH}_3\text{CHO}$  concentration at various gas mixture ratios, which clearly presents the  
 318 always small value less than 0.5  $\mu\text{mol/g}$  at the first 5 hours. But the  $\text{CH}_3\text{CHO}$   
 319 production rate increases as the chemical process continues, and it presents a higher  
 320 value at a more intensive CO concentration. Besides, as the ratio of CO to  $\text{CO}_2$   
 321 changes from 1/20 to 1/2, the  $\text{CH}_3\text{CHO}$  concentration increases from 1.5  $\mu\text{mol/g}$  to  
 322 3.75  $\mu\text{mol/g}$  after 20 hours.

323 Figs.8-10 fully explain the mechanisms of the CO dominance in the photocatalytic  
 324 process, which can be described by the following three reactions.



325



326 When a small amount of CO gas exists in the reactor, the CO reacts with CH<sub>3</sub>OH to  
327 form HCOOCH<sub>3</sub> as reaction (1). Due to the excessive H<sub>2</sub>, the HCOOCH<sub>3</sub> reacts with  
328 H<sub>2</sub> and then generates CH<sub>3</sub>OH as reaction (3). In this case, the CO promotes CH<sub>3</sub>OH  
329 production. However, if CO gas is excessive, the CO will react with CH<sub>3</sub>OH to form  
330 HCOOCH<sub>3</sub> at first, then the remaining CO continues to react with HCOOCH<sub>3</sub> to  
331 produce CH<sub>3</sub>CHO as reaction (2), which prevents HCOOCH<sub>3</sub> from reacting with H<sub>2</sub>,  
332 resulting in an indirect consumption of CH<sub>3</sub>OH.

333 The aforementioned conclusion about the gas mixture ratio can be of benefit to the  
334 design and application of photocatalytic reactor systems. For the twin reactor, the  
335 optimal CO to CO<sub>2</sub> ratio as well as reaction time can be recommended with reference  
336 to the light intensity distribution and reactor structure. Moreover, increasing the  
337 byproduct of CH<sub>3</sub>CHO during the photocatalytic process proves efficient to prevent  
338 the side effect as reaction (2).

### 339 *3.2 Effects of pressure*

340 The mixture pressure in the reactor is of great importance for photocatalytic  
341 reactions. According to Henry's law, the partial pressure of the mixture above the  
342 liquid surface can directly affect the gas solubility. Besides, the mass transfer rate  
343 between the gas and liquid is related greatly with the partial pressure in terms of the  
344 two-film theory. Fig. 11 presents the production of CH<sub>3</sub>OH at various pressures  
345 during the 20 hours. It can be seen that as the initial pressure in the reactor goes up,

346 the CH<sub>3</sub>OH yield increases. When the initial pressure reaches 20atm, the CH<sub>3</sub>OH  
347 concentration arrives at 14.5 μmol/g at 20 hours, which is 52.6% higher than that of  
348 9.5 μmol/g at the initial pressure of 1atm. As for the efficiency, increasing the initial  
349 pressure in the reactor will consume more energy, so a viable operating pressure  
350 should be determined for the photocatalytic reactor in potential engineering  
351 applications.

### 352 *3.3 Effects of temperature*

353 The Henry constant can well represent the solubility of CO<sub>2</sub> and CO in the  
354 electrolyte. As observed from Table 3, the Henry constant increases as the temperature  
355 rises. Besides, the diffusion coefficients of the gas-gas as well as gas-liquid depend  
356 also upon the temperature according to Eq.(9), so the mass transfer correlates strongly  
357 with the temperature. Fig.12 shows the CH<sub>3</sub>OH concentration change at various  
358 temperatures, from which can be seen that the CH<sub>3</sub>OH concentration increases with  
359 increasing the temperature, resulting from the comprehensive effects of the solubility  
360 and mass transfer rate. At the temperature of 273K, the ultimate CH<sub>3</sub>OH concentration  
361 at the 20th hour is 6 μmol/g, while at 333K it approaches 11μmol/g, presenting an  
362 increase of 83.2%, which shows that the conversion efficiency can be greatly  
363 improved by increasing the temperature.

### 364 *3.4 Effects of light intensity*

365 Based on the optical parameters of the physical model aforementioned, the sun

366 light model is developed and the two dimensional distribution of light intensity on a  
367 cross-section of the reactor is achieved by adopting the software SOLTRACE. Fig. 13  
368 shows transient solar flux distribution in the reactor at 8:00, 12:00 and 16:00  
369 respectively, in which the positive direction of the X-axis stands for the west of the  
370 reactor and the positive direction of the Y-axis represents the zenith of the twin reactor.  
371 The distribution of light intensity at 8:00 is shown in Fig.13(a), which presents a  
372 non-uniform light intensity scattering in the reactor with  $832\text{W/m}^2$  on the east side  
373 while only  $205\text{W/m}^2$  on the west side, and the average light intensity is about  
374  $331\text{W/m}^2$ . As observed from Fig. 13(b), the reactor receives the sunlight vertically at  
375 12:00, so the light intensity arrives at the maximum value in the center while  
376 minimum value at both sides, due to the combined effects of the reflection and  
377 refraction by the glass container and colored solution with the iron ion. The average  
378 light intensity can reach nearly  $620\text{W/m}^2$  in the reactor. Fig. 13(c) presents the  
379 irradiation at 16:00 from the west side of the reactor with the average light intensity of  
380  $330\text{W/m}^2$ .

381 From 8:00 to 16:00, the average light intensity is obtained and shown in Fig.14,  
382 which is fitted to the following equation:

$$383 \quad I = -1996 + 435Hr - 18Hr^2 \quad (14)$$

384 It can be seen from Fig.14 that the results from the fitting curve agree well with the  
385 simulated data, so the fitting equation is reliable enough to predict the average light

386 intensity change over time. Together with the chemical reaction engineering module,  
387 the photocatalytic CO<sub>2</sub> reduction combined with the water splitting process can be  
388 numerically simulated within the 8 hours (8:00-16:00) at the temperature of 293K and  
389 pressure of 1atm. Fig.15 shows the concentration changes of O<sub>2</sub>, H<sub>2</sub> and CH<sub>3</sub>OH over  
390 time, proving that the CH<sub>3</sub>OH product using the sun light source is less than that using  
391 the artificial light source in the experiment of Cheng et al.[25]. As also clearly  
392 presented, the CH<sub>3</sub>OH concentration reaches the climax of 4.6 μmol/g about 3.5 hours  
393 later (11:30), and then it begins to decrease gradually due to the weakened light  
394 intensity. Fig. 16 shows the reaction rates of the photocatalytic CO<sub>2</sub> reduction and  
395 water splitting process. It can be seen that as the light intensity decreases, the  
396 photocatalytic water splitting reaction becomes slow, resulting in the reduced H<sub>2</sub> for  
397 CO<sub>2</sub> reduction. The CH<sub>3</sub>OH generating rate is lower than the consuming rate of side  
398 reaction, leading to a reduced CH<sub>3</sub>OH concentration.

399 Since the experimental study with the artificially unchanged light intensity could  
400 not totally represent the photocatalytic CO<sub>2</sub> reduction mechanism, the numerical  
401 method with the natural sunlight changing over time demonstrates an attractive  
402 superiority, which is closer to the real chemical process.

#### 403 **4. Conclusions**

404 The photocatalytic reduction of CO<sub>2</sub> by CO co-feed combined with photocatalytic  
405 water splitting in a novel twin reactor was modeled and numerically investigated.

406 The CH<sub>3</sub>OH concentration almost linearly increases with increasing the gas mixture  
407 ratio of CO to CO<sub>2</sub>, due to the direct conversion from CO to CH<sub>3</sub>OH. However, the  
408 excessive CO will react with HCOOCH<sub>3</sub> to form CH<sub>3</sub>CHO unexpectedly, resulting in  
409 a reduced CH<sub>3</sub>OH concentration. Besides, with the temperature and pressure increase,  
410 the CH<sub>3</sub>OH production rises owing to the enhanced mass transfer.

411 The numerical method with the natural sunlight in this work proves a more accurate  
412 photocatalytic CO<sub>2</sub> reduction process compared with the experiment, and the yield of  
413 CH<sub>3</sub>OH is reduced due to the changing light intensity. It suggests the artificial light  
414 intensity adjusted with time in the photocatalytic experiment, so as to obtain a more  
415 reliable result.

#### 416 **Acknowledgment**

417 The financial support for this research from the National Natural Science  
418 Foundation of China (Grant No. 50776032) is gratefully acknowledged. The authors  
419 also thank the support provided by the Royal Society International Project of UK  
420 (IE150489).

421

422       **References**

- 423       [1] Baran T, Wojtyła S, Dibenedetto A, Aresta M, Macyk W. Zinc sulfide functionalized with  
424 ruthenium nanoparticles for photocatalytic reduction of CO<sub>2</sub>. *Applied Catalysis B: Environmental*  
425 2015;178:170-6.
- 426       [2] Huang Q, Yu J, Cao S, Cui C, Cheng B. Efficient photocatalytic reduction of CO<sub>2</sub> by  
427 amine-functionalized g-C<sub>3</sub>N<sub>4</sub>. *Appl Surf Sci* 2015;358:350-5.
- 428       [3] Tahir B, Tahir M, Amin NS. Gold–indium modified TiO<sub>2</sub> nanocatalysts for photocatalytic CO<sub>2</sub>  
429 reduction with H<sub>2</sub> as reductant in a monolith photoreactor. *Appl Surf Sci* 2015;338:1-14.
- 430       [4] Yuan K, Yang L, Du X, Yang Y. Performance analysis of photocatalytic CO<sub>2</sub> reduction in optical  
431 fiber monolith reactor with multiple inverse lights. *Energ Convers Manage* 2014;81:98-105.
- 432       [5] Yuan K, Yang L, Du X, Yang Y. Numerical analysis of photocatalytic CO<sub>2</sub> reduction in optical  
433 fiber monolith reactor with optimized structures. *Energ Convers Manage* 2014;87:258-66.
- 434       [6] Tahir M, Amin NS. Recycling of carbon dioxide to renewable fuels by photocatalysis: Prospects  
435 and challenges. *Renewable and Sustainable Energy Reviews* 2013;25:560-79.
- 436       [7] Chiu FP, Kuo HI, Chen CC, Hsu CS. The energy price equivalence of carbon taxes and  
437 emissions trading—Theory and evidence. *Appl Energ* 2015;160:164-71.
- 438       [8] Liu Y, Zhou Y, Wu W. Assessing the impact of population, income and technology on energy  
439 consumption and industrial pollutant emissions in China. *Appl Energ* 2015;155:904-17.
- 440       [9] Wang Q, Su B, Sun J, Zhou P, Zhou D. Measurement and decomposition of energy-saving and  
441 emissions reduction performance in Chinese cities. *Appl Energ* 2015;151:85-92.
- 442       [10] Sim LC, Leong KH, Saravanan P, Ibrahim S. Rapid thermal reduced graphene oxide/Pt-TiO<sub>2</sub>  
443 nanotube arrays for enhanced visible-light-driven photocatalytic reduction of CO<sub>2</sub>. *Appl Surf Sci* 2015.
- 444       [11] Tahir M, Amin NS. Photocatalytic CO<sub>2</sub> reduction with H<sub>2</sub> as reductant over copper and indium  
445 co-doped TiO<sub>2</sub> nanocatalysts in a monolith photoreactor. *Applied Catalysis A: General*  
446 2015;493:90-102.
- 447       [12] Inoue T, Fujishima A, Satoshi K, Honda K. Photoelectrocatalytic reduction of carbon dioxide in  
448 aqueous suspensions of semiconductor powders. *Nature* 1979;277:637-8.
- 449       [13] Tahir M, Amin NS. Advances in visible light responsive titanium oxide-based photocatalysts  
450 for CO<sub>2</sub> conversion to hydrocarbon fuels. *Energ Convers Manage* 2013;76:194-214.
- 451       [14] Broberg Viklund S, Johansson MT. Technologies for utilization of industrial excess heat:  
452 Potentials for energy recovery and CO<sub>2</sub> emission reduction. *Energ Convers Manage* 2014;77:369-79.
- 453       [15] Jain S, Vardia J, Ameta R, Ameta SC. Use of malachite green as photocatalyst in reduction of  
454 sodium and potassium carbonates. *Energ Convers Manage* 2004;45:1233-42.
- 455       [16] Tahir B, Tahir M, Amin NS. Performance analysis of monolith photoreactor for CO<sub>2</sub> reduction  
456 with H<sub>2</sub>. *Energ Convers Manage* 2015;90:272-81.
- 457       [17] Wang T, Yang L, Du X, Yang Y. Numerical investigation on CO<sub>2</sub> photocatalytic reduction in  
458 optical fiber monolith reactor. *Energ Convers Manage* 2013;65:299-307.
- 459       [18] Ola O, Maroto-Valer MM. Transition metal oxide based TiO<sub>2</sub> nanoparticles for visible light  
460 induced CO<sub>2</sub> photoreduction. *Applied Catalysis A: General* 2015;502:114-21.
- 461       [19] Ola O, Maroto-Valer MM. Review of material design and reactor engineering on TiO<sub>2</sub>

462 photocatalysis for CO<sub>2</sub> reduction. *Journal of Photochemistry and Photobiology C: Photochemistry*  
463 *Reviews* 2015;24:16-42.

464 [20] Nong G, Chen Y, Li M, Zhou Z. Generation of hydrogen free radicals from water for fuels by  
465 electric field induction. *Energ Convers Manage* 2015;105:545-51.

466 [21] Waskasi MM, Hashemianzadeh SM, Mostajabi Sarhangi O, Harzandi AP. Computational model  
467 of hydrogen production by Coumarin-dye-sensitized water splitting to absorb the visible light in a local  
468 electric field. *Energ Convers Manage* 2012;62:154-64.

469 [22] Thampi KR, Kiwi J, Gratzel M. Methanation and photo-methanation of carbon dioxide at room  
470 temperature and atmospheric pressure. *Nature* 1987;327:506-8.

471 [23] Lo CC, Hung CH, Yuan CS, Wu JF. Photoreduction of carbon dioxide with H<sub>2</sub> and H<sub>2</sub>O over  
472 TiO<sub>2</sub> and ZrO<sub>2</sub> in a circulated photocatalytic reactor. *Sol Energ Mat Sol C* 2007;91:1765-74.

473 [24] Shinichi I, Ryota D. Hydrogen production from water and conversion of carbon dioxide to  
474 useful chemicals by room temperature photoelectrocatalysis. *Catal Today* 1996;27:271-7.

475 [25] Cheng YH, Nguyen VH, Chan HY, Wu JCS, Wang WH. Photo-enhanced hydrogenation of CO<sub>2</sub>  
476 to mimic photosynthesis by CO co-feed in a novel twin reactor. *Appl Energ* 2015;147:318-24.

477 [26] Lee WH, Liao CH, Tsai MF, Huang CW, Wu JCS. A novel twin reactor for CO<sub>2</sub> photoreduction  
478 to mimic artificial photosynthesis. *Applied Catalysis B: Environmental* 2013;132-133:445-51.

479 [27] Yu SC, Huang CW, Liao CH, Wu JCS, Chang ST, Chen KH. A novel membrane reactor for  
480 separating hydrogen and oxygen in photocatalytic water splitting. *J Membrane Sci* 2011;382:291-9.

481 [28] Lin H, Valsaraj K. An optical fiber monolith reactor for photocatalytic wastewater treatment.  
482 *Aiche J* 2006;2271-80.

483 [29] Herrmann JM. Heterogeneous photocatalysis: an emerging discipline involving multiphase  
484 systems. *Catal Today* 1995;24:157-64.

485 [30] Denny F, Scott J, Peng GD, Amal R. Channelled optical fibre photoreactor for improved air  
486 quality control. *Chem Eng Sci* 2010;65:882-9.

487 [31] Ueyama K, Hatanaka J. Salt effect on solubility of nonelectrolyte gases and liquids. *Chem Eng*  
488 *Sci* 1982;37:790-2.

489 [32] Ryszard P, Wadysaw M. Kinetics of Reaction Between Carbon-Dioxide and Hydroxyl Ions in  
490 Aqueous-Electrolyte Solutions. *Chem Eng Sci* 1988;43:1677-84.

491 [33] Rathore M, Kapuno R. *Engineering heat transfer*: Jones & Bartlett; 2011.

492 [34] Spencer GH, Murty M. General Ray-Tracing Procedure. *Journal of the Optical Society of*  
493 *America* 1962;52:672-8.

**Table 1**Changes of enthalpy and Gibbs free energy in the CO<sub>2</sub> photoreduction reactions[25].

Reactions	$\Delta H^0$ (kJ/mol)	$\Delta G^0$ (kJ/mol)
(1) CO <sub>2</sub> (g)+3H <sub>2</sub> (g)→CH <sub>3</sub> OH (l) +H <sub>2</sub> O (l)	-137.8	-10.7
(2) CO(g)+CH <sub>3</sub> OH(l)→HCOOCH <sub>3</sub> (l)	-25.6	6.6
(3) CO <sub>2</sub> (g)+H <sub>2</sub> (g)+CH <sub>3</sub> OH(l)→HCOOCH <sub>3</sub> (l)+H <sub>2</sub> O(l)	-31.8	25.8
(4) HCOOCH <sub>3</sub> (l)+2H <sub>2</sub> (g)→2CH <sub>3</sub> OH(l)	-99.7	-35.1
(5) HCOOCH <sub>3</sub> (l)+CO(g)→CH <sub>3</sub> CHO(l)+CO <sub>2</sub> (g)	-96.5	-86.7



**Table 2**Model parameters for photocatalytic CO<sub>2</sub> reduction by CO co-feed.

Type	Variables	Values	Unit
kinetics	$k_1$	3.3E-9	m <sup>3</sup> /(s · mol)
	$k_2$	1.7E-2	m <sup>9</sup> /(s · mol <sup>3</sup> )
	$k_3$	2.3E-4	m <sup>3</sup> /(s · mol)
	$k_4$	1.7E-4	m <sup>3</sup> /(s · mol)
	$k_5$	5.8E-6	m <sup>6</sup> /(s · mol <sup>2</sup> )
	$k_6$	8.1E-3	m <sup>3</sup> /(s · mol)
Geometry	$L$	11.46	cm
	$R_1$	5	cm
	$R_2$	4	cm
Mass transfer	$D_L$	1.9809E-9	m <sup>2</sup> /s
	$D_G$	1.41E-7	m <sup>2</sup> /s
	$\delta_G$	0.1	mm
	$\delta_L$	0.1	mm
	$h_{H^+}$	0	
	$h_{Fe^{2+}}$	0.049	
	$h_{Fe^{3+}}$	0.054	
	$h_{SO_4^{2-}}$	0.029	
$h_{Cl^-}$	0.021		

	$h_{\text{CO}^2}$	-0.019	
	$h_{\text{CO}}$	0.0283	
	$H_{0\text{CO}}$	5.43E+6	kPa
	$H_{0\text{CO}_2}$	1.44E+5	kPa
Initial value	$C_{\text{CO}_2}$	30.73	mol/m <sup>3</sup>
	$C_{\text{CO}}$	0.095	mol/m <sup>3</sup>
	$C_{\text{SO}_4^{2-}}$	1.21	mol/m <sup>3</sup>
	$C_{\text{Fe}^{2+}}$	8.8	mol/m <sup>3</sup>
	$C_{\text{Fe}^{3+}}$	8.8	mol/m <sup>3</sup>
	$I$	900	W/m <sup>2</sup>
	$m$	1	
Sun position	$Day$	200	
	$Hr$	8-16	
	$L$	40°5'	
	$Shape$	Pillbox	
Optical property	$Rf_{\text{glass}}$	0.05	
	$Tr_{\text{glass}}$	0.95	
	$Ab_{\text{glass}}$	0	
	$n_{\text{glass}}$	1.6	
	$Rf_{\text{solution}}$	0.2	

$Tr_{\text{solution}}$	0.48
$Ab_{\text{solution}}$	0.32
$n_{\text{solution}}$	1.3
<i>Slope error(mrad)</i>	3.5
<i>Specularity error(mrad)</i>	0.2

---

**Table 3**

Henry constants at various temperatures.

<i>T</i> (K)	273	278	283	288	293	298	303	308	313	318	323	333
Gas												
CO ( $H_x \times 10^{-6}$ kPa)	3.57	4.01	4.48	4.95	5.43	5.88	6.28	6.68	7.05	7.39	7.71	8.32
CO <sub>2</sub> ( $H_x \times 10^{-5}$ kPa)	0.37	0.8	1.05	1.24	1.44	1.66	1.88	2.12	2.36	2.60	2.87	3.46

$$H_c = \frac{H_x M_{\text{solvent}}}{1000 \rho}$$

Fig.1. Schematic of photocatalytic CO<sub>2</sub> reduction and H<sub>2</sub>O splitting in the twin reactor.

Fig.2. H<sub>2</sub> and O<sub>2</sub> production during photocatalytic reduction of pure CO<sub>2</sub> with simultaneous H<sub>2</sub>O splitting.

Fig.3. CH<sub>3</sub>OH production during photocatalytic reduction of pure CO<sub>2</sub> with simultaneous H<sub>2</sub>O splitting.

Fig.4. CH<sub>3</sub>CHO and HCOOCH<sub>3</sub> production during photocatalytic reduction of pure CO<sub>2</sub> with simultaneous H<sub>2</sub>O splitting.

Fig.5. CH<sub>3</sub>OH concentration at the CO to CO<sub>2</sub> ratio of 1:10.

Fig.6. CH<sub>3</sub>OH concentration at the CO to CO<sub>2</sub> ratio of 1:5.

Fig.7. H<sub>2</sub>, O<sub>2</sub> and CH<sub>3</sub>OH concentrations with the pure CO as the reactant gas.

Fig.8. Total CH<sub>3</sub>OH concentration, C<sub>x</sub>H<sub>3</sub>OH and C<sub>y</sub>H<sub>3</sub>OH concentrations at the CO to CO<sub>2</sub> ratio of 1:10.

Fig.9. Total CH<sub>3</sub>OH concentration, C<sub>x</sub>H<sub>3</sub>OH and C<sub>y</sub>H<sub>3</sub>OH concentrations at the CO to CO<sub>2</sub> ratio of 1:5.

Fig.10. CH<sub>3</sub>CHO concentrations at various CO to CO<sub>2</sub> gas mixture ratios.

Fig.11. CH<sub>3</sub>OH concentration change with time at various pressures.

Fig.12. CH<sub>3</sub>OH concentration change with time at various temperatures.

Fig.13. Light intensity distribution in CO<sub>2</sub> reduction reactor. (a) 8:00, (b) 12:00, (c) 16:00.

Fig.14. Average light intensity change over time under the sun light.

Fig.15. Concentration changes of  $H_2$ ,  $O_2$  and  $CH_3OH$  over time under the sun light.

Fig.16. Reaction rate changes of water splitting and  $CO_2$  reduction over time under the sun light.

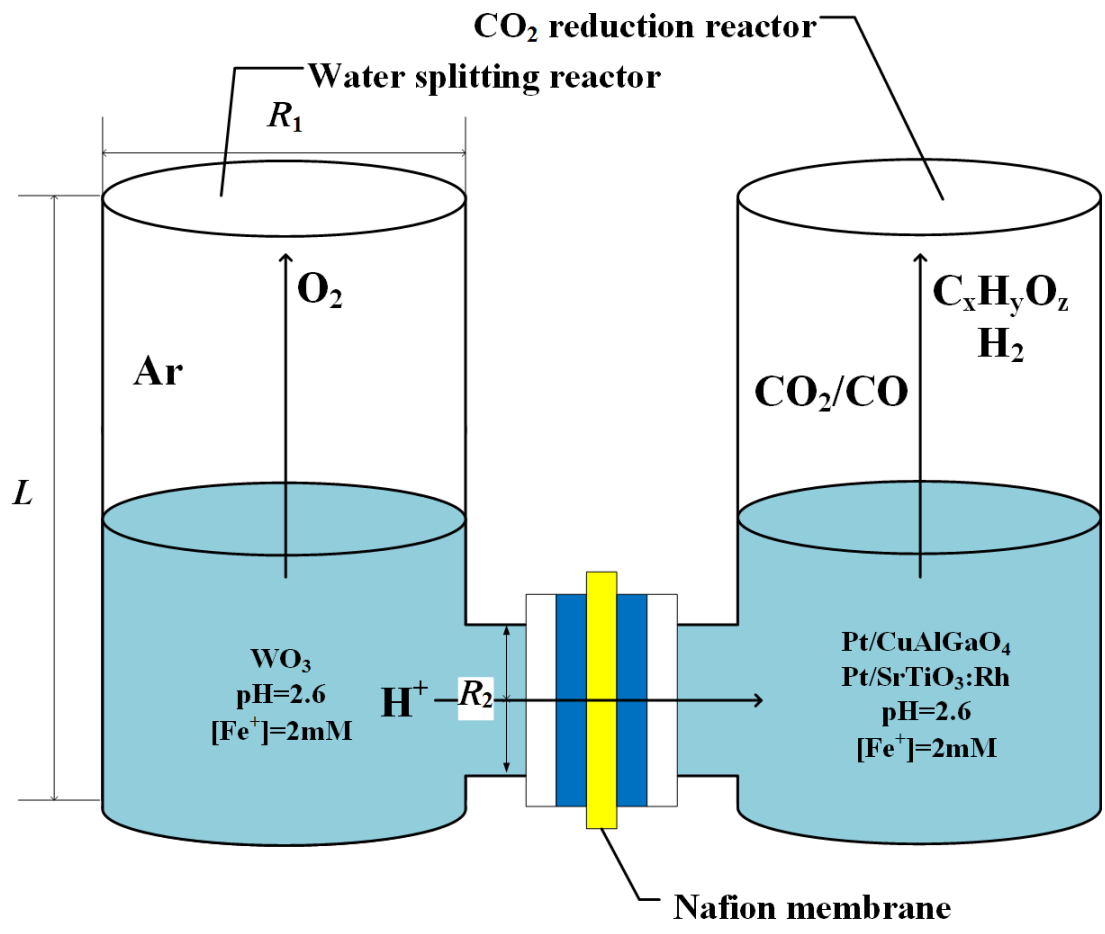


Fig.1.

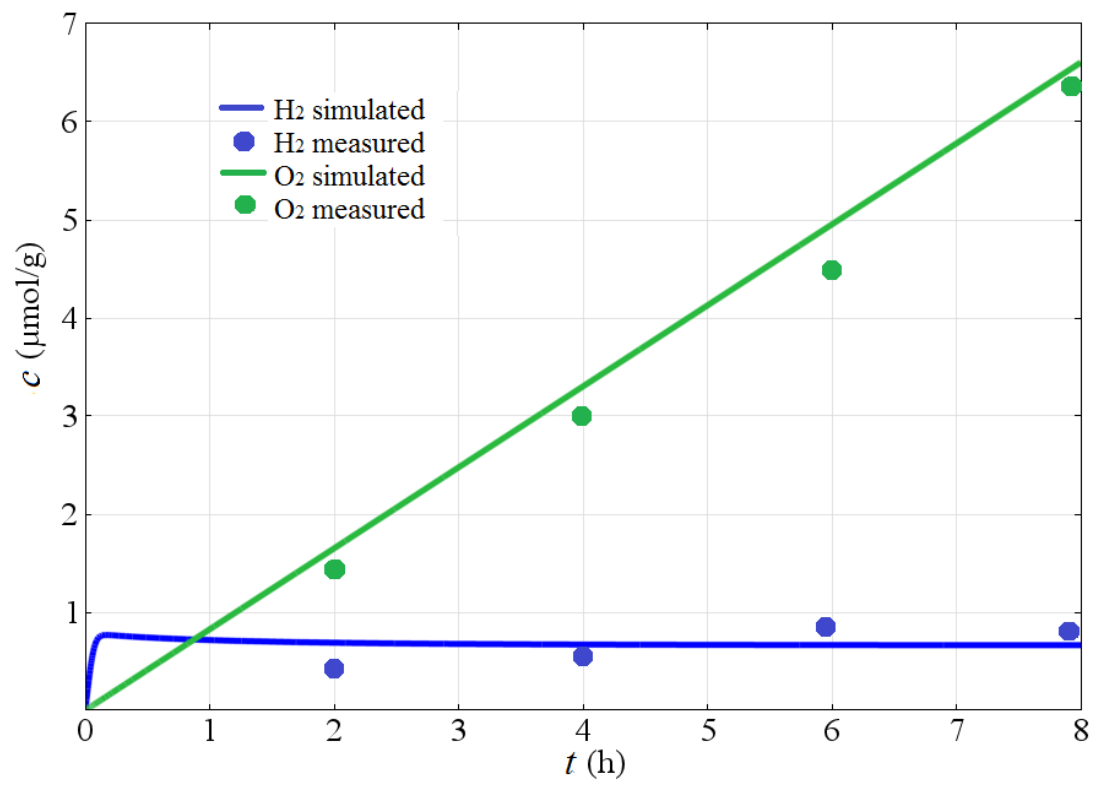


Fig.2.



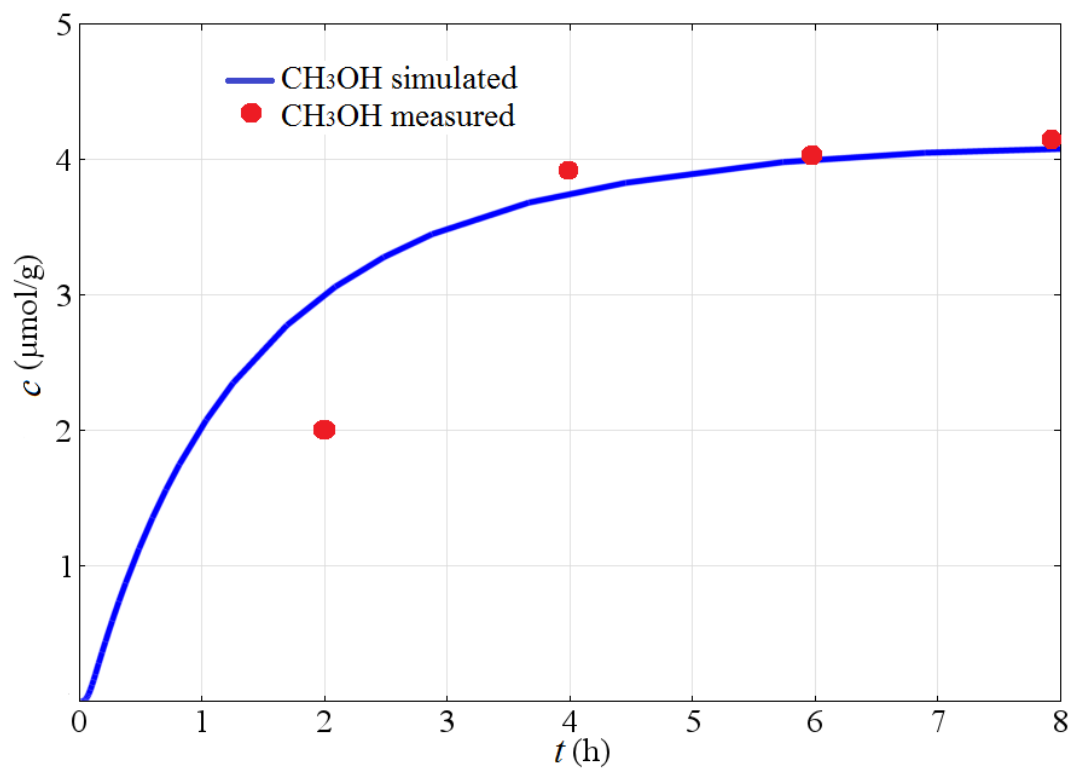


Fig.3.

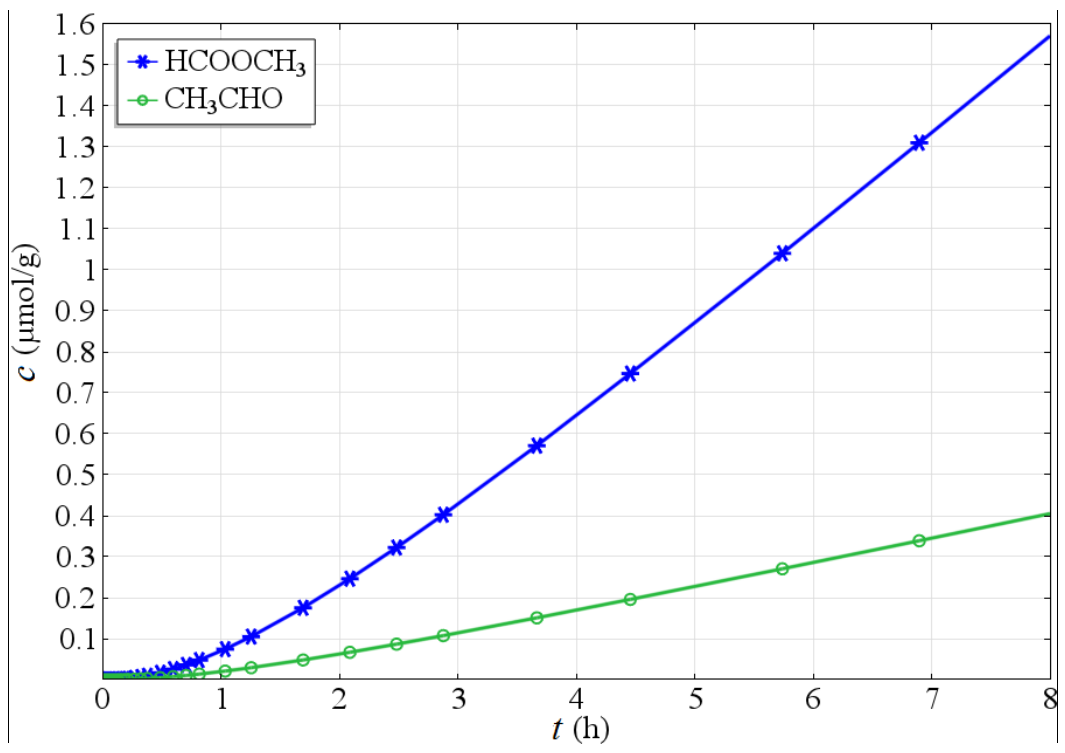


Fig.4.

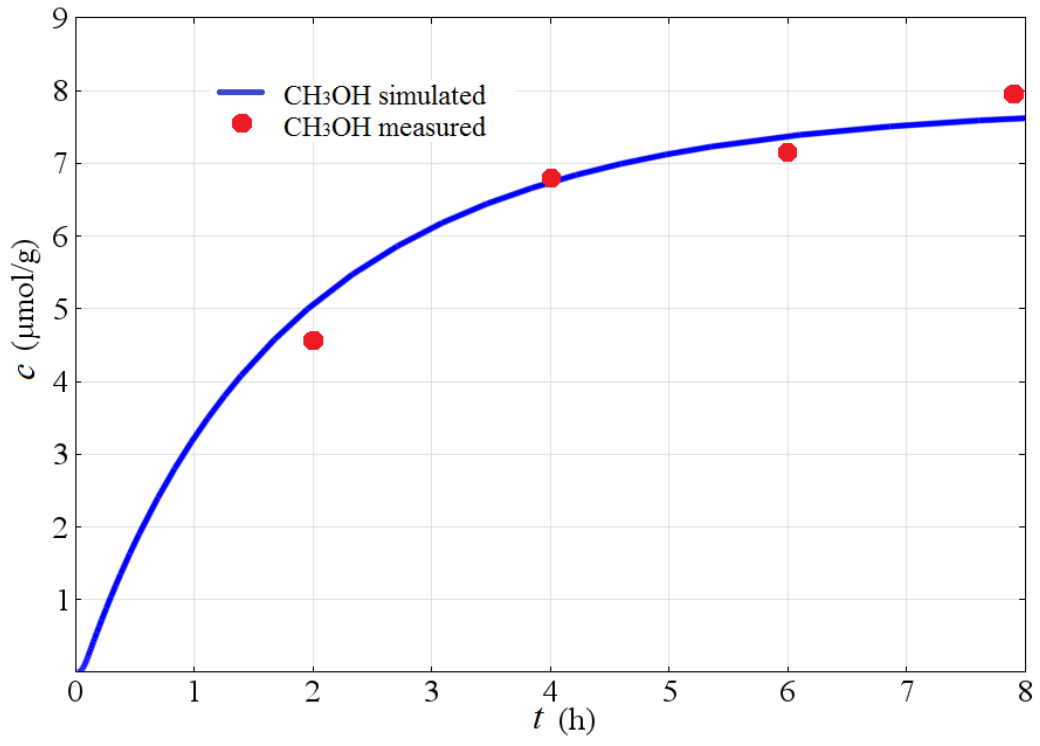


Fig.5.

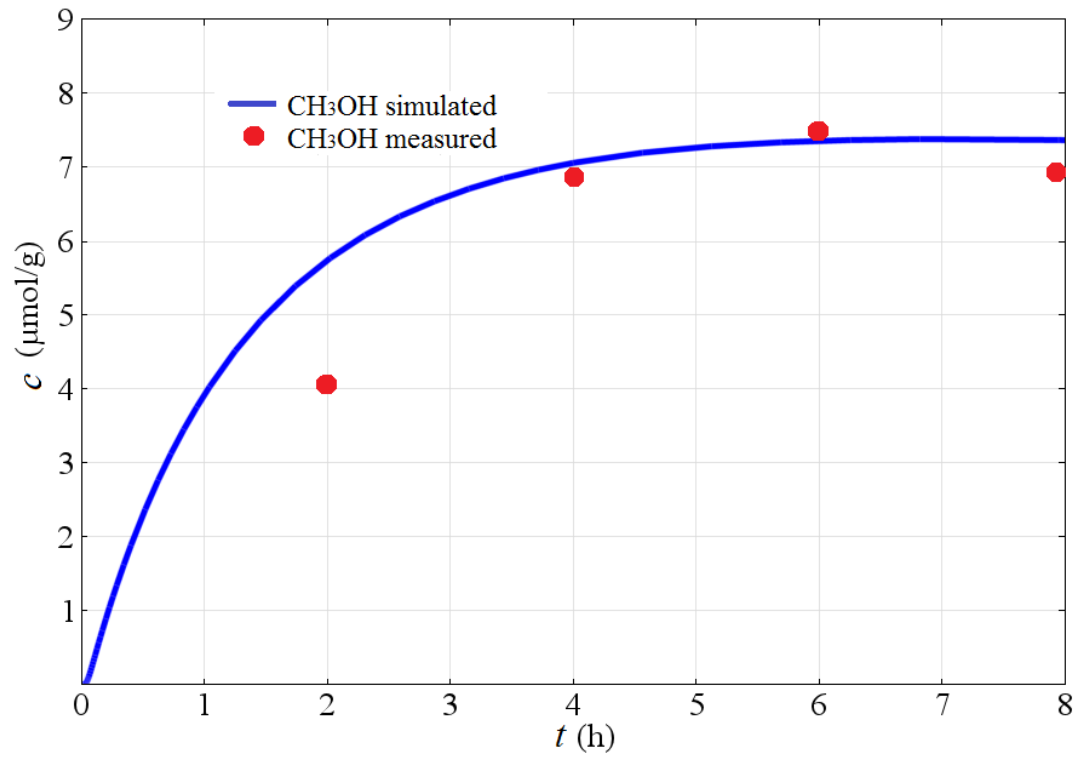


Fig.6.

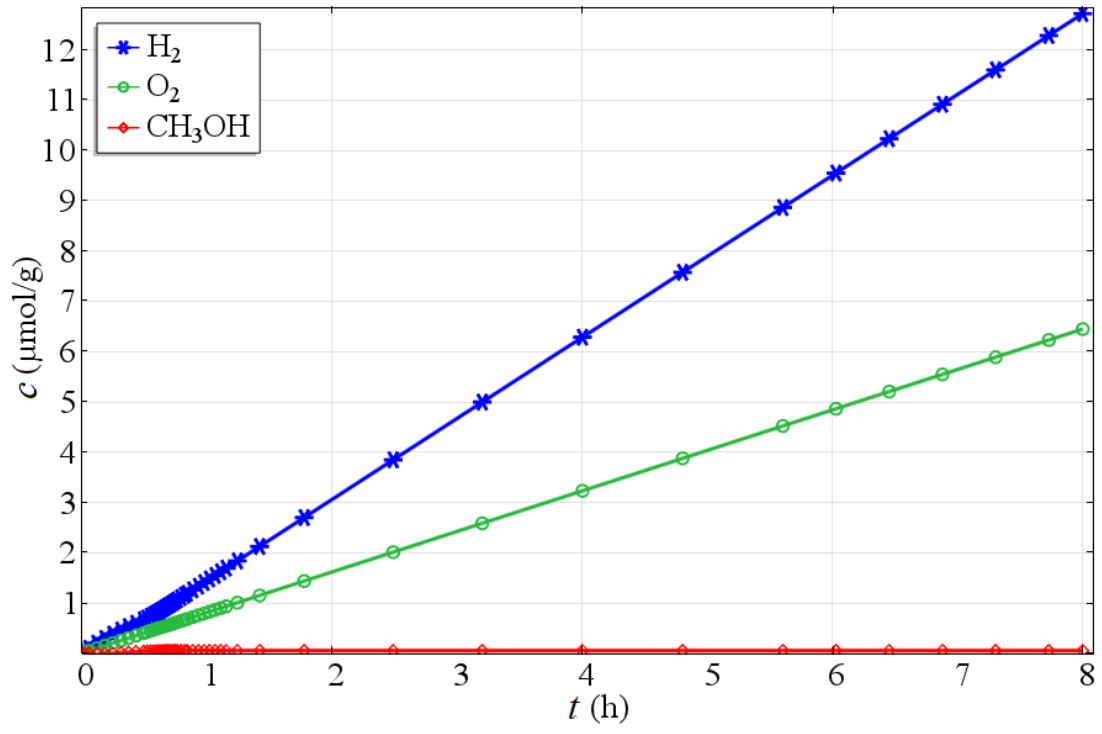


Fig.7.

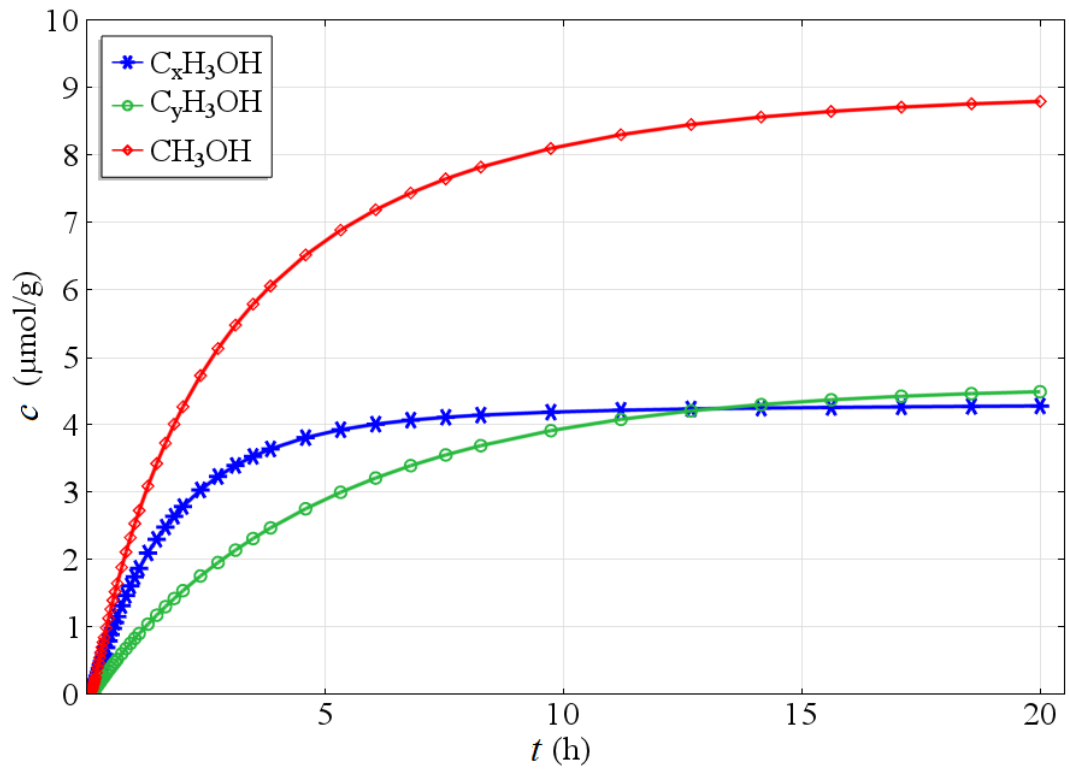


Fig.8.

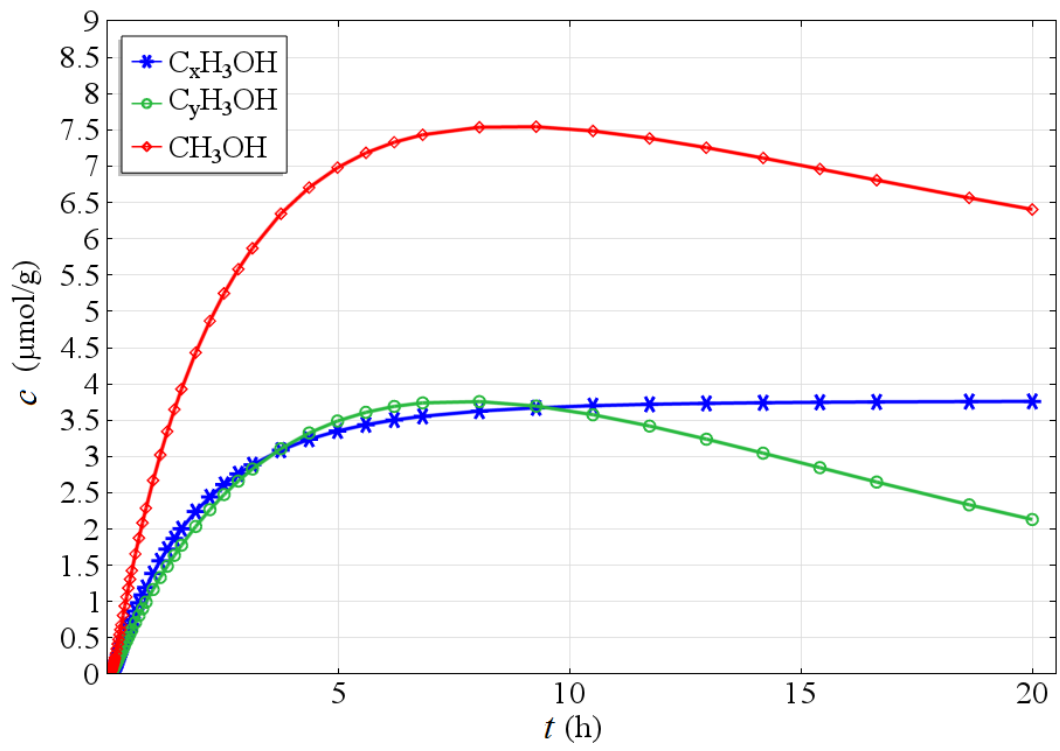


Fig.9.

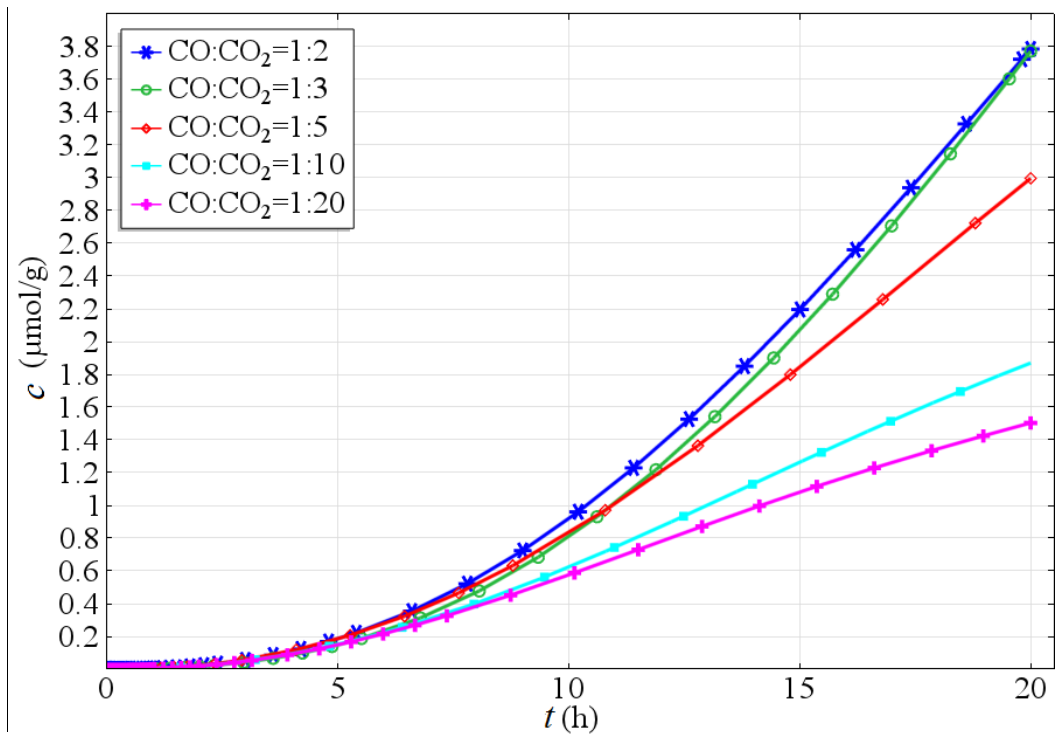


Fig.10.



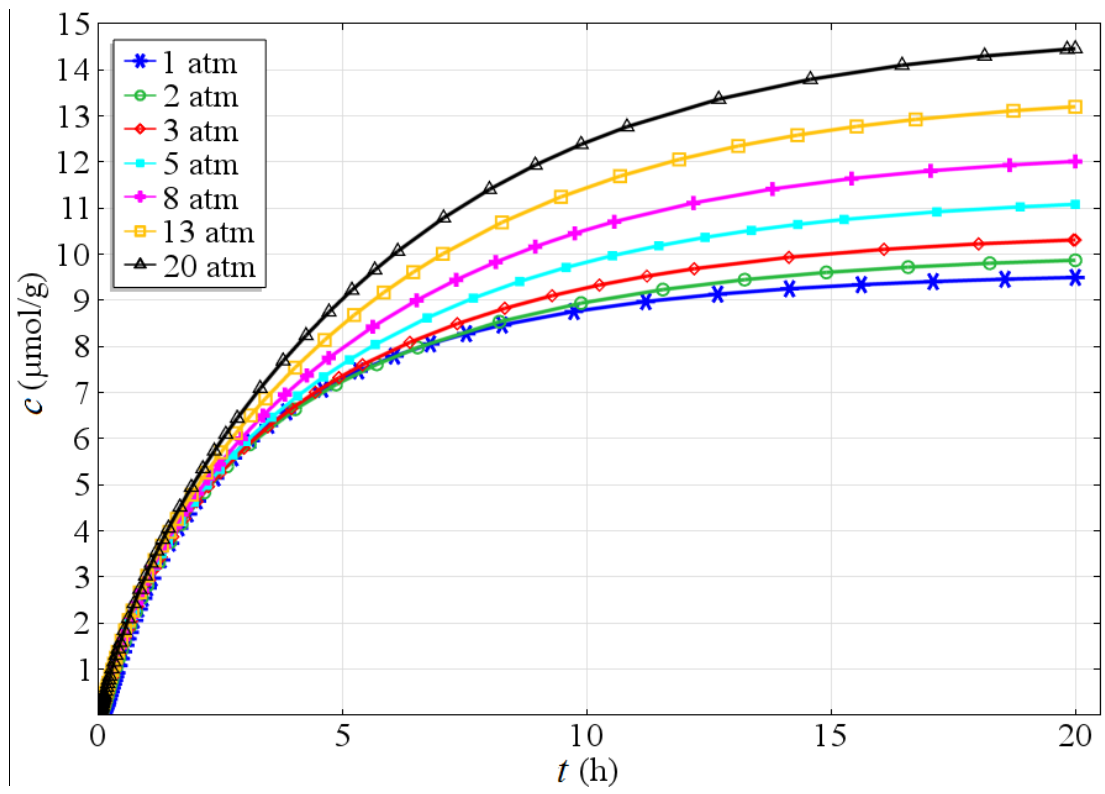


Fig.11.

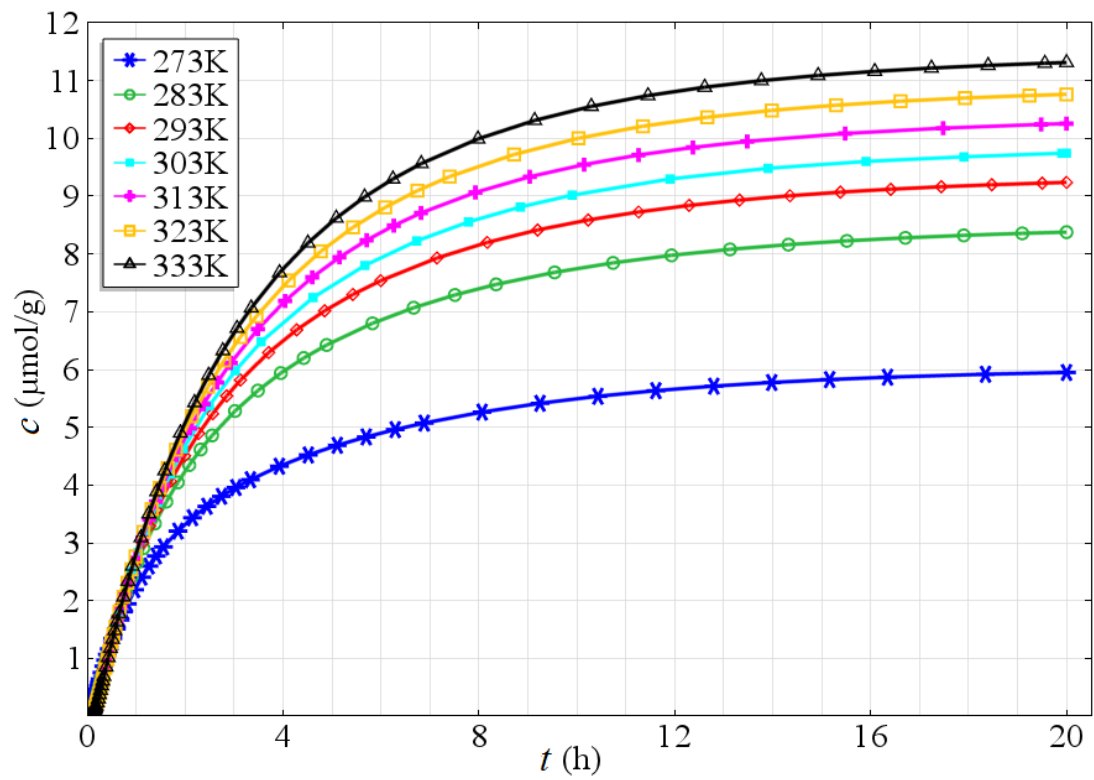
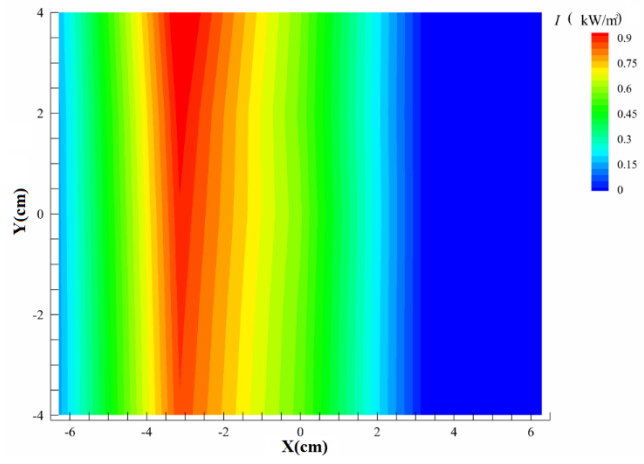
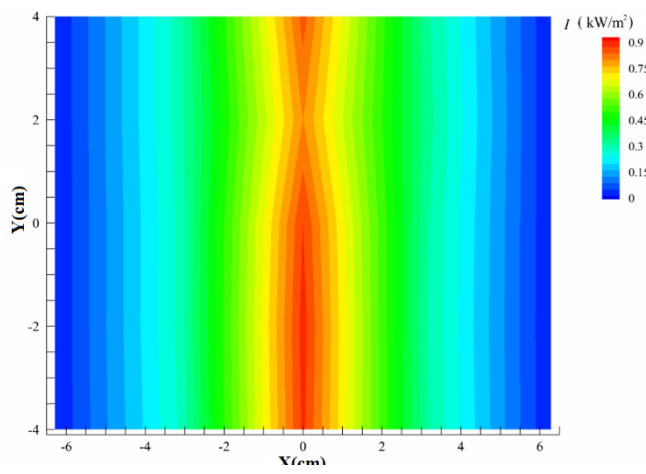


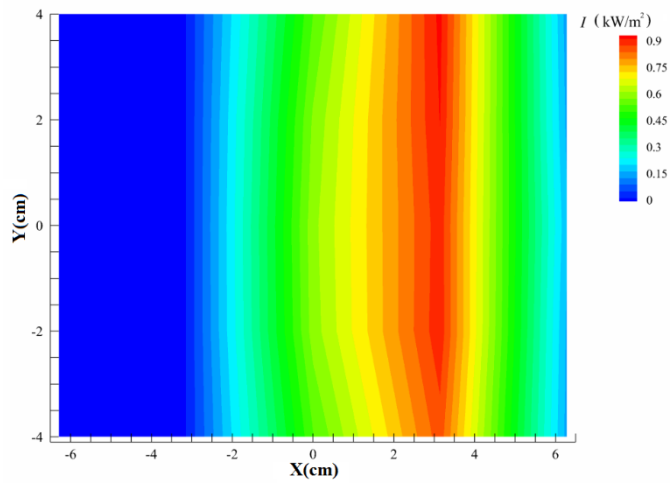
Fig.12.



(a)



(b)



(c)

Fig.13.

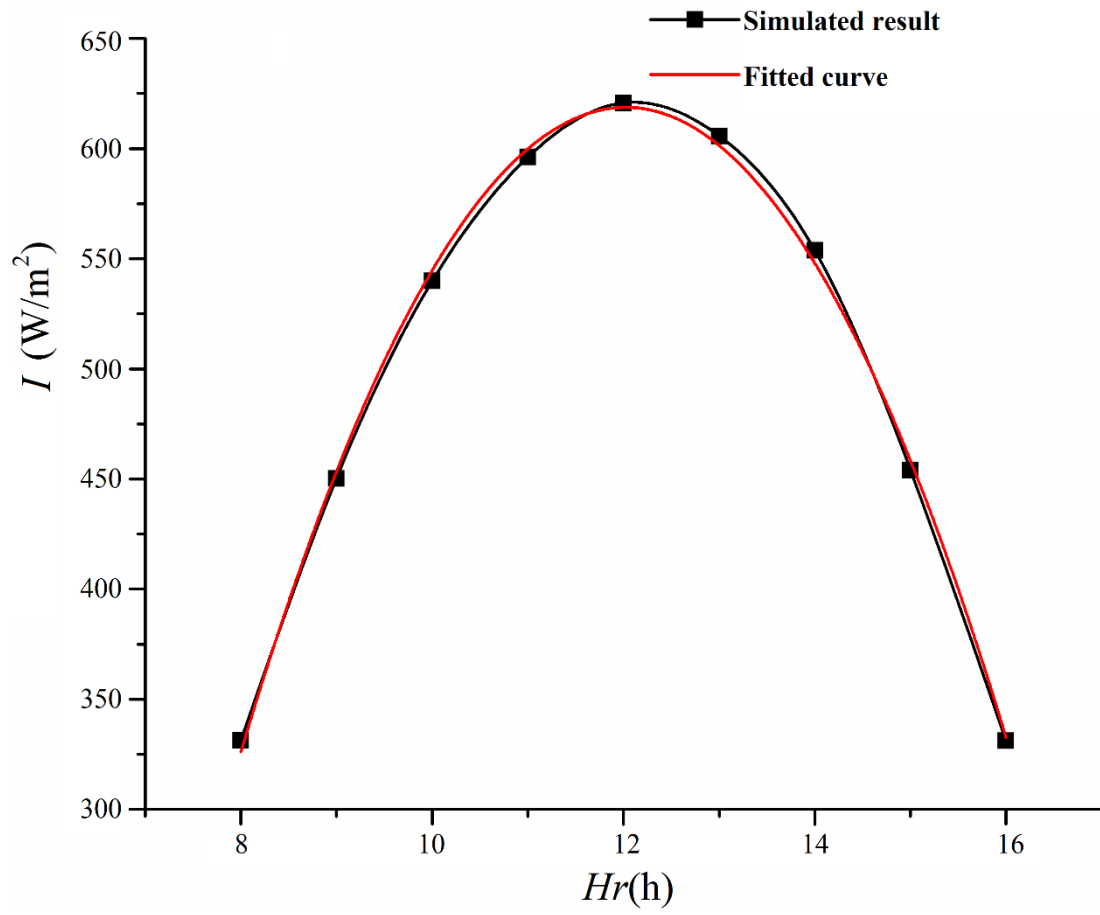


Fig.14.

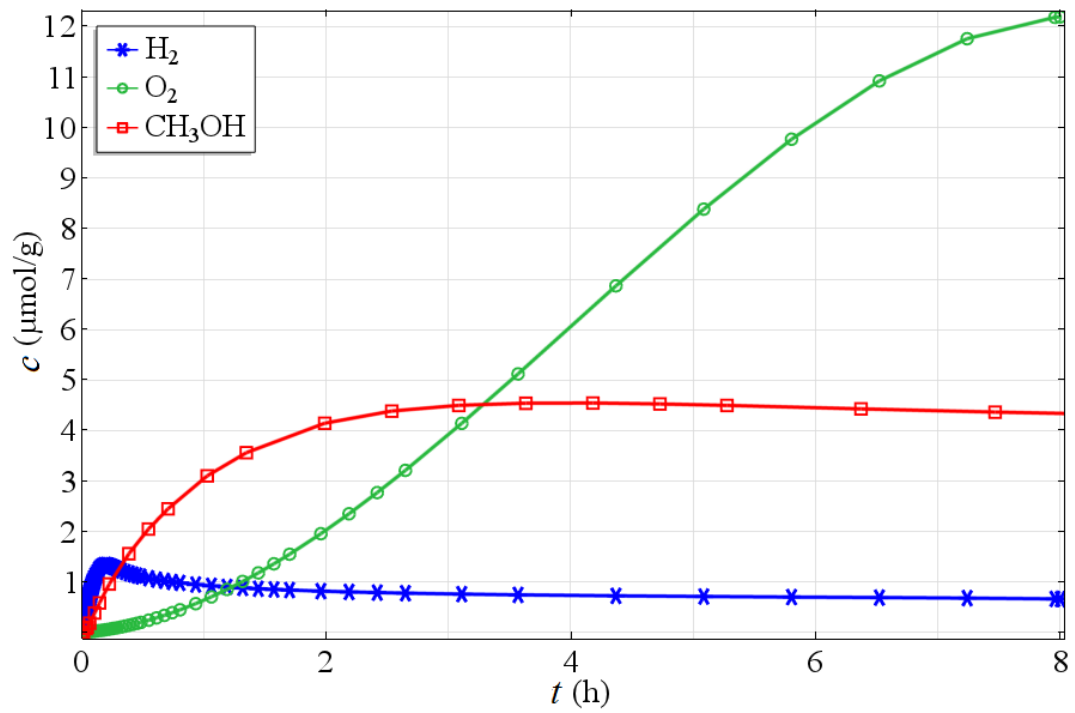


Fig.15.

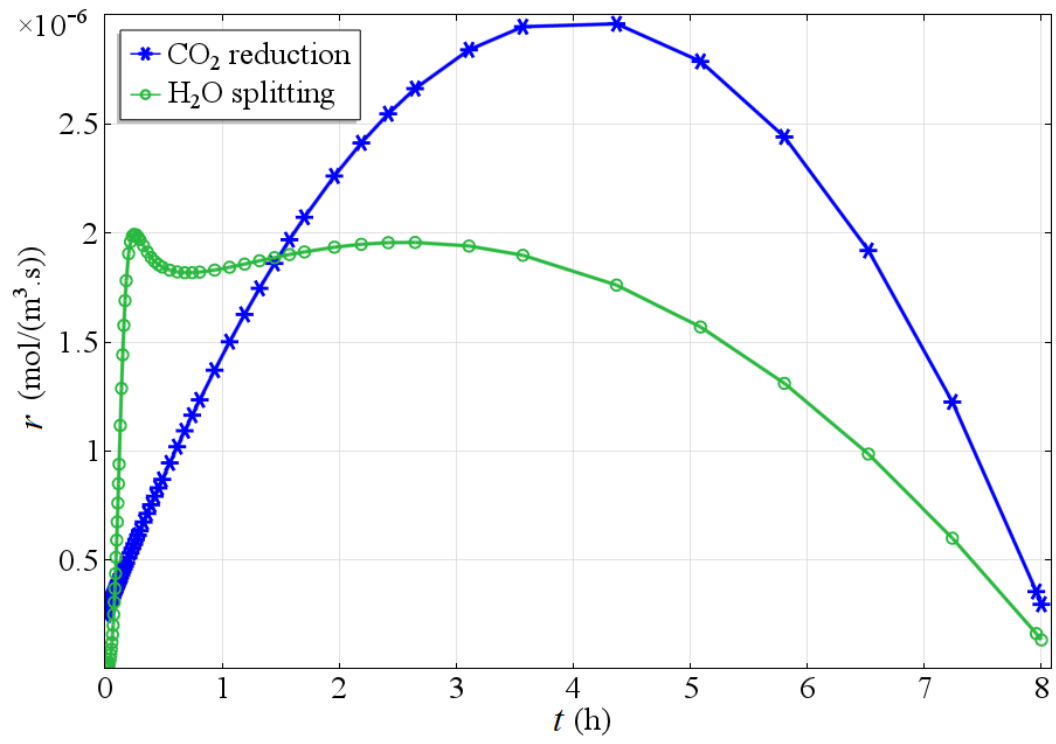


Fig.16.

## Response to Reviewers' Comments of ECM-D-16-00352

Ms. Ref. No.: ECM-D-16-00352

Title: Photocatalytic characteristics of CO<sub>2</sub> reduction by CO co-feed combined with photocatalytic water splitting  
Energy Conversion and Management

Dear Editor,

Thanks for your comments and suggestions on our manuscript. Those comments are all valuable and very helpful for revising and improving our paper, as well as important for guiding our researches. We have modified the manuscript accordingly and seriously. Detailed corrections are listed below point by point.

Reviewer #1:

The authors developed a simple two dimensional computational model to characterize the photocatalytic reduction of carbon dioxide by CO co-feed in a novel twin reactor. It has been demonstrated that photocatalytic CO<sub>2</sub> reduction combined with the water splitting is viable to produce fuels at a high yield rate. More importantly, the modeling and numerical methods are verified by previous experimental work. Therefore, the results are very interesting, which may have great potential for the applications. Therefore, I think the manuscript could be accepted after the following minor issues should be addressed carefully:

1. Some typing errors should be revised carefully throughout the manuscript. For example, Line 42 on Page 6, the number in "CO<sub>2</sub>" should be the form of subscript

**Reply:** Thanks for the reviewer's comments. We have carefully checked the spelling and grammar throughout the manuscript, and corrected all the mistakes to make sure our paper more idiomatic and acceptable.

2. The following title can be referenced: "Photocatalytic reduction of CO<sub>2</sub> by CO co-feed combined with photocatalytic water splitting in a novel twin reactor"

**Reply:** Thanks for the reviewer's comment. The proposed title is more suitable and helpful, and we have changed as the reviewer's comment in the revised manuscript.

3. Some figures can be combined together.

**Reply:** Thanks for the reviewer's suggestions. In this manuscript, some figures may contain only one curve and some points with insufficient information. We try to combine these figures together in the revised manuscript, so that more information can be presented in one figure. For example, Figs. 13, 14 and 15 have been combined to one figure, and the solar scatter plots have been deleted.

Reviewer #2:

The results provided theoretically using the proposed model is very much away from those to be produced in real experiments. The original results published for hydrogen

generation using this twin-reactor system do not provide the sufficient basis for that reaction to happen in a two-compartment cells and why the hydrogen ions should travel from water splitting compartment to CO<sub>2</sub> reducing compartment. This manuscript does not provide the essential information to make use of the information presented in this manuscript.

**Reply:** Thanks for the reviewer's comments, which can make this article more comprehensive and logical. Some theoretical basis for the reaction happening in a two-compartment cell and why the hydrogen ions should travel from water splitting compartment to CO<sub>2</sub> reducing compartment have been supplemented to the revised manuscript.

1. Why do the reactions happen in a two-compartment cell?

**Reply:** In 1987, Graetzel et al.[1] reported that with the help of TiO<sub>2</sub> nanoparticles catalyst, CH<sub>4</sub> was produced from the gas mixture of H<sub>2</sub> and CO<sub>2</sub> with the production rate of about 116μL/h. In 2007, Lo et al.[2] confirmed that the CO<sub>2</sub> photoreduction was improved by a mixture of H<sub>2</sub> and H<sub>2</sub>O compared with using solely H<sub>2</sub> or H<sub>2</sub>O. Many studies on CO<sub>2</sub> hydrogenation to yield organics have been reported, which provide a theoretical basis for the chemical reactions in this paper. Moreover, the conversion of CO<sub>2</sub> into hydrocarbons is feasible from the thermodynamic viewpoint. For instance, the photoreduction of CO<sub>2</sub> to produce CH<sub>3</sub>OH can be represented by five possible reactions as shown in Table. The enthalpies ( $\Delta H^0$ ) of all the five reactions are negative at room temperature, which proves that the reactions are exothermic. The Gibbs free energy ( $\Delta G^0$ ) of the reactions (1), (4) and (5) are negative, meaning that the reactions are spontaneous, equilibrium favorable. Moreover, although the  $\Delta G^0$  of the reactions (2) and (3) are positive, meaning that they are thermodynamically not spontaneous, those values are still much lower than that of water splitting ( $\Delta H^0=285.8$  kJ/mol; $\Delta G^0 = 237.1$  kJ/mol). Hence, the photocatalysts can convert photon energy into chemical energy accompanied by this slightly positive change in the Gibbs free energy.

Changes of enthalpy and Gibbs free energy in the CO<sub>2</sub> photoreduction reactions[3]

Reactions	$\Delta H^0$ (kJ/mol)	$\Delta G^0$ (kJ/mol)
(1) CO <sub>2</sub> (g)+3H <sub>2</sub> (g)→CH <sub>3</sub> OH (l) +H <sub>2</sub> O (l)	-137.8	-10.7
(2) CO(g)+CH <sub>3</sub> OH(l)→HCOOCH <sub>3</sub> (l)	-25.6	6.6
(3) CO <sub>2</sub> (g)+H <sub>2</sub> (g)+CH <sub>3</sub> OH(l)→ HCOOCH <sub>3</sub> (l)+H <sub>2</sub> O(l)	-31.8	25.8
(4) HCOOCH <sub>3</sub> (l)+2H <sub>2</sub> (g)→2CH <sub>3</sub> OH(l)	-99.7	-35.1
(5) HCOOCH <sub>3</sub> (l)+CO(g)→CH <sub>3</sub> CHO(l)+CO <sub>2</sub> (g)	-96.5	-86.7

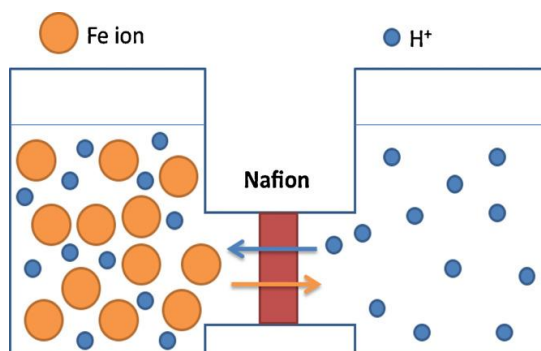
We expounded the rationality and necessity of the reaction mentioned in this paper from two points of view of past experimental research and thermodynamics, which



were added in the introduction part of the revised manuscript. More details were introduced in the references[3, 4].

2. Why should the hydrogen ions travel from water splitting compartment to CO<sub>2</sub> reducing compartment?

**Reply:** As is shown in the following figure, in the novel twin reactor, one of the key components is the modified Nafion membrane that allows not only the transport of hydrogen ions, but also the exchange of the electron mediators (Fe<sup>2+</sup>/Fe<sup>3+</sup>). The electron is shuffled via the electron mediator (Fe<sup>2+</sup>/Fe<sup>3+</sup>) through membrane. The mass and charge balances are kept concurrently by the diffusion of H<sup>+</sup> through the membrane. This information has been supplemented to the physical model of the revised manuscript. More details were introduced in the references[5].



A connected twin reactor separated by a modified Nafion membrane

Reviewer #3:

1. Please add the graphical abstract.

**Reply:** Thanks for the reviewer's comment. The graphical abstract has been provided in the revised manuscript.

2. Please consider the effects of pH in the present reactor system.

**Reply:** Thanks for the reviewer's comment. When the solution contains electrolytes, electrolyte ions will reduce the solubility of gases[6]. The Henry constant of gas in pure H<sub>2</sub>O is different from that in the electrolyte solution, hence the correction coefficient of Henry constant  $\varphi$  has been introduced in the reserach of Ueyama and Hatanaka [6]:

$$H = \varphi H^0$$

$$\lg \varphi = \sum h_i V_i \quad (1)$$

$H^0$  and  $H$  are Henry constants for the gas in the water and electrolyte, respectively.  $V_i$  is the electrolyte ionic strength calculated by Eq.(2) as follows, and  $h_i$  is the reduced coefficient of solubility caused by electrolyte, which is calculated by  $h = h^+ + h^- + h^*$ .  $h^+$ ,  $h^-$ ,  $h^*$  are influenced by the positive and negative ions, and the dissolved gases.

$$V_i = \frac{1}{2} \sum c_j z_j^2 \quad (2)$$

Where,  $c_j$  is the ion concentration,  $z_j$  is the ion valence.

The electrolytes in the system are  $H^+$ ,  $Fe^{2+}$ ,  $Fe^{3+}$ ,  $Cl^-$  and  $SO_4^{2-}$  according to the related experiments. As the physical model introduced above, the pH which has an impact on the gas dissolution process, is set as 2.6 (adjusted by adding sulfuric acid) of the solution. And in this work,  $H^+$  is considered with the same electrolyte as  $Fe^{2+}$ ,  $Fe^{3+}$  and  $Cl^-$ , so the pH effects on the solubility of  $CO_2$  are illustrated by correction coefficient  $\varphi$ . The aforementioned information has been supplemented to the mass transfer model in the revised manuscript. More details were introduced in the reference [6].

Additional Comment from the Editor: The English language used in this manuscript is rather weak. Can the authors get this manuscript to be proof read by a colleague that is a native English speaker or perhaps with the help of professional English editing?

**Reply:** We have done our best to revise this paper in detail and correct some languages throughout the manuscript to make sure our paper more idiomatic and acceptable. Thanks for the comments from the Editor.

### References

- [1] Thampi KR, Kiwi J, Gratzel M. Methanation and photo-methanation of carbon dioxide at room temperature and atmospheric pressure. *Nature* 1987;327:506-8.
- [2] Lo C-C, Hung C-H, Yuan C-S, Wu J-F. Photoreduction of carbon dioxide with  $H_2$  and  $H_2O$  over  $TiO_2$  and  $ZrO_2$  in a circulated photocatalytic reactor. *Sol Energ Mat Sol C* 2007;91:1765-74.
- [3] Cheng Y-H, Nguyen V-H, Chan H-Y, Wu JCS, Wang W-H. Photo-enhanced hydrogenation of  $CO_2$  to mimic photosynthesis by  $CO$  co-feed in a novel twin reactor. *Appl Energ* 2015;147:318-24.
- [4] Lee W-H, Liao C-H, Tsai M-F, Huang C-W, Wu JCS. A novel twin reactor for  $CO_2$  photoreduction to mimic artificial photosynthesis. *Applied Catalysis B: Environmental* 2013;132-133:445-51.
- [5] Yu S-C, Huang C-W, Liao C-H, Wu JCS, Chang S-T, Chen K-H. A novel membrane reactor for separating hydrogen and oxygen in photocatalytic water splitting. *J Membrane Sci* 2011;382:291-9.
- [6] Ueyama K, Hatanaka J. Salt effect on solubility of nonelectrolyte gases and liquids. *Chem Eng Sci* 1982;37:790-2.

1                    **Photocatalytic reduction of CO<sub>2</sub> by CO co-feed**  
2                    **combined with photocatalytic water splitting in a novel**  
3                    **twin reactor**

4                    Shang Li<sup>1</sup>, Lijun Yang\*<sup>1</sup>, Oluwafunmilola Ola\*<sup>2</sup>, Mercedes Maroto-Valer<sup>2</sup>, Xiaoze  
5                    Du<sup>1</sup>, Yongping Yang<sup>1</sup>

6                    *1. Key Laboratory of Condition Monitoring and Control for Power Plant Equipments of*  
7                    *Ministry of Education,*  
8                    *School of Energy Power and Mechanical Engineering, North China Electric Power*  
9                    *University, Beijing 102206, China*

10                    *2. Centre for Innovation in Carbon Capture and Storage (CICCS),*  
11                    *School of Engineering and Physical Sciences, Heriot-Watt University, Edinburgh, EH14 4AS,*  
12                    *UK*

13  
14                    **ABSTRACT**

15                    **As a promising way to control greenhouse gas emission and alleviate global energy**  
16                    **shortage, photocatalytic reduction of carbon dioxide attracts more attentions in recent**  
17                    **years since it can produce fuels efficiently with the combination of H<sub>2</sub> through water**  
18                    **splitting. In this work, a computational model which characterizes the photocatalytic**

---

\* Corresponding author: Lijun Yang. Tel: +86 10 61773373; Fax: +86 10 61773877. *E-mail address:*

[yanglj@ncepu.edu.cn](mailto:yanglj@ncepu.edu.cn)

Oluwafunmilola Ola. Tel: +44 (0) 131 451 4737. *E-mail address:* [O.O.Ola@hw.ac.uk](mailto:O.O.Ola@hw.ac.uk)

19 reduction of carbon dioxide by CO co-feed in a novel twin reactor is developed with  
20 three subsidiaries of chemical reaction kinetics, gas-liquid mass transfer, and transient  
21 sun light intensity distribution. Thanks to previous experimental work as the reliable  
22 verification for the numerical simulation, the variations of the CH<sub>3</sub>OH concentration  
23 with the CO/CO<sub>2</sub> ratio of gas mixture, pressure and temperature are obtained and  
24 analyzed. The results show that the carbon in CO can form CH<sub>3</sub>OH directly, however  
25 the excessive CO will react with HCOOCH<sub>3</sub> to form CH<sub>3</sub>CHO, which results in a  
26 reduced CH<sub>3</sub>OH concentration. Besides, the CH<sub>3</sub>OH concentration subsequently  
27 increases as the temperature and pressure increase, and the CH<sub>3</sub>OH product and  
28 reaction rate vary widely with time due to the changing sun light intensity during the  
29 day.

30 **Key words:** twin reactor, CO<sub>2</sub> reduction, water splitting, photocatalysis, methanol, sun  
31 light intensity

32

33 **Nomenclature**

<i>c</i>	concentration	$\text{mol}\cdot\text{m}^{-3}$
<i>D</i>	diffusion coefficient	$\text{m}^2\cdot\text{s}^{-1}$
<i>I</i>	light intensity	$\text{W}\cdot\text{m}^{-2}$
<i>k</i>	kinetic rate constant	$\text{m}^4\cdot\text{s}^{-1}\cdot\text{mol}^{-2}$
<i>L</i>	reactor height	mm
<i>M</i>	molecular weight	$\text{g}\cdot\text{mol}^{-1}$
<i>p</i>	pressure	Pa
<i>r</i>	reaction rate	$\text{mol}\cdot\text{m}^{-3}\cdot\text{s}^{-1}$
<i>R</i>	radius	mm
<i>t</i>	time	s
<i>T</i>	temperature	K
<i>V</i>	molar volume	$\text{cm}^3\cdot\text{mol}^{-1}$
<i>N</i>	mass transfer rate	$\text{mol}\cdot\text{m}^{-2}\cdot\text{s}^{-1}$
<i>K</i>	mass transfer coefficient	$\text{s}\cdot\text{mol}\cdot\text{kg}^{-1}\cdot\text{m}^{-1}$
<i>H</i>	Henry constant	$\text{Pa}\cdot\text{m}^3\cdot\text{mol}^{-1}$
<i>V</i>	ionic strength	$\text{mol}\cdot\text{m}^{-3}$
<i>E</i>	electric field intensity	$\text{V}\cdot\text{m}^{-1}$
<i>z</i>	ionic valence	
<i>h</i>	solubility coefficient	

$X$	sun unit vector
$Y$	sun unit vector
$Z$	sun unit vector
$m$	energy coefficient
$Rf$	reflectivity
$Tr$	transmissivity
$Ab$	absorptivity
$n$	refractivity
$L$	latitude
$Day$	day of year
$Hr$	local solar time

34 Greek letters

$\delta$	film thickness	mm
$\nu$	chemical calculated number	
$\rho$	density	$\text{kg}\cdot\text{m}^{-3}$
$\varphi$	correction coefficient of Henry constant	
$\psi$	proportional coefficient	S
$\omega$	hour angle	
$\delta$	declination	
$\alpha$	solar altitude	

$\gamma$  solar azimuth

Subscript and superscript

$A$  material

$B$  material

$F$  material

$O$  material

$a$  chemical calculated number

$b$  chemical calculated number

$f$  chemical calculated number

$o$  chemical calculated number

$L$  liquid phase

$G$  gas phase

$j$  number of reaction

$i$  number of reactant or ion

$m$  interface

$s$  sun

$x$  carbon source from carbon dioxide

$y$  carbon source from carbon monoxide

## 36 1. Introduction

37 Since fossil fuels dominate more than 85% of energy consumption all over the  
38 world at the status quo, the rapid depletion has concentrated the growing concerns on  
39 the global energy crisis and an increasing carbon dioxide (CO<sub>2</sub>) emission, which  
40 motivates researchers exploring the CO<sub>2</sub> reduction and utilization[1-5]. In the past  
41 decades, the conversion of CO<sub>2</sub> to value-added chemicals and renewable fuels has  
42 been investigated by various methods such as thermal conversion, plasma conversion  
43 and photoreduction[6]. Among various technologies of energy conservation and  
44 emission reduction[7-9], the photocatalytic CO<sub>2</sub> reduction into hydrocarbon fuels is a  
45 promising and eco-friendly method to prevent the increasing of greenhouse gases and  
46 depletion of fossil resources[5, 10, 11]. Since the first demonstration in 1979 by Inoue  
47 et al.[12], the approach of photocatalytic CO<sub>2</sub> reduction has received increasing  
48 attentions [13-15].

49 For the traditional photo-technology, CO<sub>2</sub> can be reduced by water (H<sub>2</sub>O) to CO,  
50 CH<sub>4</sub>, HCOOH, HCHO and CH<sub>3</sub>OH over semiconductor materials such as TiO<sub>2</sub>, ZnO,  
51 WO<sub>3</sub>, SiC, CdS, and GaP[16-19]. However, CO<sub>2</sub> is hardly reducible since H<sub>2</sub>O is a  
52 weak reductant. What's worse, the hydrocarbon products can be easily oxidized,  
53 which results in a low output ratio of hydrocarbons unexpectedly. In recent years, the  
54 technology of hydrogen production from photocatalytic water splitting has achieved a  
55 rapid progress [20, 21]. In 1987, Thampi et al.[22] reported that under the action of



56 TiO<sub>2</sub> nanoparticles catalyst, CH<sub>4</sub> was produced from the gas mixture of H<sub>2</sub> and CO<sub>2</sub>  
57 with the production rate of about 116μL/h. And in 2007, Lo et al.[23] confirmed that  
58 the CO<sub>2</sub> photoreduction was improved by a mixture of H<sub>2</sub> and H<sub>2</sub>O compared with  
59 that using solely H<sub>2</sub> or H<sub>2</sub>O. Many studies on CO<sub>2</sub> hydrogenation to yield organics  
60 have been reported, which provide a theoretical basis for the chemical reactions of  
61 photocatalytic reduction of carbon dioxide with the combination of H<sub>2</sub> through water  
62 splitting. Twin reactor system can combine the water splitting with CO<sub>2</sub> reduction  
63 because the reducibility of H<sub>2</sub> is better than H<sub>2</sub>O, so the CO<sub>2</sub> photo-reduction with H<sub>2</sub>  
64 through water splitting is more viable to produce fuels at a higher yield rate [11], as it  
65 has also been experimentally investigated in previous studies [24-26].

66 Twin reactor usually consists of two components for photocatalytic water splitting  
67 and photocatalytic CO<sub>2</sub> reduction, which are divided by an ion exchange unit. H<sup>+</sup> from  
68 water splitting is directly used to perform the CO<sub>2</sub> photo-hydrogenation with the  
69 participation of the light at the room temperature. The conversion of CO<sub>2</sub> into  
70 hydrocarbons is feasible from the thermodynamic viewpoint. For instance, the  
71 photoreduction of CO<sub>2</sub> to produce CH<sub>3</sub>OH can be represented by five possible  
72 reactions as listed in Table 1. The enthalpies ( $\Delta H^0$ ) of all the five reactions are  
73 negative at room temperature, which proves that the reactions are exothermic. The  
74 Gibbs free energies ( $\Delta G^0$ ) of the reactions (1), (4) and (5) are negative, meaning that  
75 the reactions are spontaneous, equilibrium favorable. Moreover, although the  $\Delta G^0$  of

76 the reactions (2) and (3) are positive, meaning that they are thermodynamically not  
77 spontaneous, those values are still much lower than that of water splitting ( $\Delta H^0 =$   
78  $285.8 \text{ kJ/mol}$ ;  $\Delta G^0 = 237.1 \text{ kJ/mol}$ ). Hence, the photocatalysts can convert photon  
79 energy into chemical energy accompanied by this slightly positive change in the  
80 Gibbs free energy[25]. The combination of photocatalytic  $\text{CO}_2$  reduction with water  
81 splitting in the twin reactor presents a better performance than the  $\text{CO}_2$  reduction by  
82  $\text{H}_2\text{O}$ , and prevents the oxygenation of hydrocarbon products.

83 CO was considered as a co-feed to enhance the production efficiency of  $\text{CH}_3\text{OH}$ ,  
84 and a certain amount of CO mixed with the reaction gases can promote  $\text{CH}_3\text{OH}$   
85 production under the same conditions because CO is thermodynamically more  
86 favorable as compared to the  $\text{CO}_2$ . However, due to the limitation of experimental  
87 conditions, it did not address how the CO affects the methanol production. When the  
88 reaction gas is pure CO,  $\text{CH}_3\text{OH}$  cannot be produced, which was not clarified in detail  
89 by previous studies. Other operating conditions such as the pressure and temperature  
90 in the twin reactor, which are crucial to the photocatalytic reduction of  $\text{CO}_2$ , were also  
91 not deeply investigated. What's more, there are few related studies about the sun light  
92 effect on the photocatalytic  $\text{CO}_2$  reduction in twin reactors, since most of the  
93 experiments were carried out in an indoor environment with the artificial light instead  
94 of natural sources. Adopting the software SOLTRACE in this work, the principle of  
95 CO effect on the  $\text{CH}_3\text{OH}$  production and the impacts of operation conditions on the

96 conversion efficiency from CO<sub>2</sub> to CH<sub>3</sub>OH in the twin reactor are deeply investigated  
97 by unveiling the sun light distribution as well as the photocatalytic CO<sub>2</sub> reduction  
98 mechanism. It can be of benefit to the optimal design and operation of twin reactors  
99 by investigating the photocatalytic reduction of CO<sub>2</sub> by CO co-feed combined with  
100 photocatalytic water splitting.

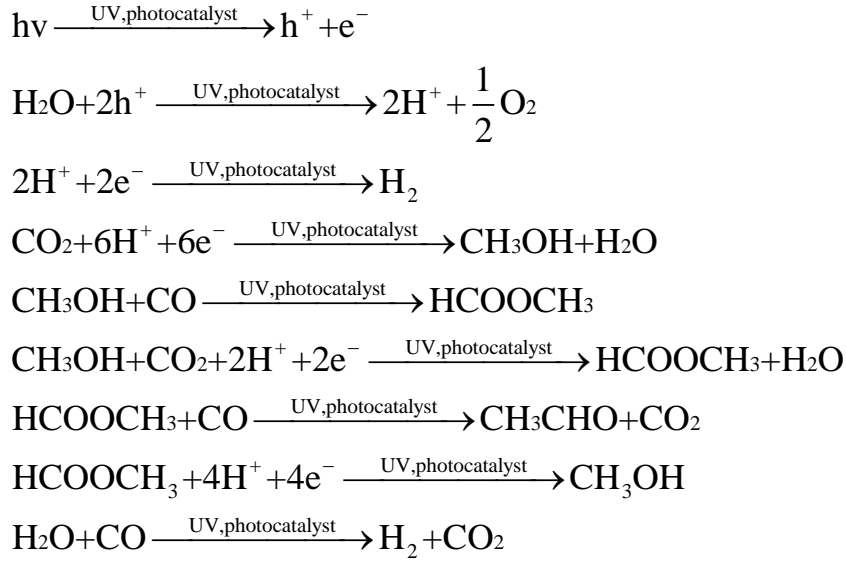
## 101 **2. Model development**

### 102 *2.1 Physical model*

103 The physical model of the twin reactor can be simplified as Fig.1, which has been  
104 described in detail and experimentally investigated in some of the photocatalytic  
105 characteristics [24-26]. With a Nafion membrane for segregation, 0.15 g of  
106 Pt/CuAlGaO<sub>4</sub> and 0.15 g of Pt/SrTiO<sub>3</sub>:Rh in 2mM FeCl<sub>2</sub> were placed in the CO<sub>2</sub>  
107 reduction reactor solution, while 0.30 g of commercial WO<sub>3</sub> in 2mM FeCl<sub>3</sub> solution  
108 were put in the water splitting reactor. In the novel twin reactor, one of the key  
109 components is the modified Nafion membrane that allows not only the transport of  
110 hydrogen ions, but also the exchange of the electron mediators (Fe<sup>2+</sup>/Fe<sup>3+</sup>). The  
111 electron is shuffled via the electron mediator (Fe<sup>2+</sup>/Fe<sup>3+</sup>) through membrane. The mass  
112 and charge balances are kept concurrently by the diffusion of H<sup>+</sup> through the  
113 membrane[27]. The pH of the solution is 2.6 (adjusted by adding sulfuric acid) and  
114 the volume of each compartment of the twin reactor is 225 mL. The H<sup>+</sup> generated by  
115 H<sub>2</sub>O splitting goes through the Nafion membrane and forms H<sub>2</sub>, which reacts with

116 CO<sub>2</sub> to produce organic compounds. In this work, the multi-physics coupling software  
117 is used to simulate the above process with the following necessary assumptions, based  
118 on which the model can be well simplified without introducing unexpected errors.

- 119 1) Since the driving force of the photoreaction originates from the light energy  
120 but not the thermal energy (i.e. molecular kinetics at high temperatures) in  
121 the traditional catalytic reaction, most photoreactions work at about the room  
122 temperature. As a result, the thermodynamic effects of the reactions at  
123 various temperatures can be ignored because of the extremely weak  
124 provoking energy in the photocatalysis.
- 125 2) Thanks to the magnetic stirrer in the experiment for the uniform catalyst  
126 distribution in the solution, the reaction rate is assumed to be a function of  
127 the time rather than the location.
- 128 3) Since CO and CO<sub>2</sub> are free from liquidation at the room temperature and  
129 atmospheric pressure, the mixture can be seen as an ideal gas so as to easily  
130 calculate the partial pressure based on the ideal gas equation. Besides, the  
131 chemical process at the interface of the gas and liquid is not taken into  
132 account.
- 133 4) The effects of the catalyst surface topography, concentration, band gap, and  
134 absorption or desorption existing on the surface of catalyst particles are  
135 ignored.
- 136 5) The chemical reactions in the twin reactor take the following forms, which  
137 are regarded as single step reactions [25].



138

139 With the aforementioned equations, the inferior middle processes are reasonably  
 140 ignored for clearly uncovering the chemical mechanism from the reactants to  
 141 products.

## 142 2.2 Chemical reaction kinetics model

143 For the chemical reaction  $aA + bB = fF + oO$  under constant volume conditions, the  
 144 reaction rate can be expressed as follows:

$$r = -\frac{1}{a} \frac{dc_A}{dt} = -\frac{1}{b} \frac{dc_B}{dt} = \frac{1}{f} \frac{dc_F}{dt} = \frac{1}{o} \frac{dc_o}{dt} \quad (1)$$

145

146 When the reaction is an elementary reaction, the above formula can be written as:

$$r = k c_A^a c_B^b \quad (2)$$

147

148 Where  $k$  is the reaction rate constant.

149 In previous studies, it has been noticed that the photocatalytic reaction rate follows  
 150 a power law expression of the light intensity[28]. By experimental studies, Herrmann  
 151 suggested that the reaction rate is proportional to the light intensity at low light

152 intensities, and when the light intensity is high, the reaction rate is proportional to the  
 153 square root of the light intensity [29]. According to the work of Wang et al., the  
 154 photocatalytic reaction rate was considered proportional to the n-th power of the light  
 155 intensity[17], where n is a factor to describe the reaction rate dependency on light  
 156 irradiance. The higher n value of the reactor represents that the incident photons can  
 157 be more effectively utilized for photocatalytic reactions[30]. Therefore, the reversible  
 158 catalytic reaction rate equation can be written with the following form:

$$159 \quad r_j = I^m \left( k_j \prod_{i=1}^{\nu_i} c_i^{\nu_i} \right) \quad (3)$$

160 Where  $r_j$  is the reaction rate,  $k_j$  is the kinetic rate constant,  $c_i$  is the concentration,  $\nu_i$  is  
 161 the chemical calculated number,  $I$  is the light intensity,  $m$  is the energy coefficient.

### 162 2.3 Mass transfer model

163 Many physical models, such as two-film, Higbie penetration, Danckwerts surface  
 164 renewal and turbulent mass transfer theories, all formerly clarified the process of  
 165 gas-liquid mass transfer. With two-film theory adopted in this work, a static film on  
 166 each side of the gas-liquid interface is assumed as the gas membrane and liquid  
 167 membrane. Moreover, the mass transfer rate of gas-liquid interphase depends on the  
 168 diffusion rate of gas and liquid membranes.

$$169 \quad N = \frac{D_G}{RT\delta_G}(p_G - p_m) = \frac{D_L}{\delta_L}(c_m - c_L) \quad (4)$$

170 Where  $N$  is the mass transfer rate,  $D_G$  and  $D_L$  are the diffusion coefficients of  
 171 components in gases and liquids respectively.  $\delta_G$  and  $\delta_L$  are the gas and liquid film  
 172 thicknesses, which are about 0.1mm according to the experiment.  $c_m$  and  $p_m$  represent

173 the concentration and partial pressure at the interface of the membranes.  $p_G$  is the  
 174 partial pressure of components in gas phase while  $c_L$  is the concentration of  
 175 components in liquid phase.  $R$  is the perfect gas constant and  $T$  is temperature.

176 By eliminating the interface concentration  $c_m$  and the interface pressure  $p_m$  in the  
 177 above formula, the mass transfer rate is expressed as:

$$178 \quad N = K_G(p_G - p^*) = K_L(c^* - c_L) \quad (5)$$

$$p^* = Hc_L; c^* = \frac{p_G}{H}$$

179 Where  $p^*$  is the partial pressure in equilibrium with  $c_L$ ,  $c^*$  is the concentration in  
 180 equilibrium with  $p_G$ ,  $H$  is the Henry constant,  $K_G$  and  $K_L$  represent gas phase total  
 181 mass transfer coefficient and liquid phase total mass transfer coefficient:

$$182 \quad K_G = \frac{1}{\frac{RT\delta_G}{D_G} + \frac{H\delta_L}{D_L}} \quad (6)$$

$$K_L = \frac{1}{\frac{RT\delta_G}{HD_G} + \frac{\delta_L}{D_L}}$$

183 When the solution contains electrolytes, electrolyte ions will reduce the solubility  
 184 of gases[31]. The Henry constant of gas in pure H<sub>2</sub>O is different from that in the  
 185 electrolyte solution, hence the correction coefficient of Henry constant  $\varphi$  has been  
 186 introduced in the research of Ueyama and Hatanaka [31]:

$$187 \quad H = \varphi H^0$$

$$\lg \varphi = \sum h_i V_i \quad (7)$$

188  $H^0$  and  $H$  are Henry constants for the gas in the water and electrolyte, respectively.  $V_i$   
 189 is the electrolyte ionic strength calculated by Eq.(8) as followed, and  $h_i$  is the reduced  
 190 coefficient of solubility caused by electrolyte, which is calculated by  $h = h^+ + h^- + h^*$ .  $h^+$ ,

191  $h^-$ ,  $h^*$  are influenced by the positive and negative ions, and the dissolved gases.

192 
$$V_i = \frac{1}{2} \sum c_j z_j^2 \quad (8)$$

193 Where,  $c_j$  is the ion concentration,  $z_j$  is the ion valence.

194 The electrolytes in the system are  $H^+$ ,  $Fe^{2+}$ ,  $Fe^{3+}$ ,  $Cl^-$  and  $SO_4^{2-}$  according to the  
195 related experiments.

196 As the physical model introduced above, the pH which has an impact on gas  
197 dissolution process, is set as 2.6 (adjusted by adding sulfuric acid) of the solution. In  
198 this work,  $H^+$  is considered with the same electrolyte as  $Fe^{2+}$ ,  $Fe^{3+}$  and  $Cl^-$ , so the pH  
199 effects on the solubility of  $CO_2$  are illustrated by the correction coefficient  $\varphi$ .

200 Diffusion coefficients of  $CO_2$  in the mixed gas and the solution can be calculated  
201 according to the following formula [32, 33]:

202 
$$\log D_L = -8.1764 + \frac{712.5}{T} - \frac{2.591 \times 10^5}{T^2}$$
$$D_G = \frac{435.7T^{3/2}}{P(V_A^{1/3} + V_B^{1/3})^2} \sqrt{\frac{1}{M_A} + \frac{1}{M_B}} \quad (9)$$

203 Where  $A$ ,  $B$  are two kinds of gas in the reactor,  $p$  is the total pressure,  $T$  is the  
204 temperature in the reactor and equals to 293K and  $M$  is the molar mass of the gas.  $V$  is  
205 the molar volume with the constant of 22.4 L/mol, due to the fact that the  $CO_2$  and  
206 CO are ideal gases in the reactor.

#### 207 2.4 Sun light model

208 Since the photocatalytic  $CO_2$  reduction cannot work without sun light input in the  
209 twin reactor, most of the experiments were carried out in an indoor environment with



210 the artificial light for substitute. Unfortunately, few related studies emphasized on the  
 211 sun light distribution. While in this work, with the software SOLTRACE based on the  
 212 theory from Spencer and Murty[34], the sun light distribution is obtained and  
 213 analyzed for its optical performance, which is highly affected by the light diffusion as  
 214 a key factor that can be predicted by setting up accurate parameters in SOLTRACE.

215 The angular intensity distribution and position of the light together define the  
 216 natural energy source, and in Beijing (northern latitude  $40^{\circ}5'$ , east longitude  $116^{\circ}16'$ ),  
 217 the 200nd day during the year with the maximum sun declination is usually selected  
 218 for sunlight acquisition. Although the Gaussian and Pillbox apparatus can together  
 219 determine the sun shape, it cannot represent the real sunlight condition due to the  
 220 complex atmospheric factors as well as inevitable errors from the optical equipment.  
 221 Since the Gaussian leads to an obviously higher error than pillbox, it is dismissed in  
 222 this paper. The sunlight position ( $X_s, Y_s, Z_s$ ) can be calculated by latitude ( $L$ : +N, -S),  
 223 day of year ( $Day$ ) and local solar time ( $Hr$ ) as follows.

$$\begin{aligned}
 X_s &= \sin\gamma_s \cos\alpha_s \\
 Y_s &= \sin\alpha_s \\
 Z_s &= \cos\gamma_s \cos\alpha_s
 \end{aligned}
 \tag{10}$$

225 Where  $\alpha_s$  is the solar altitude and  $\gamma_s$  is the solar azimuth, which can be obtained by  
 226 the following form.

$$\begin{aligned}
 \alpha_s &= \sin^{-1}(\cos L \cos \delta \cos \omega + \sin L \sin \delta) \\
 \gamma_s &= \cos^{-1}\left[\frac{\sin \alpha_s \sin L - \sin \delta}{\cos \alpha_s \cos L}\right]
 \end{aligned}
 \tag{11}$$

228 Where  $\omega$  is the hour angle,  $\omega=15(Hr-12)$ .  $Hr$  is the local solar time, which is set  
229 from 8:00 to 16:00.  $\delta$  is the declination,  $\delta= 23.45\sin (360(284+Day)/365)$ .  $Day$  is set  
230 as 200, implying the maximum sun declination, and  $L$  as  $40^{\circ}5'$ , representing the  
231 latitude of Beijing.

232 Optical properties can be obtained from the movement of rays when they hit the  
233 surfaces. According to the experiment of Chen et al.[25], the body of the reactor is  
234 made of glass which can be treated as fully transparent, so the absorptivity is set to 0.  
235 The reflectivity and the transmissivity of the twin reactor can be obtained by the  
236 following forms.

$$237 \quad Rf = \frac{(n_1 - n_2)}{(n_1 + n_2)} \quad (12)$$
$$Rf + Tr = 1$$

238 Where  $Rf$  is reflectivity,  $Tr$  is transmissivity,  $n$  is refractivity that can be obtained  
239 from the relevant literature. In addition, due to the effect of the element surface shape  
240 on ray direction, surface slope error and surface specularly can be included, which  
241 together affect ray interaction at the surface in a combined form as follows

$$242 \quad \sigma_{\text{optical}} = (4\sigma_{\text{slope}}^2 + \sigma_{\text{specularity}}^2)^{1/2} \quad (13)$$

243 Where  $\sigma_{\text{optical}}$  is the comprehensive factor,  $\sigma_{\text{slope}}$  means the surface slope error, and  
244  $\sigma_{\text{specularity}}$  represents the surface specularly error.

## 245 2.5 Evaluation of model parameters

246 The variables and constants used in this model are listed in Table 2 with specific

247 meanings. The geometric parameters were obtained based on the real dimensions of  
248 the reactor and the kinetics parameters by fitting the experimental data. Since the  
249 reaction rate constant is not known in advance, should it be assumed at first. The  
250 CH<sub>3</sub>OH production can be numerically calculated and then compared with the  
251 experimental data. If the error is not within the allowed value, should the reaction rate  
252 constant as aforementioned above be reassumed for expecting results. The mass  
253 transfer parameters were estimated by Eqs.(7-9) with the initials referring to the  
254 experiment, and the sun position parameters by Eqs.(10) and (11) with the optical  
255 variables determined by Eqs.(12) and (13).

## 256 *2.6 Validation of numerical results*

257 Adopting the reaction engineering and diluted species transport modules, Eqs.(2-3)  
258 and (4-9) can be solved respectively by the commercial software COMSOL. Besides,  
259 the reaction rate can be iterated as the light intensity was taken into account by  
260 setting global variables.

261 The initial conditions with pure CO<sub>2</sub> are simulated as shown in Figs. 2 and 3. As  
262 observed, the H<sub>2</sub> concentration increases sharply at the beginning since the H<sup>+</sup>  
263 generated by water decomposition penetrates directly through the ion exchange  
264 membrane to form H<sub>2</sub>. Meanwhile, the O<sub>2</sub> concentration in the water splitting reactor  
265 also rises with a half production of H<sub>2</sub>. However as the O<sub>2</sub> increases stably, the H<sub>2</sub> in  
266 the CO<sub>2</sub> reduction reactor no longer increases and keeps at the rate of nearly

267 0.85 $\mu\text{mol/g}$ , showing that  $\text{H}_2$  already reaches a balance since it generated by water  
268 splitting transforms directly into the  $\text{CH}_3\text{OH}$  and other organic compounds. So at the  
269 beginning five hours, even the increasing rate declines gradually, the  $\text{CH}_3\text{OH}$  rises  
270 conspicuously with an average speed of 0.8  $\mu\text{mol/g/h}$ , while it then keeps almost no  
271 change with the ultimate concentration of 4 $\mu\text{mol/g}$  as shown in Fig. 3. Besides, Fig. 3  
272 shows that the average error between the simulation and experimental results is about  
273 13.12%, which is quite small. Moreover, Fig. 4 shows the concentration of methyl  
274 formate ( $\text{HCOOCH}_3$ ) and acetaldehyde ( $\text{CH}_3\text{CHO}$ ) as the two by-products during the  
275 reaction process, which reaches 1.5 $\mu\text{mol/g}$  and 0.4  $\mu\text{mol/g}$  with the average rate of  
276 0.1875  $\mu\text{mol/g/h}$  and 0.05  $\mu\text{mol/g/h}$  respectively within the 8 hours. The  $\text{CO}_2$  and  $\text{CO}$   
277 composite process is also numerically calculated with the initial partial pressure of  
278  $\text{CO}$  set in accordance with the mixing ratio of 1:10 and 1:5 respectively as shown in  
279 Figs. 5 and 6, which clearly present that the final  $\text{CH}_3\text{OH}$  concentrations are  
280 7.8  $\mu\text{mol/g}$  and 7.4 $\mu\text{mol/g}$  after 8 hours with the relative errors between the  
281 simulating and experimental results of 4.41% and 2.92% respectively.

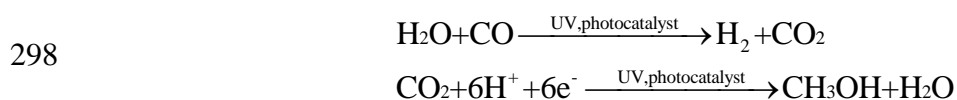
282 The comparisons show that the numerical and experimental results agree well with  
283 each other, so the modelling approach is reliable and accurate enough to predict the  
284 photocatalytic  $\text{CO}_2$  reduction performances in the twin reactor system. Since the  
285 photocatalytic  $\text{CO}_2$  reduction gradually recedes with an ultimately constant  $\text{CH}_3\text{OH}$   
286 concentration, the working conditions of the twin reactor system can be optimized by

287 means of numerical simulations.

### 288 **3. Results and discussion**

#### 289 *3.1 Effects of gas mixture ratio*

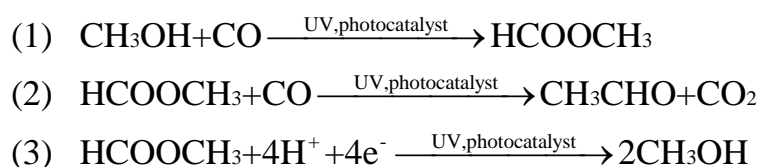
290 Pure CO as the reactant gas is specifically simulated so as to unveil its  
291 characteristics during the overall process at the ambient pressure and temperature of  
292 1atm and 293K respectively. Fig. 7 shows that the H<sub>2</sub> presents almost twice the  
293 concentration of O<sub>2</sub>, while the CH<sub>3</sub>OH concentration displays nearly zero due to the  
294 non-conversion from hydrogen, which clearly shows the unavailable direct chemical  
295 reaction between the pure CO and hydrogen or hydrogen ions. However, very small  
296 amount of CH<sub>3</sub>OH (less than 0.1μmol/g) exists inevitably due to the following  
297 reaction in the reduction reactor:



299 The overall process at various gas mixture ratios of CO to CO<sub>2</sub> was numerically  
300 simulated during the whole 20 hours with the carbon elements symbolized as C<sub>x</sub> from  
301 CO<sub>2</sub> and C<sub>y</sub> from CO for easy analysis of the carbon trails existing in methanol. Fig.8  
302 displays the processing amount of C<sub>x</sub>H<sub>3</sub>OH as well as C<sub>y</sub>H<sub>3</sub>OH at the CO to CO<sub>2</sub> ratio  
303 of 1:10. During the first 8 hours, it can be observed that the C<sub>x</sub>H<sub>3</sub>OH has a higher  
304 production rate of 0.53 μmol/g/h, while only 0.45 μmol/g/h for the C<sub>y</sub>H<sub>3</sub>OH. After  
305 then, it changes little for the concentration of C<sub>x</sub>H<sub>3</sub>OH with a stable amount of  
306 4.2μmol/g at the 20th hour. But for C<sub>y</sub>H<sub>3</sub>OH, the concentration always increases and

307 eventually reaches about 4.6  $\mu\text{mol/g}$  after 20 hours. It shows that the CO can easily  
 308 transform into the methanol and other organic compounds through the chemical  
 309 chains as aforementioned above compared with  $\text{CO}_2$ . As shown in Fig. 9, the  
 310 production of  $\text{C}_x\text{H}_3\text{OH}$  declines with the CO to  $\text{CO}_2$  ratio of 1:5 compared with the  
 311 case of 1:10, and only arrives at 3.6 $\mu\text{mol/g}$  for the maximum concentration. As for  
 312  $\text{C}_y\text{H}_3\text{OH}$ , the concentration reaches the peak of nearly 3.75  $\mu\text{mol/g}$  at the time of 7.5h,  
 313 then it decreases to 2.1  $\mu\text{mol/g}$  after 20 hours and finally presents a declining  
 314 tendency. Since CO plays a double role during the  $\text{CH}_3\text{OH}$  production, may the  
 315  $\text{CH}_3\text{OH}$  increase due to its positive effect with a small amount, while should other  
 316 organic compounds unexpectedly emerge with an excessive CO ratio. Fig. 10 shows  
 317 the  $\text{CH}_3\text{CHO}$  concentration at various gas mixture ratios, which clearly presents the  
 318 always small value less than 0.5  $\mu\text{mol/g}$  at the first 5 hours. But the  $\text{CH}_3\text{CHO}$   
 319 production rate increases as the chemical process continues, and it presents a higher  
 320 value at a more intensive CO concentration. Besides, as the ratio of CO to  $\text{CO}_2$   
 321 changes from 1/20 to 1/2, the  $\text{CH}_3\text{CHO}$  concentration increases from 1.5  $\mu\text{mol/g}$  to  
 322 3.75  $\mu\text{mol/g}$  after 20 hours.

323 Figs.8-10 fully explain the mechanisms of the CO dominance in the photocatalytic  
 324 process, which can be described by the following three reactions.



325

326 When a small amount of CO gas exists in the reactor, the CO reacts with CH<sub>3</sub>OH to  
327 form HCOOCH<sub>3</sub> as reaction (1). Due to the excessive H<sub>2</sub>, the HCOOCH<sub>3</sub> reacts with  
328 H<sub>2</sub> and then generates CH<sub>3</sub>OH as reaction (3). In this case, the CO promotes CH<sub>3</sub>OH  
329 production. However, if CO gas is excessive, the CO will react with CH<sub>3</sub>OH to form  
330 HCOOCH<sub>3</sub> at first, then the remaining CO continues to react with HCOOCH<sub>3</sub> to  
331 produce CH<sub>3</sub>CHO as reaction (2), which prevents HCOOCH<sub>3</sub> from reacting with H<sub>2</sub>,  
332 resulting in an indirect consumption of CH<sub>3</sub>OH.

333 The aforementioned conclusion about the gas mixture ratio can be of benefit to the  
334 design and application of photocatalytic reactor systems. For the twin reactor, the  
335 optimal CO to CO<sub>2</sub> ratio as well as reaction time can be recommended with reference  
336 to the light intensity distribution and reactor structure. Moreover, increasing the  
337 byproduct of CH<sub>3</sub>CHO during the photocatalytic process proves efficient to prevent  
338 the side effect as reaction (2).

### 339 *3.2 Effects of pressure*

340 The mixture pressure in the reactor is of great importance for photocatalytic  
341 reactions. According to Henry's law, the partial pressure of the mixture above the  
342 liquid surface can directly affect the gas solubility. Besides, the mass transfer rate  
343 between the gas and liquid is related greatly with the partial pressure in terms of the  
344 two-film theory. Fig. 11 presents the production of CH<sub>3</sub>OH at various pressures  
345 during the 20 hours. It can be seen that as the initial pressure in the reactor goes up,

346 the CH<sub>3</sub>OH yield increases. When the initial pressure reaches 20atm, the CH<sub>3</sub>OH  
347 concentration arrives at 14.5 μmol/g at 20 hours, which is 52.6% higher than that of  
348 9.5 μmol/g at the initial pressure of 1atm. As for the efficiency, increasing the initial  
349 pressure in the reactor will consume more energy, so a viable operating pressure  
350 should be determined for the photocatalytic reactor in potential engineering  
351 applications.

### 352 *3.3 Effects of temperature*

353 The Henry constant can well represent the solubility of CO<sub>2</sub> and CO in the  
354 electrolyte. As observed from Table 3, the Henry constant increases as the temperature  
355 rises. Besides, the diffusion coefficients of the gas-gas as well as gas-liquid depend  
356 also upon the temperature according to Eq.(9), so the mass transfer correlates strongly  
357 with the temperature. Fig.12 shows the CH<sub>3</sub>OH concentration change at various  
358 temperatures, from which can be seen that the CH<sub>3</sub>OH concentration increases with  
359 increasing the temperature, resulting from the comprehensive effects of the solubility  
360 and mass transfer rate. At the temperature of 273K, the ultimate CH<sub>3</sub>OH concentration  
361 at the 20th hour is 6 μmol/g, while at 333K it approaches 11μmol/g, presenting an  
362 increase of 83.2%, which shows that the conversion efficiency can be greatly  
363 improved by increasing the temperature.

### 364 *3.4 Effects of light intensity*

365 Based on the optical parameters of the physical model aforementioned, the sun



366 light model is developed and the two dimensional distribution of light intensity on a  
367 cross-section of the reactor is achieved by adopting the software SOLTRACE. Fig. 13  
368 shows transient solar flux distribution in the reactor at 8:00, 12:00 and 16:00  
369 respectively, in which the positive direction of the X-axis stands for the west of the  
370 reactor and the positive direction of the Y-axis represents the zenith of the twin reactor.  
371 The distribution of light intensity at 8:00 is shown in Fig.13(a), which presents a  
372 non-uniform light intensity scattering in the reactor with  $832\text{W/m}^2$  on the east side  
373 while only  $205\text{W/m}^2$  on the west side, and the average light intensity is about  
374  $331\text{W/m}^2$ . As observed from Fig. 13(b), the reactor receives the sunlight vertically at  
375 12:00, so the light intensity arrives at the maximum value in the center while  
376 minimum value at both sides, due to the combined effects of the reflection and  
377 refraction by the glass container and colored solution with the iron ion. The average  
378 light intensity can reach nearly  $620\text{W/m}^2$  in the reactor. Fig. 13(c) presents the  
379 irradiation at 16:00 from the west side of the reactor with the average light intensity of  
380  $330\text{W/m}^2$ .

381 From 8:00 to 16:00, the average light intensity is obtained and shown in Fig.14,  
382 which is fitted to the following equation:

$$383 \quad I = -1996 + 435Hr - 18Hr^2 \quad (14)$$

384 It can be seen from Fig.14 that the results from the fitting curve agree well with the  
385 simulated data, so the fitting equation is reliable enough to predict the average light

386 intensity change over time. Together with the chemical reaction engineering module,  
387 the photocatalytic CO<sub>2</sub> reduction combined with the water splitting process can be  
388 numerically simulated within the 8 hours (8:00-16:00) at the temperature of 293K and  
389 pressure of 1atm. Fig.15 shows the concentration changes of O<sub>2</sub>, H<sub>2</sub> and CH<sub>3</sub>OH over  
390 time, proving that the CH<sub>3</sub>OH product using the sun light source is less than that using  
391 the artificial light source in the experiment of Cheng et al.[25]. As also clearly  
392 presented, the CH<sub>3</sub>OH concentration reaches the climax of 4.6 μmol/g about 3.5 hours  
393 later (11:30), and then it begins to decrease gradually due to the weakened light  
394 intensity. Fig. 16 shows the reaction rates of the photocatalytic CO<sub>2</sub> reduction and  
395 water splitting process. It can be seen that as the light intensity decreases, the  
396 photocatalytic water splitting reaction becomes slow, resulting in the reduced H<sub>2</sub> for  
397 CO<sub>2</sub> reduction. The CH<sub>3</sub>OH generating rate is lower than the consuming rate of side  
398 reaction, leading to a reduced CH<sub>3</sub>OH concentration.

399 Since the experimental study with the artificially unchanged light intensity could  
400 not totally represent the photocatalytic CO<sub>2</sub> reduction mechanism, the numerical  
401 method with the natural sunlight changing over time demonstrates an attractive  
402 superiority, which is closer to the real chemical process.

#### 403 **4. Conclusions**

404 The photocatalytic reduction of CO<sub>2</sub> by CO co-feed combined with photocatalytic  
405 water splitting in a novel twin reactor was modeled and numerically investigated.

406 The CH<sub>3</sub>OH concentration almost linearly increases with increasing the gas mixture  
407 ratio of CO to CO<sub>2</sub>, due to the direct conversion from CO to CH<sub>3</sub>OH. However, the  
408 excessive CO will react with HCOOCH<sub>3</sub> to form CH<sub>3</sub>CHO unexpectedly, resulting in  
409 a reduced CH<sub>3</sub>OH concentration. Besides, with the temperature and pressure increase,  
410 the CH<sub>3</sub>OH production rises owing to the enhanced mass transfer.

411 The numerical method with the natural sunlight in this work proves a more accurate  
412 photocatalytic CO<sub>2</sub> reduction process compared with the experiment, and the yield of  
413 CH<sub>3</sub>OH is reduced due to the changing light intensity. It suggests the artificial light  
414 intensity adjusted with time in the photocatalytic experiment, so as to obtain a more  
415 reliable result.

#### 416 **Acknowledgment**

417 The financial support for this research from the National Natural Science  
418 Foundation of China (Grant No. 50776032) is gratefully acknowledged. The authors  
419 also thank the support provided by the Royal Society International Project of UK  
420 (IE150489).

421

422       **References**

- 423       [1] Baran T, Wojtyła S, Dibenedetto A, Aresta M, Macyk W. Zinc sulfide functionalized with  
424 ruthenium nanoparticles for photocatalytic reduction of CO<sub>2</sub>. *Applied Catalysis B: Environmental*  
425 2015;178:170-6.
- 426       [2] Huang Q, Yu J, Cao S, Cui C, Cheng B. Efficient photocatalytic reduction of CO<sub>2</sub> by  
427 amine-functionalized g-C<sub>3</sub>N<sub>4</sub>. *Appl Surf Sci* 2015;358:350-5.
- 428       [3] Tahir B, Tahir M, Amin NS. Gold–indium modified TiO<sub>2</sub> nanocatalysts for photocatalytic CO<sub>2</sub>  
429 reduction with H<sub>2</sub> as reductant in a monolith photoreactor. *Appl Surf Sci* 2015;338:1-14.
- 430       [4] Yuan K, Yang L, Du X, Yang Y. Performance analysis of photocatalytic CO<sub>2</sub> reduction in optical  
431 fiber monolith reactor with multiple inverse lights. *Energ Convers Manage* 2014;81:98-105.
- 432       [5] Yuan K, Yang L, Du X, Yang Y. Numerical analysis of photocatalytic CO<sub>2</sub> reduction in optical  
433 fiber monolith reactor with optimized structures. *Energ Convers Manage* 2014;87:258-66.
- 434       [6] Tahir M, Amin NS. Recycling of carbon dioxide to renewable fuels by photocatalysis: Prospects  
435 and challenges. *Renewable and Sustainable Energy Reviews* 2013;25:560-79.
- 436       [7] Chiu FP, Kuo HI, Chen CC, Hsu CS. The energy price equivalence of carbon taxes and  
437 emissions trading—Theory and evidence. *Appl Energ* 2015;160:164-71.
- 438       [8] Liu Y, Zhou Y, Wu W. Assessing the impact of population, income and technology on energy  
439 consumption and industrial pollutant emissions in China. *Appl Energ* 2015;155:904-17.
- 440       [9] Wang Q, Su B, Sun J, Zhou P, Zhou D. Measurement and decomposition of energy-saving and  
441 emissions reduction performance in Chinese cities. *Appl Energ* 2015;151:85-92.
- 442       [10] Sim LC, Leong KH, Saravanan P, Ibrahim S. Rapid thermal reduced graphene oxide/Pt-TiO<sub>2</sub>  
443 nanotube arrays for enhanced visible-light-driven photocatalytic reduction of CO<sub>2</sub>. *Appl Surf Sci* 2015.
- 444       [11] Tahir M, Amin NS. Photocatalytic CO<sub>2</sub> reduction with H<sub>2</sub> as reductant over copper and indium  
445 co-doped TiO<sub>2</sub> nanocatalysts in a monolith photoreactor. *Applied Catalysis A: General*  
446 2015;493:90-102.
- 447       [12] Inoue T, Fujishima A, Satoshi K, Honda K. Photoelectrocatalytic reduction of carbon dioxide in  
448 aqueous suspensions of semiconductor powders. *Nature* 1979;277:637-8.
- 449       [13] Tahir M, Amin NS. Advances in visible light responsive titanium oxide-based photocatalysts  
450 for CO<sub>2</sub> conversion to hydrocarbon fuels. *Energ Convers Manage* 2013;76:194-214.
- 451       [14] Broberg Viklund S, Johansson MT. Technologies for utilization of industrial excess heat:  
452 Potentials for energy recovery and CO<sub>2</sub> emission reduction. *Energ Convers Manage* 2014;77:369-79.
- 453       [15] Jain S, Vardia J, Ameta R, Ameta SC. Use of malachite green as photocatalyst in reduction of  
454 sodium and potassium carbonates. *Energ Convers Manage* 2004;45:1233-42.
- 455       [16] Tahir B, Tahir M, Amin NS. Performance analysis of monolith photoreactor for CO<sub>2</sub> reduction  
456 with H<sub>2</sub>. *Energ Convers Manage* 2015;90:272-81.
- 457       [17] Wang T, Yang L, Du X, Yang Y. Numerical investigation on CO<sub>2</sub> photocatalytic reduction in  
458 optical fiber monolith reactor. *Energ Convers Manage* 2013;65:299-307.
- 459       [18] Ola O, Maroto-Valer MM. Transition metal oxide based TiO<sub>2</sub> nanoparticles for visible light  
460 induced CO<sub>2</sub> photoreduction. *Applied Catalysis A: General* 2015;502:114-21.
- 461       [19] Ola O, Maroto-Valer MM. Review of material design and reactor engineering on TiO<sub>2</sub>

462 photocatalysis for CO<sub>2</sub> reduction. *Journal of Photochemistry and Photobiology C: Photochemistry*  
463 *Reviews* 2015;24:16-42.

464 [20] Nong G, Chen Y, Li M, Zhou Z. Generation of hydrogen free radicals from water for fuels by  
465 electric field induction. *Energ Convers Manage* 2015;105:545-51.

466 [21] Waskasi MM, Hashemianzadeh SM, Mostajabi Sarhangi O, Harzandi AP. Computational model  
467 of hydrogen production by Coumarin-dye-sensitized water splitting to absorb the visible light in a local  
468 electric field. *Energ Convers Manage* 2012;62:154-64.

469 [22] Thampi KR, Kiwi J, Gratzel M. Methanation and photo-methanation of carbon dioxide at room  
470 temperature and atmospheric pressure. *Nature* 1987;327:506-8.

471 [23] Lo CC, Hung CH, Yuan CS, Wu JF. Photoreduction of carbon dioxide with H<sub>2</sub> and H<sub>2</sub>O over  
472 TiO<sub>2</sub> and ZrO<sub>2</sub> in a circulated photocatalytic reactor. *Sol Energy Mat Sol C* 2007;91:1765-74.

473 [24] Shinichi I, Ryota D. Hydrogen production from water and conversion of carbon dioxide to  
474 useful chemicals by room temperature photoelectrocatalysis. *Catal Today* 1996;27:271-7.

475 [25] Cheng YH, Nguyen VH, Chan HY, Wu JCS, Wang WH. Photo-enhanced hydrogenation of CO<sub>2</sub>  
476 to mimic photosynthesis by CO co-feed in a novel twin reactor. *Appl Energ* 2015;147:318-24.

477 [26] Lee WH, Liao CH, Tsai MF, Huang CW, Wu JCS. A novel twin reactor for CO<sub>2</sub> photoreduction  
478 to mimic artificial photosynthesis. *Applied Catalysis B: Environmental* 2013;132-133:445-51.

479 [27] Yu SC, Huang CW, Liao CH, Wu JCS, Chang ST, Chen KH. A novel membrane reactor for  
480 separating hydrogen and oxygen in photocatalytic water splitting. *J Membrane Sci* 2011;382:291-9.

481 [28] Lin H, Valsaraj K. An optical fiber monolith reactor for photocatalytic wastewater treatment.  
482 *Aiche J* 2006;2271-80.

483 [29] Herrmann JM. Heterogeneous photocatalysis: an emerging discipline involving multiphase  
484 systems. *Catal Today* 1995;24:157-64.

485 [30] Denny F, Scott J, Peng GD, Amal R. Channelled optical fibre photoreactor for improved air  
486 quality control. *Chem Eng Sci* 2010;65:882-9.

487 [31] Ueyama K, Hatanaka J. Salt effect on solubility of nonelectrolyte gases and liquids. *Chem Eng*  
488 *Sci* 1982;37:790-2.

489 [32] Ryszard P, Wadysaw M. Kinetics of Reaction Between Carbon-Dioxide and Hydroxyl Ions in  
490 Aqueous-Electrolyte Solutions. *Chem Eng Sci* 1988;43:1677-84.

491 [33] Rathore M, Kapuno R. *Engineering heat transfer*: Jones & Bartlett; 2011.

492 [34] Spencer GH, Murty M. General Ray-Tracing Procedure. *Journal of the Optical Society of*  
493 *America* 1962;52:672-8.

**Table 1**Changes of enthalpy and Gibbs free energy in the CO<sub>2</sub> photoreduction reactions[25].

Reactions	$\Delta H^0$ (kJ/mol)	$\Delta G^0$ (kJ/mol)
(1) CO <sub>2</sub> (g)+3H <sub>2</sub> (g)→CH <sub>3</sub> OH (l) +H <sub>2</sub> O (l)	-137.8	-10.7
(2) CO(g)+CH <sub>3</sub> OH(l)→HCOOCH <sub>3</sub> (l)	-25.6	6.6
(3) CO <sub>2</sub> (g)+H <sub>2</sub> (g)+CH <sub>3</sub> OH(l)→HCOOCH <sub>3</sub> (l)+H <sub>2</sub> O(l)	-31.8	25.8
(4) HCOOCH <sub>3</sub> (l)+2H <sub>2</sub> (g)→2CH <sub>3</sub> OH(l)	-99.7	-35.1
(5) HCOOCH <sub>3</sub> (l)+CO(g)→CH <sub>3</sub> CHO(l)+CO <sub>2</sub> (g)	-96.5	-86.7

**Table 2**Model parameters for photocatalytic CO<sub>2</sub> reduction by CO co-feed.

Type	Variables	Values	Unit
kinetics	$k_1$	3.3E-9	m <sup>3</sup> /(s · mol)
	$k_2$	1.7E-2	m <sup>9</sup> /(s · mol <sup>3</sup> )
	$k_3$	2.3E-4	m <sup>3</sup> /(s · mol)
	$k_4$	1.7E-4	m <sup>3</sup> /(s · mol)
	$k_5$	5.8E-6	m <sup>6</sup> /(s · mol <sup>2</sup> )
	$k_6$	8.1E-3	m <sup>3</sup> /(s · mol)
Geometry	$L$	11.46	cm
	$R_1$	5	cm
	$R_2$	4	cm
Mass transfer	$D_L$	1.9809E-9	m <sup>2</sup> /s
	$D_G$	1.41E-7	m <sup>2</sup> /s
	$\delta_G$	0.1	mm
	$\delta_L$	0.1	mm
	$h_{H^+}$	0	
	$h_{Fe^{2+}}$	0.049	
	$h_{Fe^{3+}}$	0.054	
	$h_{SO_4^{2-}}$	0.029	
$h_{Cl^-}$	0.021		

	$h_{\text{CO}^2}$	-0.019	
	$h_{\text{CO}}$	0.0283	
	$H_{0\text{CO}}$	5.43E+6	kPa
	$H_{0\text{CO}_2}$	1.44E+5	kPa
Initial value	$C_{\text{CO}_2}$	30.73	mol/m <sup>3</sup>
	$C_{\text{CO}}$	0.095	mol/m <sup>3</sup>
	$C_{\text{SO}_4^{2-}}$	1.21	mol/m <sup>3</sup>
	$C_{\text{Fe}^{2+}}$	8.8	mol/m <sup>3</sup>
	$C_{\text{Fe}^{3+}}$	8.8	mol/m <sup>3</sup>
	$I$	900	W/m <sup>2</sup>
	$m$	1	
Sun position	$Day$	200	
	$Hr$	8-16	
	$L$	40°5'	
	$Shape$	Pillbox	
Optical property	$Rf_{\text{glass}}$	0.05	
	$Tr_{\text{glass}}$	0.95	
	$Ab_{\text{glass}}$	0	
	$n_{\text{glass}}$	1.6	
	$Rf_{\text{solution}}$	0.2	



$Tr_{\text{solution}}$	0.48
$Ab_{\text{solution}}$	0.32
$n_{\text{solution}}$	1.3
<i>Slope error(mrad)</i>	3.5
<i>Specularity error(mrad)</i>	0.2

---

**Table 3**

Henry constants at various temperatures.

<i>T</i> (K)	273	278	283	288	293	298	303	308	313	318	323	333
Gas												
CO ( $H_x \times 10^{-6}$ kPa)	3.57	4.01	4.48	4.95	5.43	5.88	6.28	6.68	7.05	7.39	7.71	8.32
CO <sub>2</sub> ( $H_x \times 10^{-5}$ kPa)	0.37	0.8	1.05	1.24	1.44	1.66	1.88	2.12	2.36	2.60	2.87	3.46

$$H_c = \frac{H_x M_{\text{solvent}}}{1000 \rho}$$

Fig.1. Schematic of photocatalytic CO<sub>2</sub> reduction and H<sub>2</sub>O splitting in the twin reactor.

Fig.2. H<sub>2</sub> and O<sub>2</sub> production during photocatalytic reduction of pure CO<sub>2</sub> with simultaneous H<sub>2</sub>O splitting.

Fig.3. CH<sub>3</sub>OH production during photocatalytic reduction of pure CO<sub>2</sub> with simultaneous H<sub>2</sub>O splitting.

Fig.4. CH<sub>3</sub>CHO and HCOOCH<sub>3</sub> production during photocatalytic reduction of pure CO<sub>2</sub> with simultaneous H<sub>2</sub>O splitting.

Fig.5. CH<sub>3</sub>OH concentration at the CO to CO<sub>2</sub> ratio of 1:10.

Fig.6. CH<sub>3</sub>OH concentration at the CO to CO<sub>2</sub> ratio of 1:5.

Fig.7. H<sub>2</sub>, O<sub>2</sub> and CH<sub>3</sub>OH concentrations with the pure CO as the reactant gas.

Fig.8. Total CH<sub>3</sub>OH concentration, C<sub>x</sub>H<sub>3</sub>OH and C<sub>y</sub>H<sub>3</sub>OH concentrations at the CO to CO<sub>2</sub> ratio of 1:10.

Fig.9. Total CH<sub>3</sub>OH concentration, C<sub>x</sub>H<sub>3</sub>OH and C<sub>y</sub>H<sub>3</sub>OH concentrations at the CO to CO<sub>2</sub> ratio of 1:5.

Fig.10. CH<sub>3</sub>CHO concentrations at various CO to CO<sub>2</sub> gas mixture ratios.

Fig.11. CH<sub>3</sub>OH concentration change with time at various pressures.

Fig.12. CH<sub>3</sub>OH concentration change with time at various temperatures.

Fig.13. Light intensity distribution in CO<sub>2</sub> reduction reactor. (a) 8:00, (b) 12:00, (c) 16:00.

Fig.14. Average light intensity change over time under the sun light.

Fig.15. Concentration changes of  $H_2$ ,  $O_2$  and  $CH_3OH$  over time under the sun light.

Fig.16. Reaction rate changes of water splitting and  $CO_2$  reduction over time under the sun light.

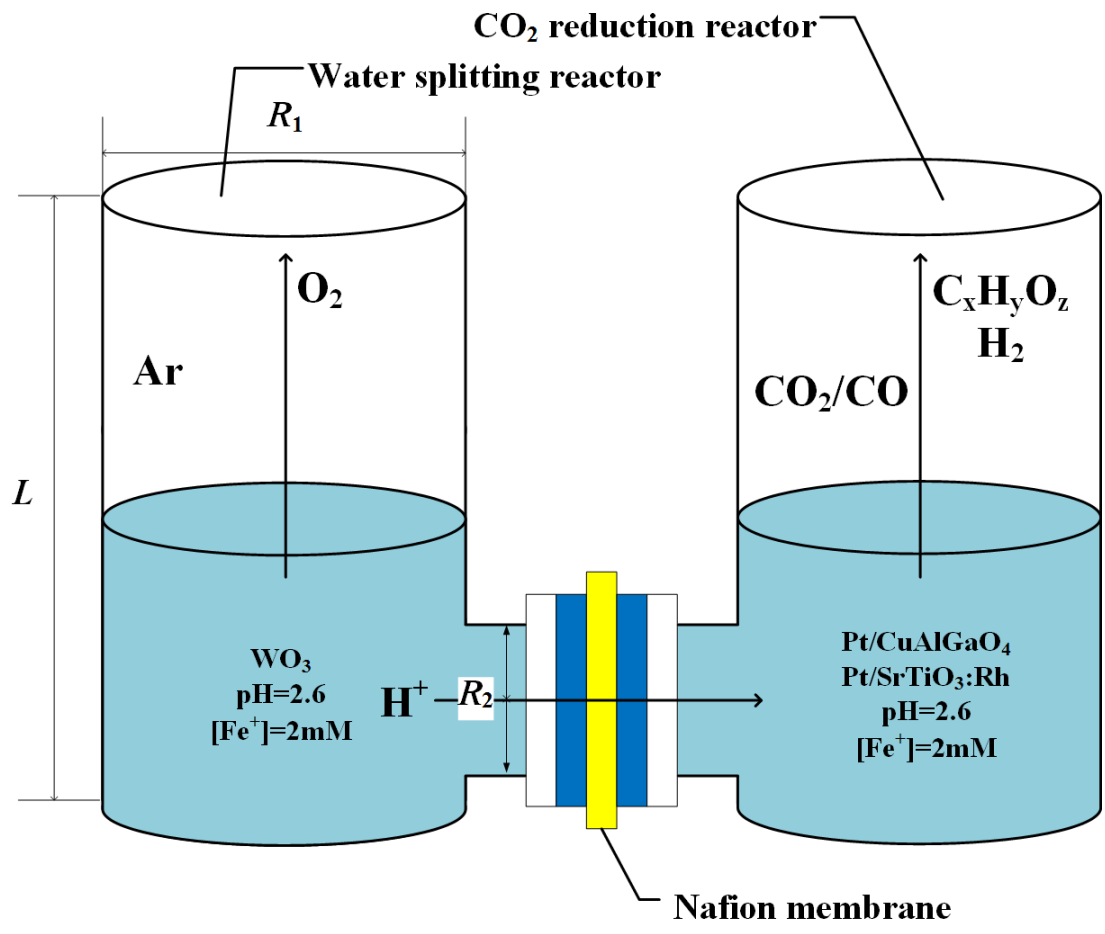


Fig.1.

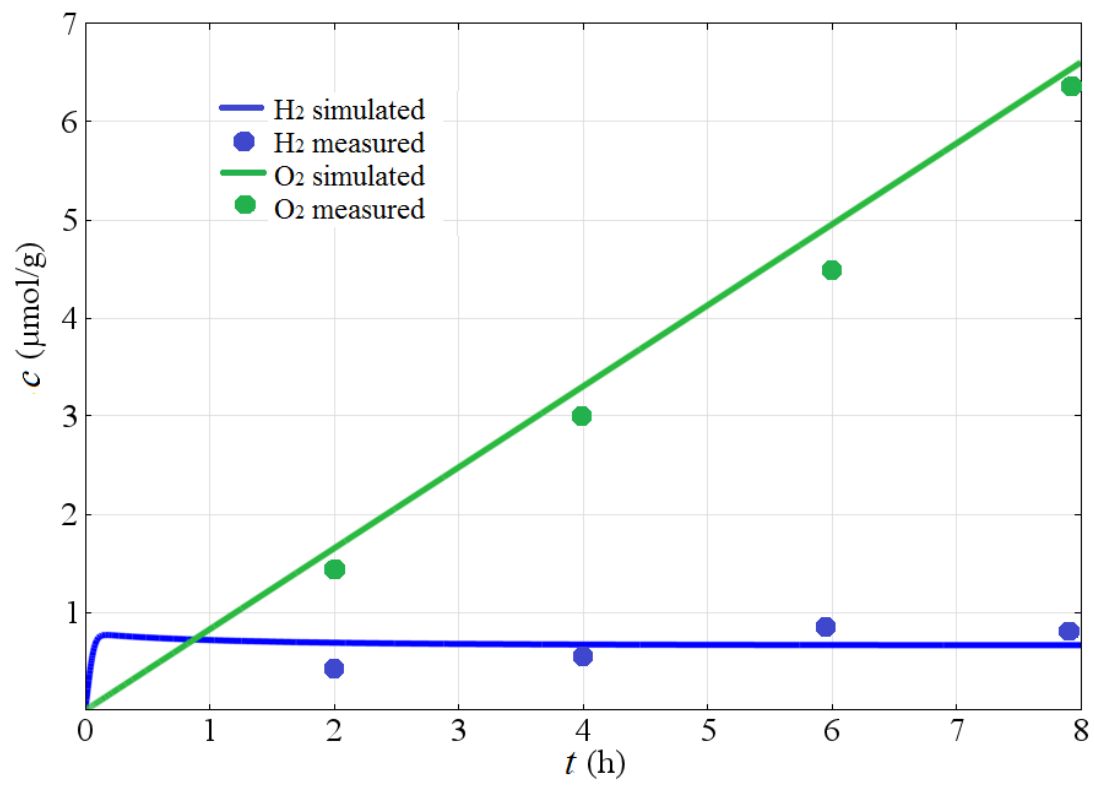


Fig.2.

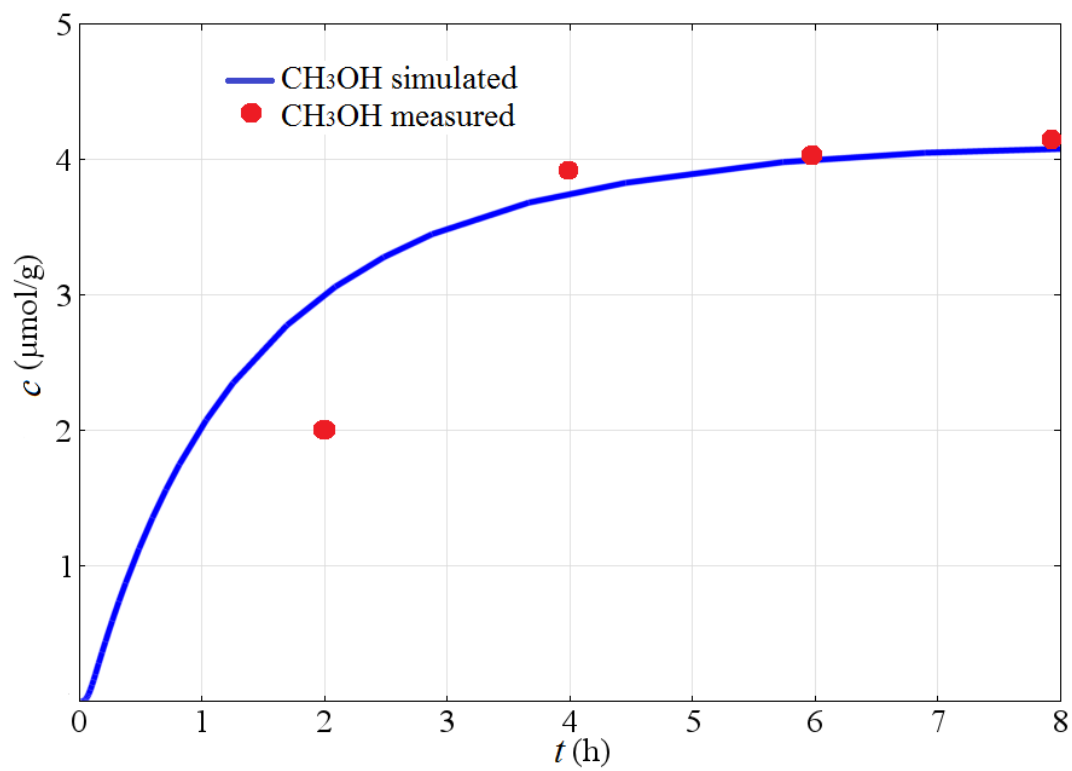


Fig.3.

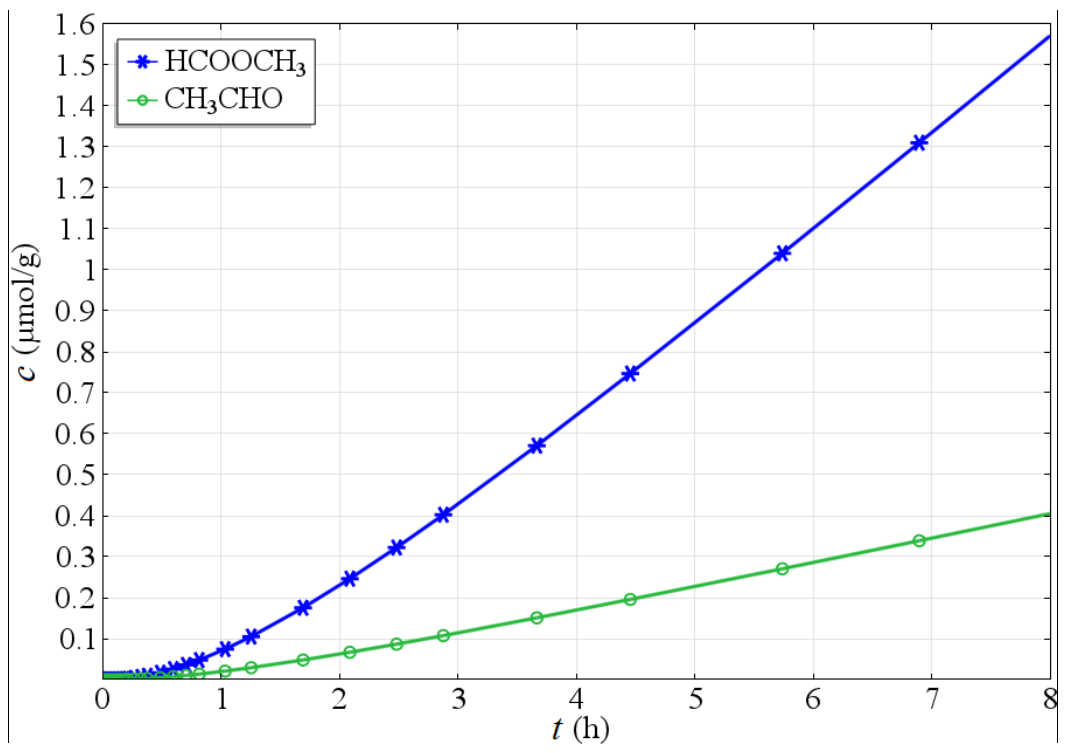


Fig.4.



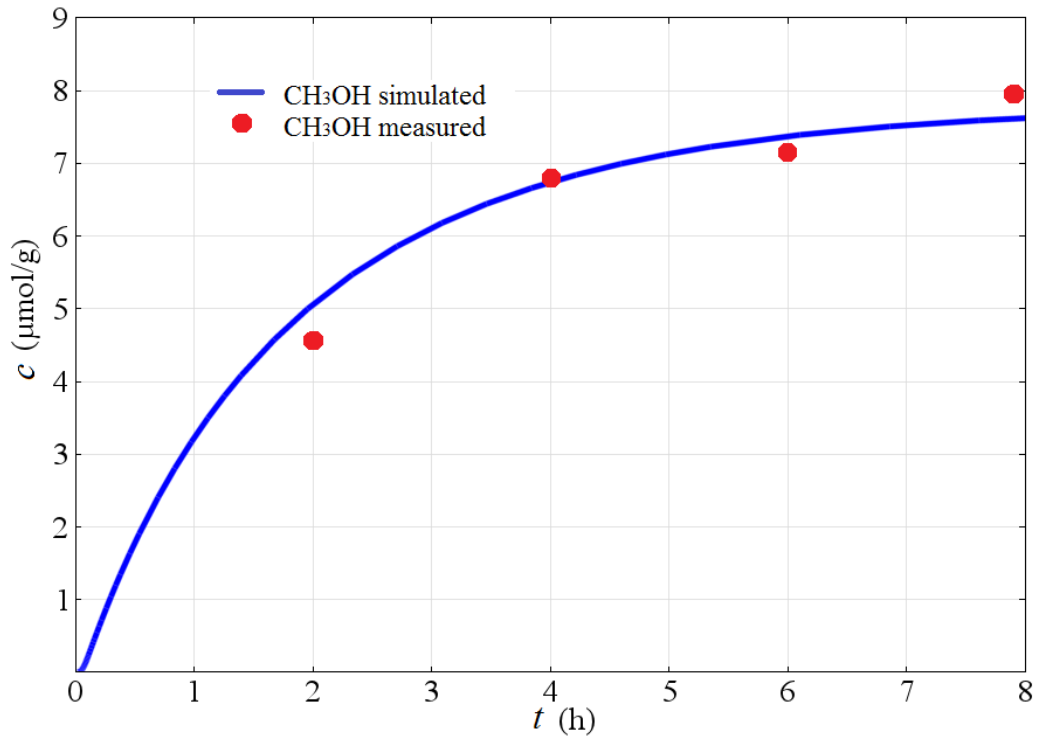


Fig.5.

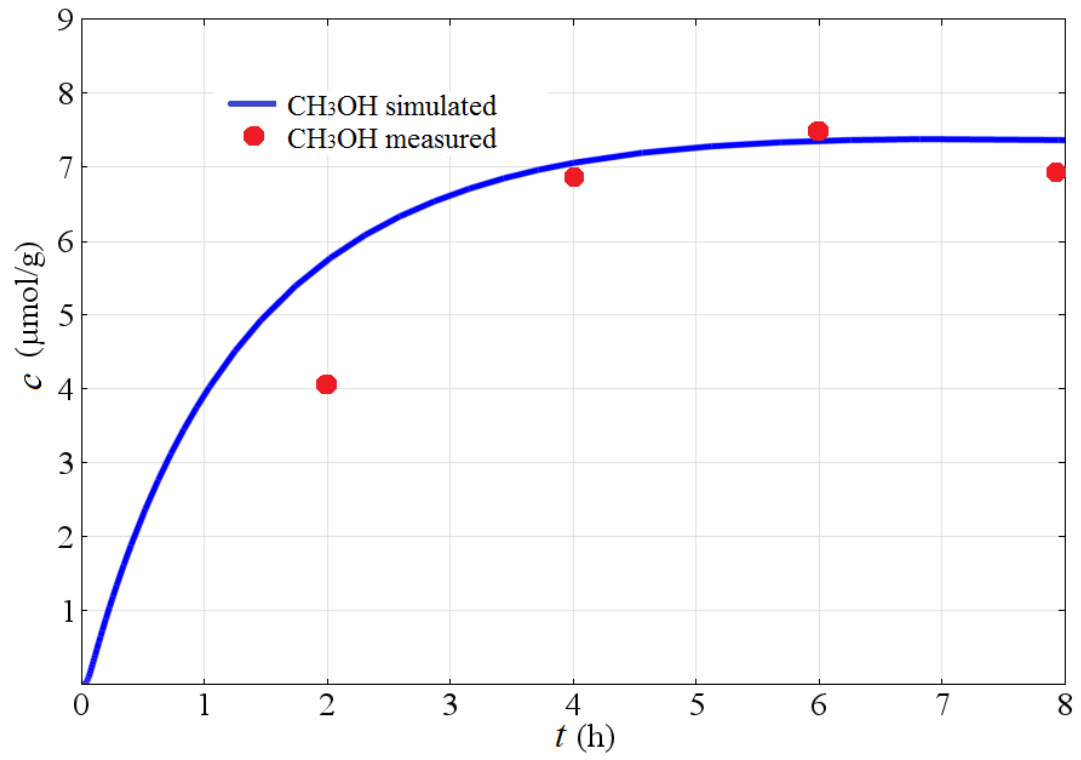


Fig.6.

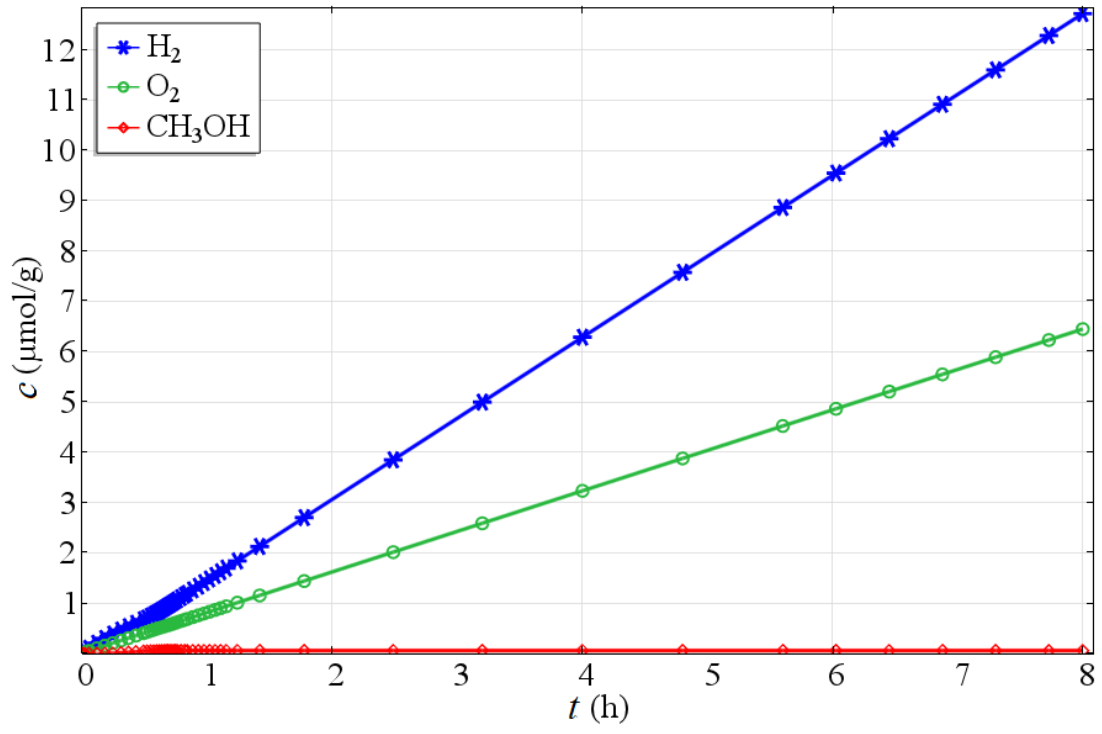


Fig.7.

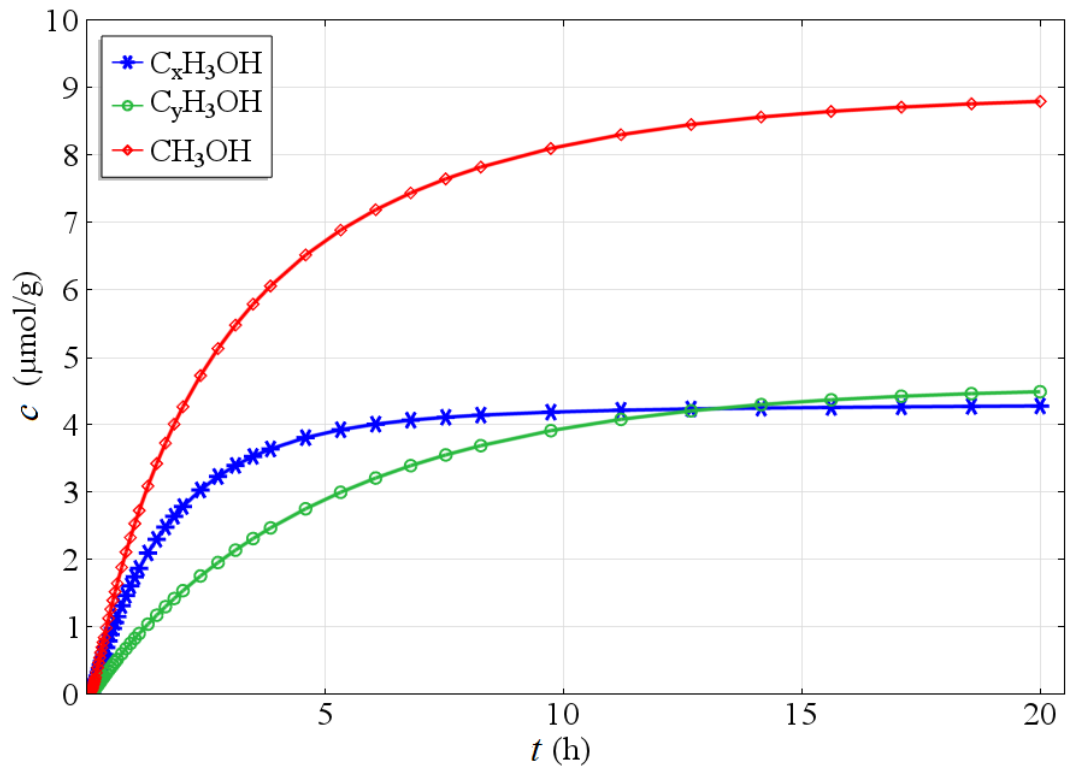


Fig.8.

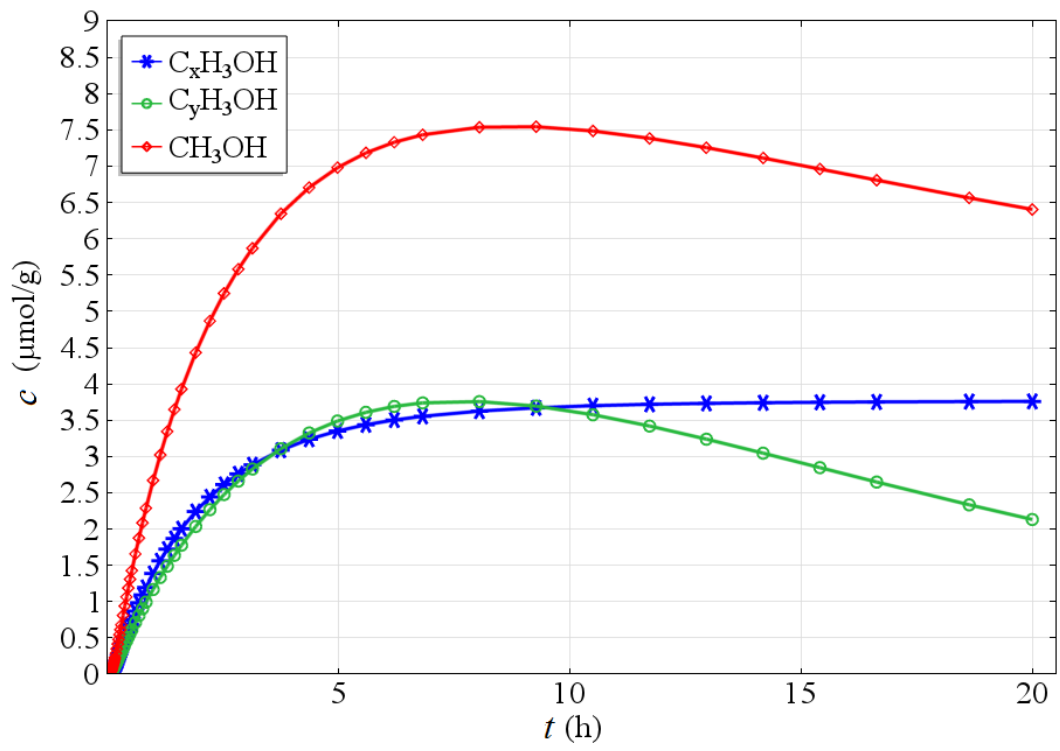


Fig.9.

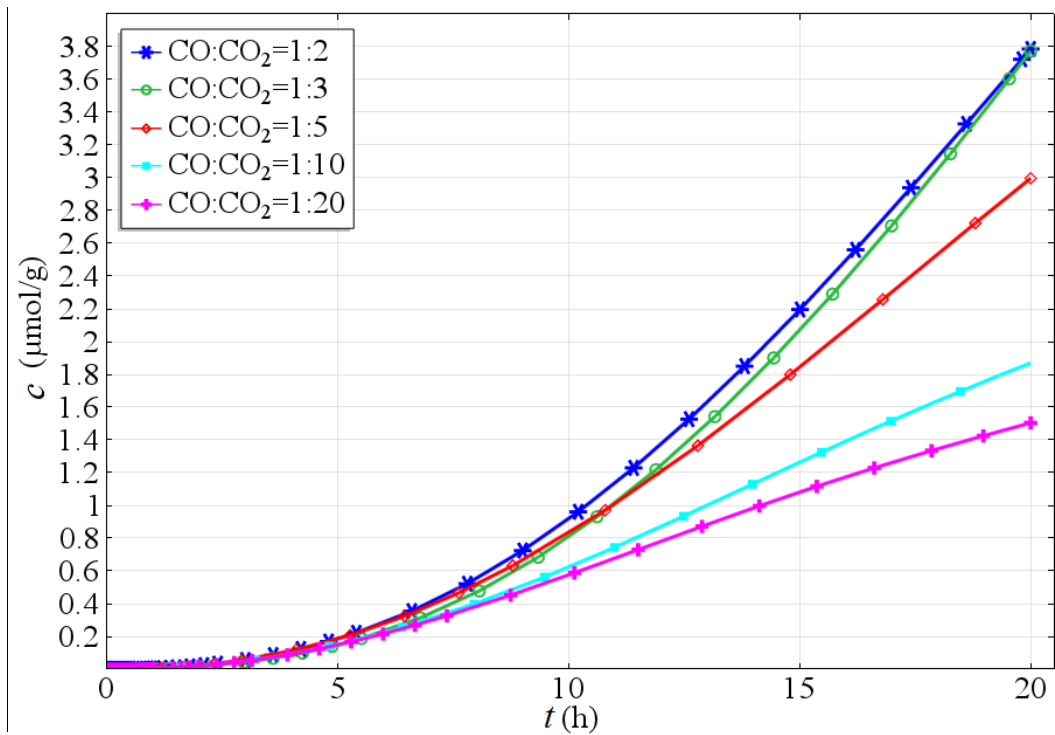


Fig.10.

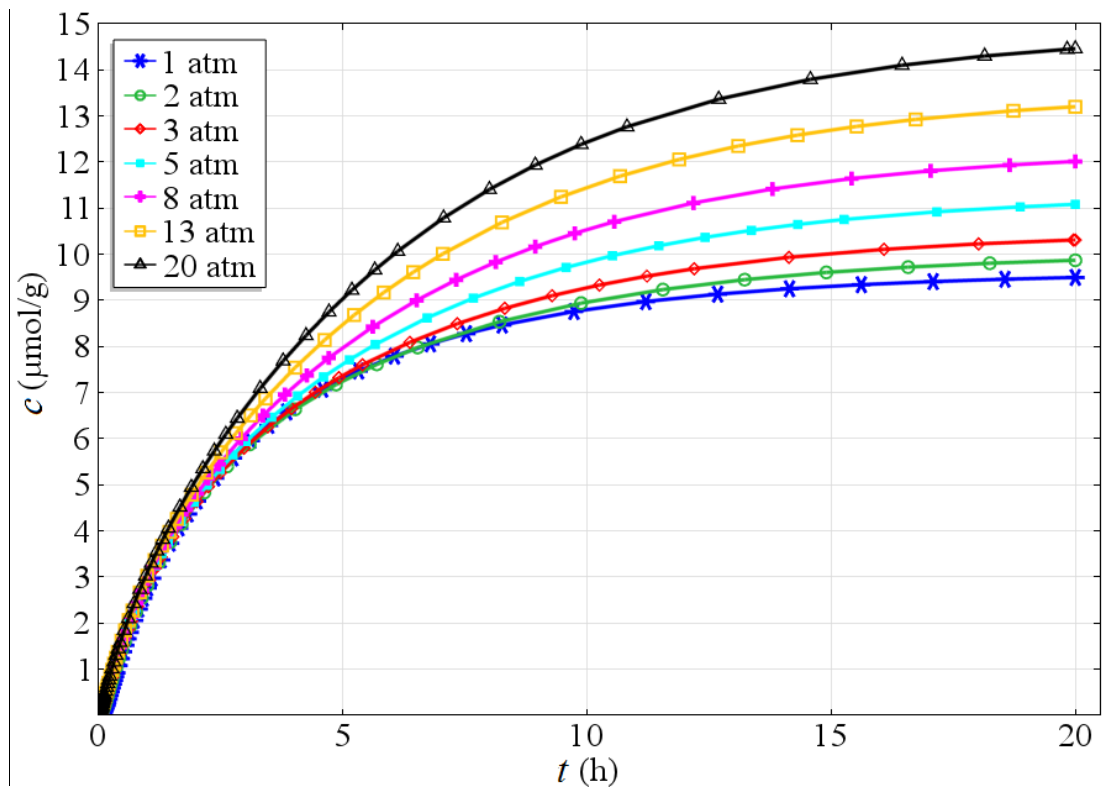


Fig.11.

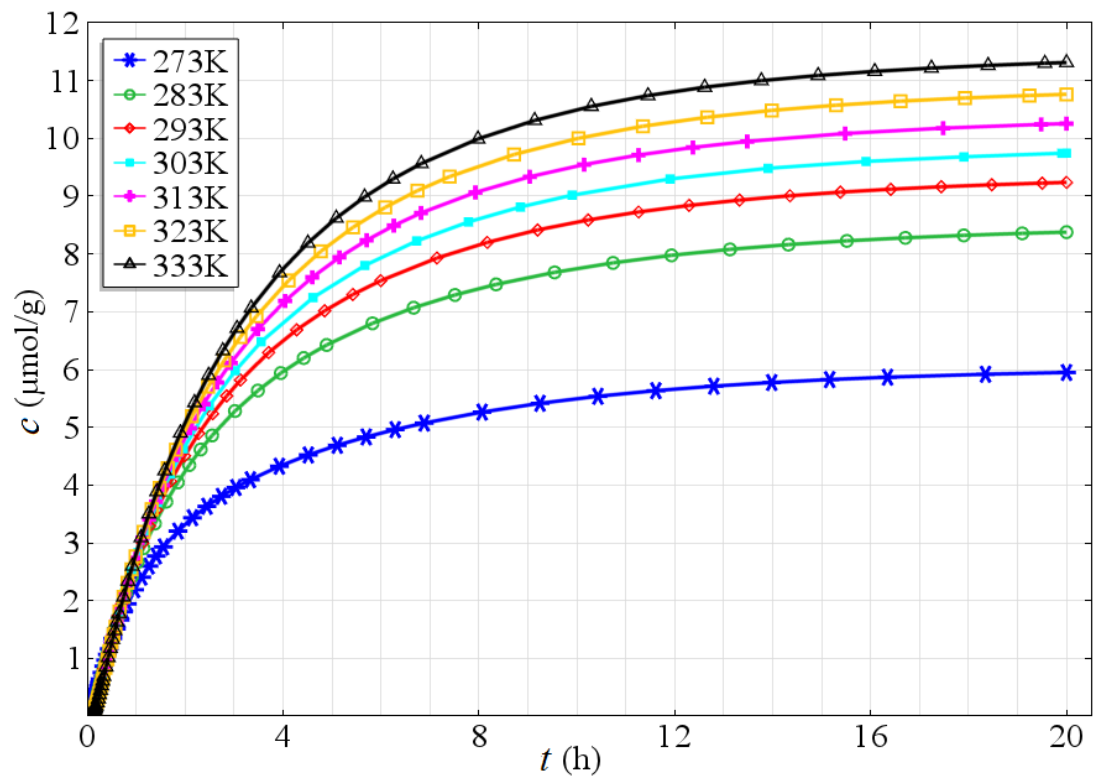
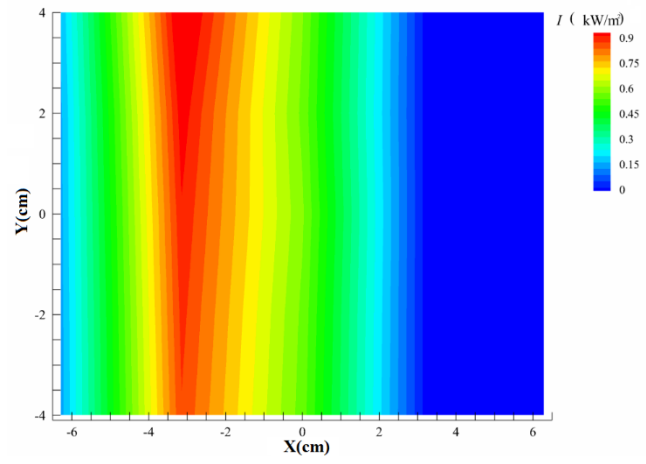
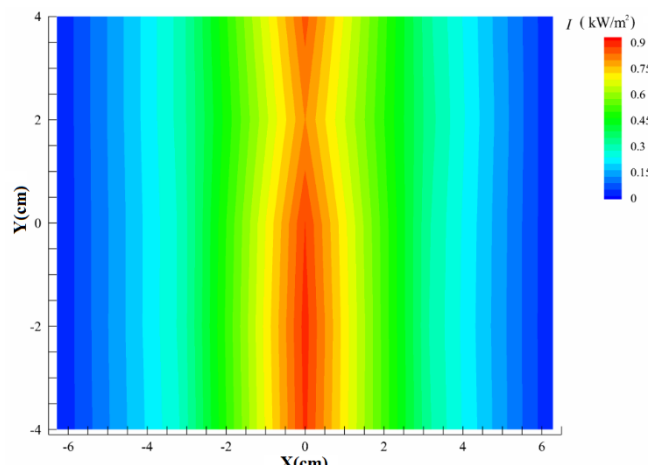


Fig.12.

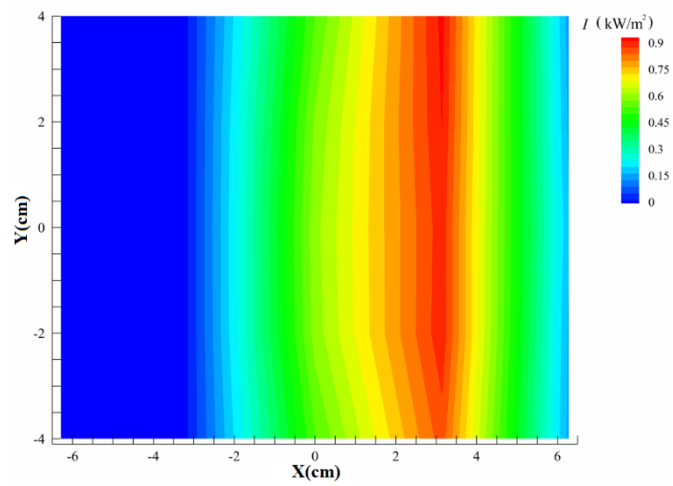




(a)



(b)



(c)

Fig.13.

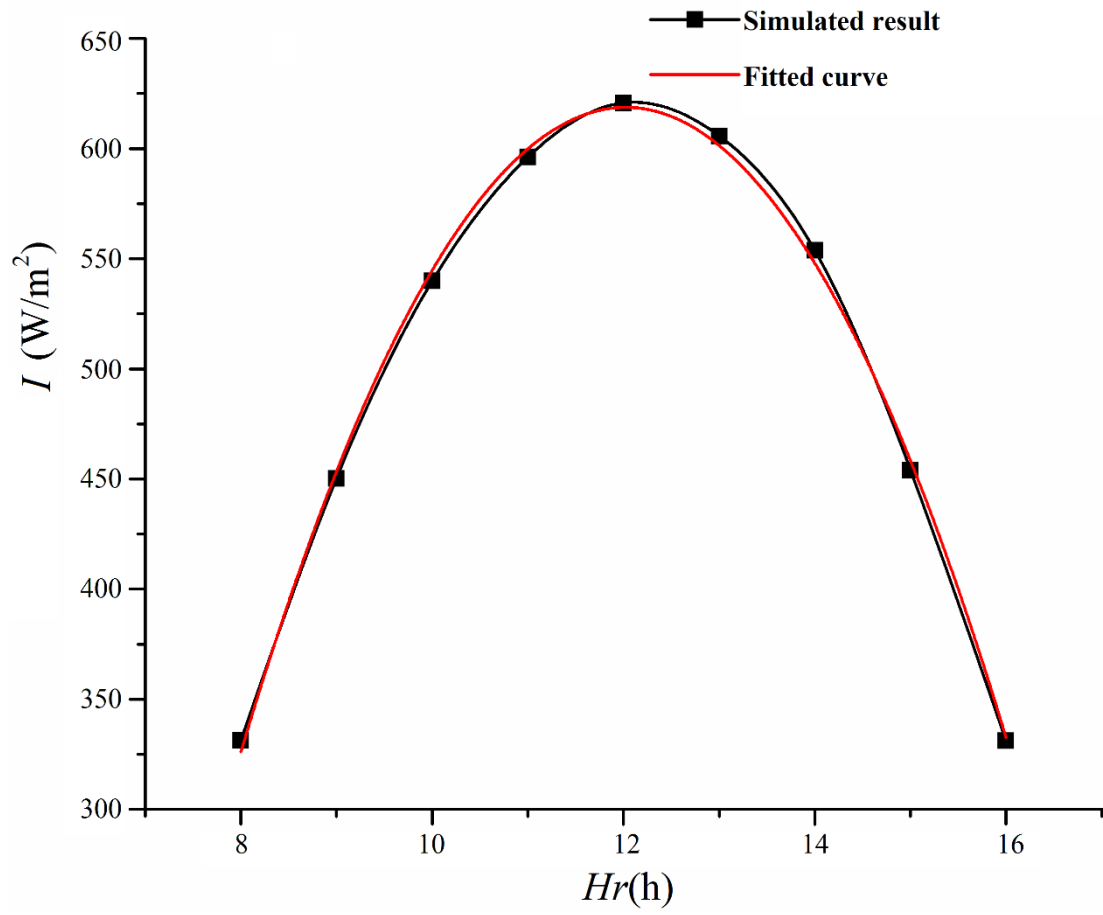


Fig.14.

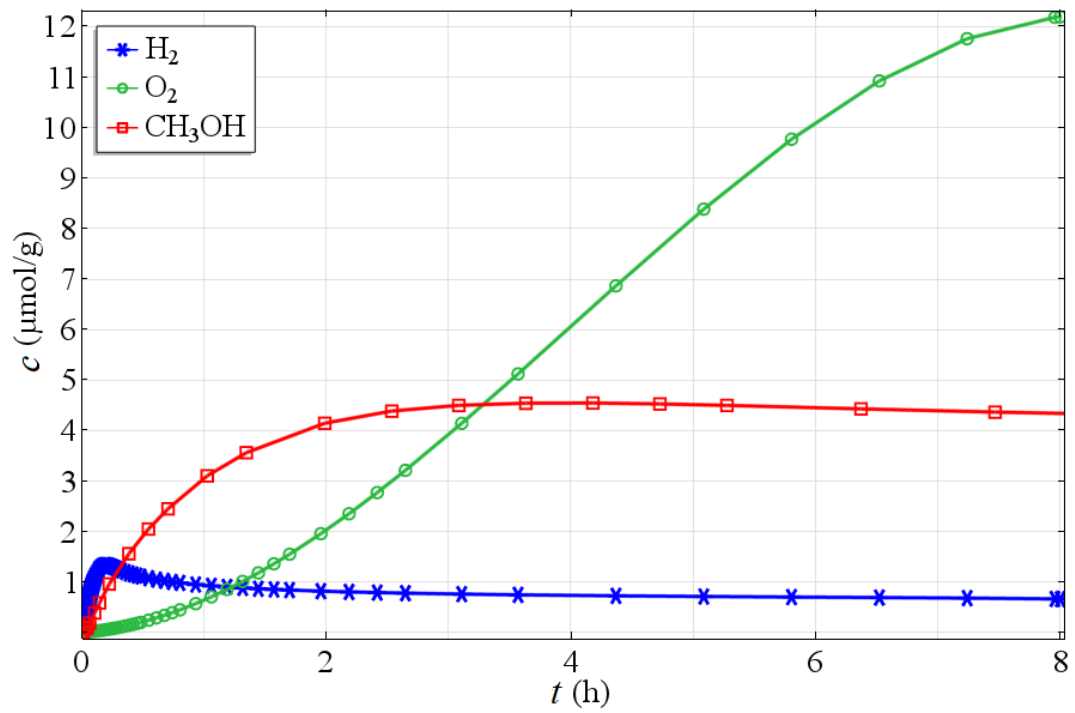


Fig.15.

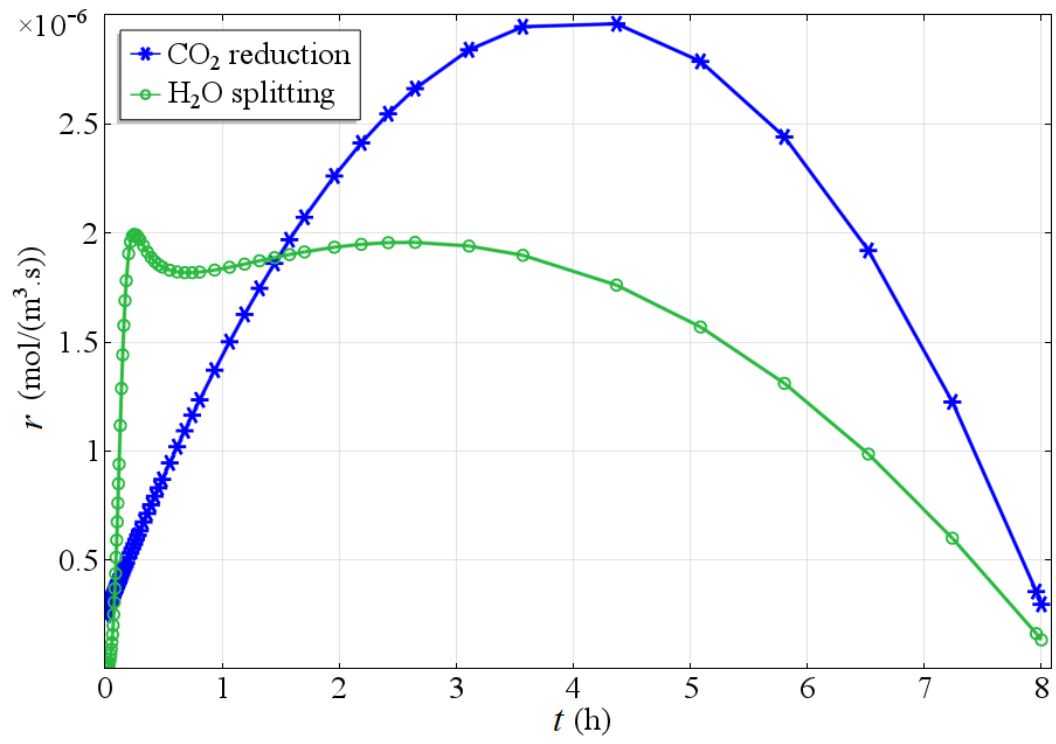


Fig.16.